Applicators and methods to achieve precise spatial control of the treatment zone during microwave ablation

by

Austin Pfannenstiel

B.S., Kansas State University, 2009
MBA, Kansas State University, 2017
M.S., Kansas State University, 2018

AN ABSTRACT OF A DISSERTATION

submitted in partial fulfillment of the requirements for the degree

DOCTOR OF PHILOSOPHY

Mike Wiegers Department of Electrical & Computer Engineering
Carl R. Ice College of Engineering

KANSAS STATE UNIVERSITY
Manhattan, Kansas

2020

Abstract

Cancer is a large and growing societal concern. According to the World Health Organization, one in five men and one in six women worldwide will develop cancer during their lifetime. However, some patients cannot be treated with established therapeutic modalities such as surgery, radiation, or chemotherapy because of challenges with performing these complex procedures for some tumors, the potential for complication due to other medical conditions, and/or dose limiting toxicities. Thermal ablation offers a low-cost, minimally invasive therapy that can be used to treat tumors, usually as an outpatient procedure. Of the possible thermal ablation energy modalities, microwave ablation (MWA) is gaining increasing clinical adoption due to its ability to rapidly heat large volumes of tissue, radiate through charred or other high impedance tissues, and avoid expensive and cumbersome ancillary equipment.

However, a significant problem limiting MWA technologies is that the growth of the thermal treatment zone cannot be precisely targeted or visualized in real time and it is therefore extremely difficult to reliably ensure the entire tumor is fully treated without also causing unintended thermal injury to adjacent critical anatomy. This limitation leaves doctors with a difficult choice of risking undertreatment and disease recurrence or risking overtreatment and damage to critical healthy anatomy that may cause pain or life-threatening complications. The fundamental technical barrier to precise targeting, and therefore to broader MWA clinical acceptance is that all currently available MWA systems can only produce a roughly spherical, ellipsoidal, or teardrop-shaped treatment zone centered on the axis near the tip of the applicator, which is not suitable for treating tumors with irregular shapes or those located near critical anatomy. This dissertation focuses on the development of a MWA applicator and methods to

achieve precise spatial control of the treatment zone during microwave ablation in diverse tissue targets.

A 14-gauge directional MWA (DMWA) applicator design is presented which would allow the physician to instead place the applicator alongside the tumor and direct heat towards the target and away from nearby sensitive tissues. DMWA may also be used with multiple applicators to "bracket" the tumor and clinical margin to enable a procedure with less chance of complications and disease recurrence, or applied on the surface of a target aiming inward in an even less-invasive non-penetrating approach. Coupled electromagnetic-bioheat transfer computational models were used for design and simulation of this DMWA applicator. Proof-of-concept applicators were evaluated in *ex vivo* liver at 60, 80, and 100 W generator settings for 3, 5 and 10 minutes (n=4 per combination) and *in vivo* tissue at 80 and 100 W generator settings for 5 or 10 minutes (n=2 or 3 per combination). Mean *ex vivo* ablation forward depth was 8–15.5 mm. No backward heating was observed at 60 W, 3–5 minutes; directivity (the ratio of forward ablation depth to backward ablation depth) was 4.7–11.0 for the other power and time combinations. *In vivo* ablation forward depth was 10.3–11.5 mm and directivity was 11.5-16.1. No visible or microscopic thermal damage to non-target tissues in direct contact with the back side of the applicator was observed.

As the resulting thermal treatment zone from MWA is comprised of regions exposed to direct electromagnetic heating as well as regions indirectly heated by thermal conduction from the temperature gradients created during thermal ablation, using excessive treatment power or duration during a DMWA procedure may still result in undesired heating of non-target sectors through the thermally conductive surrounding tissues. A method is presented to cycle microwave power on and off to allow blood perfusion in the surrounding tissue to cool the margins of the

treatment zone and improve the directivity of the DMWA procedure. Coupled electromagnetic-bioheat transfer computational models were used to evaluate equivalent energy delivery power pulsing protocols with periods of 5, 10, or 20 seconds, duty cycles of 50, 75, or 100%, and a 100 W generator power setting. A 10 second period, 70% duty cycle, 80 W generator setting power pulsing protocol in *ex vivo* liver showed a 51.7% reduction in the backward ablation depth, a 2.3% increase in the forward ablation depth, and a 115.2% increase in the directivity ratio. A 10 second period, 70% duty cycle, 100 W generator setting power pulsing protocol in *in vivo* liver showed a 40.1% reduction in the backward ablation depth, a 1.0% reduction in the forward ablation depth, and a 59.6% increase in the directivity ratio.

Once many common types of cancer metastasize, a common site to which they spread is bone. Should cancer form in the vertebral bodies, the resulting tumor growth can cause significant pain and neurological problems including paralysis. Due to the proximity of a significant amount of critical anatomy, including the spinal cord and other nerves, treating these tumors can be exceedingly challenging. DMWA may offer the ability to provide enough spatial control of the ablation zone to attempt more palliative treatments of vertebral tumors in proximity to critical nerves and the spinal cord. However, there is limited published literature describing the interactions of microwave energy in bone tissues in detail; of specific importance is the degree of microwave absorption/transmission in bone tissue relative to tissues types that would comprise metastatic disease and how that may affect the resultant size and shape of the resultant treatment zone. Presented are three-dimensional simulations of spinal DMWA treatment zones based on coupled electromagnetic-bioheat transfer computational models with tissue domains that mimic the anatomical dimensions and the biophysical properties of each different type of tissue, including cortical bone, cancellous bone, spinal cord, cartilage, and

metastatic and primary tumor. DMWA experimental ablations at 80 or 120 W generator settings for 3.5 or 5 minutes with two fiber optic temperature sensors in *ex vivo* vertebrae showed a temperature rise of 33.5 – 63.2 °C in the vertebral body 9.5 mm from the DMWA applicator (T1) and a temperature rise of 10.8 – 32.3 °C in the spinal canal 2.5 mm from the backside of the applicator (T2). A computational model with static bone tissue biophysical properties was able to predict the temperature change in the forward direction within 3 – 7% and in the backward direction within 11 – 37% of the experimental observation. This computational model was further modified to include tissue-specific perfusion values and demonstrated two DMWA applicators operated at 80 W generator setting for 5 minutes could heat the entirety of a 2 cm metastatic tumor in the vertebral body to ablative temperature (55 °C) without exceeding 45 °C in the spinal canal.

Applicators and methods to achieve precise spatial control of the treatment zone during microwave ablation

by

Austin Pfannenstiel

B.S., Kansas State University, 2009
MBA, Kansas State University, 2017
M.S., Kansas State University, 2018

A DISSERTATION

submitted in partial fulfillment of the requirements for the degree

DOCTOR OF PHILOSOPHY

Mike Wiegers Department of Electrical & Computer Engineering
Carl R. Ice College of Engineering

KANSAS STATE UNIVERSITY
Manhattan, Kansas

2020

Approved by:

Co-Major Professor
Dr. Don Gruenbacher

Approved by:

Co-Major Professor
Dr. Punit Prakash

Copyright

Abstract

Cancer is a large and growing societal concern. According to the World Health Organization, one in five men and one in six women worldwide will develop cancer during their lifetime. However, some patients cannot be treated with established therapeutic modalities such as surgery, radiation, or chemotherapy because of challenges with performing these complex procedures for some tumors, the potential for complication due to other medical conditions, and/or dose limiting toxicities. Thermal ablation offers a low-cost, minimally invasive therapy that can be used to treat tumors, usually as an outpatient procedure. Of the possible thermal ablation energy modalities, microwave ablation (MWA) is gaining increasing clinical adoption due to its ability to rapidly heat large volumes of tissue, radiate through charred or other high impedance tissues, and avoid expensive and cumbersome ancillary equipment.

However, a significant problem limiting MWA technologies is that the growth of the thermal treatment zone cannot be precisely targeted or visualized in real time and it is therefore extremely difficult to reliably ensure the entire tumor is fully treated without also causing unintended thermal injury to adjacent critical anatomy. This limitation leaves doctors with a difficult choice of risking undertreatment and disease recurrence or risking overtreatment and damage to critical healthy anatomy that may cause pain or life-threatening complications. The fundamental technical barrier to precise targeting, and therefore to broader MWA clinical acceptance is that all currently available MWA systems can only produce a roughly spherical, ellipsoidal, or teardrop-shaped treatment zone centered on the axis near the tip of the applicator, which is not suitable for treating tumors with irregular shapes or those located near critical anatomy. This dissertation focuses on the development of a MWA applicator and methods to

achieve precise spatial control of the treatment zone during microwave ablation in diverse tissue targets.

A 14-gauge directional MWA (DMWA) applicator design is presented which would allow the physician to instead place the applicator alongside the tumor and direct heat towards the target and away from nearby sensitive tissues. DMWA may also be used with multiple applicators to "bracket" the tumor and clinical margin to enable a procedure with less chance of complications and disease recurrence, or applied on the surface of a target aiming inward in an even less-invasive non-penetrating approach. Coupled electromagnetic-bioheat transfer computational models were used for design and simulation of this DMWA applicator. Proof-of-concept applicators were evaluated in *ex vivo* liver at 60, 80, and 100 W generator settings for 3, 5 and 10 minutes (n=4 per combination) and *in vivo* tissue at 80 and 100 W generator settings for 5 or 10 minutes (n=2 or 3 per combination). Mean *ex vivo* ablation forward depth was 8–15.5 mm. No backward heating was observed at 60 W, 3–5 minutes; directivity (the ratio of forward ablation depth to backward ablation depth) was 4.7–11.0 for the other power and time combinations. *In vivo* ablation forward depth was 10.3–11.5 mm and directivity was 11.5-16.1. No visible or microscopic thermal damage to non-target tissues in direct contact with the back side of the applicator was observed.

As the resulting thermal treatment zone from MWA is comprised of regions exposed to direct electromagnetic heating as well as regions indirectly heated by thermal conduction from the temperature gradients created during thermal ablation, using excessive treatment power or duration during a DMWA procedure may still result in undesired heating of non-target sectors through the thermally conductive surrounding tissues. A method is presented to cycle microwave power on and off to allow blood perfusion in the surrounding tissue to cool the margins of the

treatment zone and improve the directivity of the DMWA procedure. Coupled electromagnetic-bioheat transfer computational models were used to evaluate equivalent energy delivery power pulsing protocols with periods of 5, 10, or 20 seconds, duty cycles of 50, 75, or 100%, and a 100 W generator power setting. A 10 second period, 70% duty cycle, 80 W generator setting power pulsing protocol in *ex vivo* liver showed a 51.7% reduction in the backward ablation depth, a 2.3% increase in the forward ablation depth, and a 115.2% increase in the directivity ratio. A 10 second period, 70% duty cycle, 100 W generator setting power pulsing protocol in *in vivo* liver showed a 40.1% reduction in the backward ablation depth, a 1.0% reduction in the forward ablation depth, and a 59.6% increase in the directivity ratio.

Once many common types of cancer metastasize, a common site to which they spread is bone. Should cancer form in the vertebral bodies, the resulting tumor growth can cause significant pain and neurological problems including paralysis. Due to the proximity of a significant amount of critical anatomy, including the spinal cord and other nerves, treating these tumors can be exceedingly challenging. DMWA may offer the ability to provide enough spatial control of the ablation zone to attempt more palliative treatments of vertebral tumors in proximity to critical nerves and the spinal cord. However, there is limited published literature describing the interactions of microwave energy in bone tissues in detail; of specific importance is the degree of microwave absorption/transmission in bone tissue relative to tissues types that would comprise metastatic disease and how that may affect the resultant size and shape of the resultant treatment zone. Presented are three-dimensional simulations of spinal DMWA treatment zones based on coupled electromagnetic-bioheat transfer computational models with tissue domains that mimic the anatomical dimensions and the biophysical properties of each different type of tissue, including cortical bone, cancellous bone, spinal cord, cartilage, and

metastatic and primary tumor. DMWA experimental ablations at 80 or 120 W generator settings for 3.5 or 5 minutes with two fiber optic temperature sensors in *ex vivo* vertebrae showed a temperature rise of 33.5 – 63.2 °C in the vertebral body 9.5 mm from the DMWA applicator (T1) and a temperature rise of 10.8 – 32.3 °C in the spinal canal 2.5 mm from the backside of the applicator (T2). A computational model with static bone tissue biophysical properties was able to predict the temperature change in the forward direction within 3 – 7% and in the backward direction within 11 – 37% of the experimental observation. This computational model was further modified to include tissue-specific perfusion values and demonstrated two DMWA applicators operated at 80 W generator setting for 5 minutes could heat the entirety of a 2 cm metastatic tumor in the vertebral body to ablative temperature (55 °C) without exceeding 45 °C in the spinal canal.

Table of Contents

List of Figures

List of Tables

Acknowledgements

I would like to acknowledge the students and post-doctoral researchers in Kansas State University's Biomedical Computing and Devices Lab for all their help and support with my research. I would like to especially thank Dr. Jan Sebek for his years of help with COMSOL, MATLAB, and antenna fabrication as well as his assistance with animal studies. I would also like to especially thank Dr. Hojjat Fallahi for his collaboration and help with many experiments.

I would also like to acknowledge Dr. Damian Dupuy, Dr. Jason Iannuccilli, and Dr. Francois Cornelis for their continued interest in the DMWA project and their willingness to share so much of their time over many years providing invaluable clinical insights that helped guide development of the technology described in this dissertation.

I would also like to acknowledge Dr. Warren Beard, Dr. Margaret Highland, and Dr. Chanran Ganta, as well as several of their colleagues in the College of Veterinary Medicine, for their critical help in performing animal studies and analyzing the experimental results.

I would like to thank my co-major professor, Dr. Gruenbacher, my committee members Dr. Warren Beard, Dr. William Kuhn, and Dr. Jungkwun Kim, and my Chairperson Dr. Daniel Rolles for helping me review and improve this dissertation.

I would like to especially thank my major professor Dr. Prakash for sharing so much of his time, mentorship, and experience with me over the last five years. His role in my life and education has gone far beyond academic advising and I cannot express enough thanks for the opportunities he has provided me.

Dedication

I would like to dedicate this work to my wife, Sarah. She is the perfect partner who has made incalculable personal sacrifices to lovingly support me, both while I served in the Navy and now while I indulge myself in as much education as I can.

I would also like to dedicate this work to my parents Robin and Mitchell, who taught me to always do my best and that I can accomplish anything I set my mind to. With every year that passes and accomplishment I achieve, I realize more and more how significant their constant love and encouragement has been in my life.

Chapter 1 - Introduction

1.1 The Clinical Need

According to the American Cancer Society, an estimated 42,810 new cases of primary liver cancer, 228,820 new cases of lung cancer, and 73,750 new cases of kidney cancer will be diagnosed in the United States in 2020; of those with the disease, it is estimated about 30,160 will die from liver cancer, 135,720 will die from lung cancer, and 14,830 will die from kidney cancer [2]–[4]. For liver cancer, worldwide incidence and mortality rates are considerably higher, with 841,080 cases and 781,631 deaths in 2018 [5]. Unfortunately, some patients simply cannot be treated with established treatment modalities such as surgery, ionizing radiation, or chemotherapy because they are too old or frail or have other medical conditions that prevent them from being physically able to withstand the side effects.

For other patients, their tumors may not currently be malignant, but they may cause pain or induce secondary effects such as high blood pressure or uncontrolled weight gain. Because of the high risk of complications and side effects of current treatments, patients often must rely on chronic medication (with its own set of side effects) or simply clinical observation of the tumor.

1.1 Microwave Ablation Overview

Thermal therapy is a growing medical field which utilizes a wide range of biomedical devices and systems to heat tissue for direct or indirect treatment of disease. Some thermal therapy systems are designed to moderately heat tissue (~41 - 43 °C) for a sustained duration (~30 – 60 minutes) in a process called “hyperthermia” with the typical goal of increasing blood flow to the region and locally enhancing the effects of drug delivery or ionizing radiation

treatment [6]. Other thermal therapy processes, commonly referred to as “thermal ablation,” aim to directly destroy disease by raising tissue temperatures above which irreversible damage occurs. Cell death by thermal ablation is probabilistic and depends both on the intensity of heating (i.e. the temperature achieved) and the time exposed to elevated temperatures [7]. However, at temperatures near 55 – 60 °C, cell death is almost instantaneous [8]. Several different energy modalities have been utilized for thermal therapy including high-intensity focused ultrasound, laser, thermal conduction, radiofrequency, and microwave in a range of non-invasive or minimally invasive systems [9]–[13]. There are also numerous non-oncological applications of thermal therapy such as treatment of cardiac arrhythmias, benign prostate hyperplasia, or chronic nerve pain [14]–[16].

Typically, thermal ablation is a low-cost, minimally invasive treatment which can be provided as an outpatient procedure [1]. In addition to being much less invasive and expensive than traditional treatments, it also provides a non-toxic, localized, and repeatable option. These features enable treatment for some high-risk patients who would otherwise be ineligible for surgical resection or other physically demanding therapies, such as radiation or chemotherapy, due to the risk of medical complications or severity of side effects.

Microwave ablation (MWA) is a type of thermal therapy where physicians insert needle-applicators embedded with specially designed antennas into a target tumor, typically using image computed tomography (CT) and/or ultrasound (US) image guidance, and then energize the applicator to radiate microwaves into a target tissue with sufficient energy to heat the target to lethal temperatures. Most systems in current clinical use radiate microwave power at frequencies of 915 MHz or 2.45 GHz. MWA may also be performed via open or laparoscopic surgery, or via flexible catheters under endoscopic guidance. During microwave ablation, the cellular damage

results from kinetic heating of polar molecules (such as water and proteins) that rapidly oscillate as they try to align with the applied electromagnetic waves. The goal of MWA is to heat a target area surrounding a tumor to toxic temperatures while minimizing damage to surrounding healthy tissues and the probability of medical complications. The target ablation zone typically includes a 5 – 10 mm margin on all sides of the tumor to ensure complete destruction of the known diseased tissue as well as any microscopic disease surrounding the tumor that may be undetected on diagnostic imaging (see Figure 1-1: Illustration of a microwave ablation zone encompassing a target tumor and 5 – 10 mm margin).

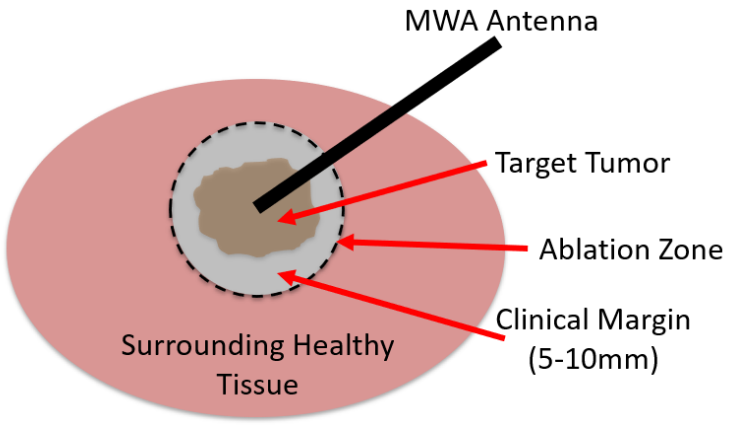

Figure 1-1: Illustration of a microwave ablation zone encompassing a target tumor and 5 – 10 mm margin of surrounding normal tissue

Of the possible thermal ablation energy modalities, MWA is quickly becoming a clinical favorite due to its ability to rapidly heat large volumes of tissue, radiate through charred or other high impedance tissues (lung & bone), and avoid expensive and cumbersome ancillary equipment such as grounding pads, gas tanks, or complex power switching systems [17].

1.2 Research approach

MWA is an established treatment modality for localized tumors; however, despite its numerous potential advantages, MWA has failed to supplant surgical resection, chemotherapy, or radiation therapy as gold standard of care. A major reason MWA is still not a primary choice for cancer treatment is there is a lack of consistency, predictability, and control of the thermal treatment zone with existing clinical applicators. There are no practical methods to monitor the growth of the thermal treatment zone in real time during MWA and heterogenous tissues and the heat sink effect of vessels and arteries can cause undesired and difficult to predict effects on the ablation size and shape. Should physicians be too conservative with the treatment dose, they risk disease recurrence; should they be too aggressive, they risk thermal injury to nearby critical anatomy. The clinical users have few tools available to them other than individual experience to balance these risks. Furthermore, the rapid and intense heating produced by most clinical MWA systems (which were specifically designed to create large volume ablations in highly perfused organs) can limit usability in small targets with sensitive and critical nearby tissues, such as in glands, the kidneys, and spine.

The goal of this dissertation is to determine if a practical MWA system employing directional MWA (DMWA) applicators can be developed to provide improved spatial control of the ablation zone and expand this minimally invasive treatment option to a wider range of patients and cases. The questions which must be answered to accomplish this goal include:

(1) What are the limitations of current clinical MWA applicators and what new potential clinical use cases can be envisioned for a directional MWA applicator?

(2) Can a directional MWA applicator be designed and fabricated which meets the necessary clinical usability requirements while still providing compelling electromagnetic performance?

(3) Will the applicator perform as designed and meet usability requirements in a clinically relevant testing environment?

(4) What system-level features or functions can support a directional MWA system that would otherwise not be considered for existing omni-directional systems?

(5) What other potential clinical sites can be treated with a MWA system which are not being treated effectively now?

1.3 Contributions

To address the aforementioned questions, this dissertation contributes to the state of the art as follows:

Contribution 1: All current clinical MWA applicators are limited to producing a cylindrically-symmetric ellipsoidal treatment zone. Most MWA applicator research and development activities have been focused on increasing the ablation volume, improving the axial ratio (more spherical), and reducing applicator diameter. MWA applicators with spatial control of the radiation pattern have been proposed in the literature, tested experimentally, and even obtained FDA-clearance, but have failed to gain commercial traction due to a number of practical limitations in the designs [18]–[21]. We have conducted extensive research in the clinical needs and requirements and developed a practical MWA applicator which provides spatial (angular and lengthwise) control of the radiation pattern. This contribution is discussed in

Chapters 3 and 4 and in the following peer-reviewed journal article, pending patent application, and funded grants from the National Science Foundation (NSF):

- [32] Pfannenstiel A, Sebek J, Fallahi H, Beard W, Ganta C, Dupuy D, Prakash P, "Directional Microwave Ablation: Experimental Evaluation of a 2.45-GHz Applicator in Ex Vivo and In Vivo Liver," Journal of Vascular and Interventional Radiology, vol. 31, no. 7, pp. 1170-1177.e2, Jul. 2020, doi: 10.1016/j.jvir.2020.01.016.
- Pfannenstiel A, Fallahi H, Prakash P. "Minimally invasive Microwave Ablation Device." PCT Patent Application No. PCT/US20/34290. Filed 5/22/2020
- NSF award #1819177 "SBIR Phase I: Directional minimally invasive microwave antenna for precise spatial control of thermal ablation" PI: Pfannenstiel A.
- NSF award #1951186 "SBIR Phase II: Microwave ablation system for creating precision directed ablation zones" PI: Pfannenstiel A.

Contribution 2: During the early development of a directional MWA applicator, the expected clinical use focused on liver tumors near critical anatomy that are challenging to treatment with existing MWA applicators. However, this is a relatively niche potential market. As development of the directional MWA applicator evolved, many more clinical techniques were envisioned which could be enabled by this new technology. Chapter 2 provides an in-depth review describing the status and limitations of the state-of-the-art clinical MWA systems and provides clinical users with an introduction of how directional MWA can be applied clinically in the future. This contribution was also supported through participation in a National Science Foundation (NSF) Innovation Corps (I-Corps) grant:

- NSF award #1711833 “I-Corps: Directional microwave antenna for precise thermal tissue ablation” PI: Prakash P.
- Pfannenstiel A, Iannuccilli J, Cornelis F, Dupuy D, Prakash P, “Directional Microwave Ablation: A Review of New Techniques and Potential Clinical Applications,” In preparation for submission

Contribution 3: Upon development (Chapter 3) and experimental evaluation (Chapter 4) of a novel DMWA applicator, it became evident that despite attempts to shape the electromagnetic radiation pattern, the ultimate directivity ratio of any DMWA applicator may be limited by heat transfer from the forward direction to the backward direction through the thermally conductive surrounding tissue. Power pulsing has been previously explored, with little success, as an option to develop larger or more spherical thermal ablation zones with omni-directional applicators [22] but had not been investigated as an option to improve the directivity of DMWA applicators. Briefly, the hypothesis tested was that periodically cycling MW power off would allow the effect of blood perfusion to cool the ablation margins, reducing backward heating, while MW radiation would penetrate further though desiccated tissue in the forward direction each cycle, improving overall directivity. Chapter 5 describes MW power pulsing’s ability to impact the forward ablation depth, backward ablation depth, and resultant ablation zone directivity.

- Pfannenstiel A, Beard W, Highland M, Iannuccilli J, Dupuy D, Prakash P, “Directional Microwave Ablation: The Effect of Applied Power Pulsing on Directivity Ratio,” In preparation for submission

Contribution 4: Although radiofrequency ablation (RFA) and cryoablation are currently used clinically for the ablation of metastatic tumors within bone sites such as the vertebral bodies [23] (but each with their own limitations in this application), and RFA is in use to treat osteoid osteoma [24], MWA in bone targets has not been thoroughly discussed in the literature from a biophysical perspective. This is likely because the use of current omni-directional, large-volume MWA devices would not be practical for treating relatively small tumors in the bone. As a result, despite having a good understanding of how MWA affects soft tissue, MWA's effects in bone are not well understood. Due to bone's low electrical conductivity, it could be expected microwaves would be absorbed less in bone and propagate further – potentially causing thermal injury to non-target critical anatomy further from a MWA applicator than anticipated. Conversely, less MW absorption in bone may cause less intense heating, reducing the risk to non-target anatomy. Chapter 6 describes a computational modeling and simulation approach combined with *ex vivo* experimentation to describe the effects of MWA in bone. This data was used to develop an anatomically representative computational model that shows DMWA has potential to safely treat various types of tumors within the vertebral body near the spinal cord.

- Pfannenstiel A, Highland M, Beard W, Cornelis F, Prakash P, "Directional Microwave Ablation: Computational Modeling and Experimental Evaluation in *Ex Vivo* Bone," In preparation for submission

1.4 Dissertation outline

The rest of this dissertation is organized as follows. Chapter 2 presents a review of current clinical MWA systems combined with new treatment techniques and approaches enabled by the advent of a directional MWA applicator. Development of a directional microwave

ablation applicator is discussed in Chapter 3. Experimental testing and characterization of the applicator developed in Chapter 3 is described in Chapter 4. An investigation into the effect on directionality when pulsing power is applied to the directional MWA is described in Chapter 5. Chapter 6 provides computational modeling and simulation and ex vivo experimentation of MWA in bone. Finally, Chapter 7 provides a discussion of future work and concluding remarks.

Chapter 2 - Background

2.1 Introduction

Thermal ablation has become a well-established treatment alternative for localized cancers in patients who are otherwise not good candidates for surgery or other physically demanding treatments such as radiation therapy, or chemotherapy [25], [26]. Thermal ablation is also gaining acceptance as a low cost, minimally invasive method for palliative care [27], [28]. Among thermal ablation energy modalities, microwave ablation (MWA) is becoming an increasingly important and popular treatment for localized tumors in many tissues [17]. Driving this growth are MWA's inherent advantages over other energy modalities including the ability to rapidly heat large volumes of tissue, achieve high peak temperatures which are better able to overcome the effects of local heat sinks, radiate through high impedance tissues, and operate without the need for ancillary components (such as ground pads) [17], [29].

However, despite its advantages, MWA has failed to supplant surgical resection, chemotherapy, or radiation therapy as a standard of care. A major reason MWA is still not the primary choice for cancer treatment is a lack of consistency, predictability, and control of the thermal treatment zone with existing clinical applicators. There are no practical methods to monitor the growth of the thermal treatment zone in real time during MWA and heterogenous tissues and the heat sink effect of vessels and arteries can cause undesired and difficult to predict impacts to the resulting ablation size and shape. Should physicians be too conservative with the treatment dose, they risk disease recurrence; should they be too aggressive, they risk thermal injury to nearby critical anatomy. Clinical users have few tools available to them other than individual experience to balance these risks. Furthermore, the rapid and intense heating and

relatively large ablation zones produced by most clinical MWA systems (which were designed for large-volume ablation in highly perfused organs) can limit usability in small targets with sensitive and critical nearby tissues, such as in glands, the kidneys, and spine.

2.2 Current Clinical MWA applicators

MWA systems currently in clinical use almost exclusively consist of a needle-like applicator which is inserted centrally into a target tumor, typically using CT or US guidance, and with a percutaneous or open surgical approach [30]. The applicator outer shaft is typically made of steel or other similarly rigid material such as fiberglass or PEEK to provide the stiffness necessary for accurate placement in the target. Contained within the outer shaft is a small diameter coaxial cable which carries the microwave power from the applicator handle/hub to the distal end of the applicator where the microwave antenna is located (a larger diameter, lower-loss transmission cable connects the applicator hub/handle to the microwave generator). The microwave antenna is typically a linear antenna which may be as simple as a segment of the inner conductor of the coaxial transmission line stripped of its outer conductor. Additional elements may be soldered or otherwise connected to the inner conductor or additional modifications made to the outer conductor to improve the electrical performance of the antenna. In some cases, a metallic trocar point with the appropriate dimensions can be electrically connected to the coaxial inner conductor to act as the microwave antenna.

Linear antennas are often considered “omni-directional” in the sense that they radiate uniformly across the angular expanse around the axis of the antenna. However, they do not radiate out of the end-fires (the ideal radiation pattern resembles a toroid or donut), and as a result, the ablation zones produced by clinical MWA systems typically do not extend appreciably

beyond the distal tip of the applicator. Furthermore, because the linear antennas used in MWA systems are comprised of the coaxial transmission line itself, with the outer conductor acting as a non-optimal second leg or ground plane, they are unbalanced, with a radiation pattern that extends proximally along the shaft of the applicator. Some current MWA applicators include additional structures, such as chokes or sleeves, to help constrain the length of the radiation pattern, though many current applicators still produce thermal ablation zones with a “tail” or a “teardrop” or “comet” shape when sliced across the longitudinal plane. Finally, the physical dimensions of the MW antenna in the applicator must be well matched to the electrical properties of the surrounding tissue (which vary among tissue and tumor types and also change dynamically during an ablation procedure), otherwise a portion of the applied power to be reflected back along the transmission cable rather than being transmitted into the tissue, potentially reducing the diameter of tissue ablated. When in clinical use, this would be observed as a high “reflected power” on the generator display and could also indicate applicator placement in a void or a defect in a transmission cable or connector.

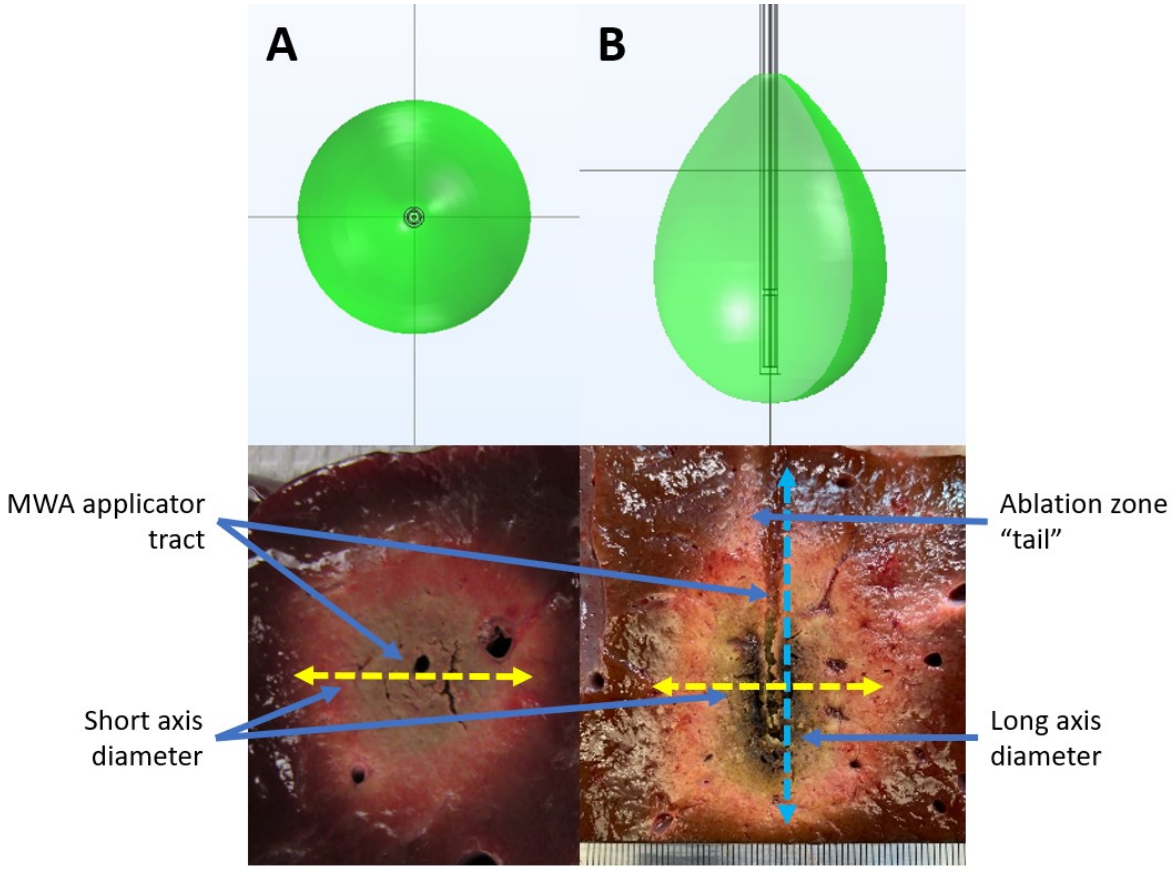

Figure 2-1: Omni-directional microwave ablation zone cross-sectional slice (A) and longitudinal slice (B). The top row is the simulated 55 °C isothermal contour while the bottom row is from experiments in *ex vivo* liver tissues.

To deliver sufficient power to ablate tissue, the very small diameter microwave transmission lines within a MWA applicator are often operated at almost an order of magnitude higher power than they would be otherwise rated if exposed and cooled by ambient air. Therefore, almost all clinical MWA systems include an active cooling system, without which the applicator shaft may heat sufficiently to cause unintended thermal ablation of tissue along its length or the applicator may face material failure [31]. Most systems use circulating water while one uses compressed gas expansion [32]. In addition to cooling the internal transmission line, active cooling of the MWA applicator internals and shaft can cool the surrounding tissue, reducing the "tail" of ablation zone and improving its sphericity.

When water cooling is used, current MWA systems differ in whether the cooling water encompasses the active antenna element or terminates and returns at some point proximal to the antenna. When surrounding the antenna, water has a high relative permittivity, which acts as a dielectric load and enables the antenna to have a shorter physical length and maintain a better impedance match even as the electrical properties of the surrounding tissue change during thermal ablation. Enabling a shorter antenna length also contributes to improved sphericity of the resulting ablation zone. Directly cooling the active portion of the applicator may also reduce the chance of tissue charring and adhering to the applicator shaft that can make post-ablation applicator removal more difficult. However, water is also conductive and therefore creates internal losses as microwave power is radiated through it and absorbed. All else equal, a MWA applicator with water surrounding the antenna will produce a smaller ablation zone compared to an applicator omitting such a lossy material, though it may be more spherical.

Current MWA applicators are compared and evaluated based on three main criteria:

1. Short-axis diameter – This is the maximal width the thermal ablation zone extends measured perpendicular to the applicator shaft. This is often used to describe the maximum ablation zone size achievable by a particular applicator with a single measurement. Many clinical MWA applicators can achieve short axis diameters of approximately 4 cm in 5 -10 minutes in *ex vivo* liver tissue, which has emerged as a de facto standard environment for evaluating ablation devices [33].
2. Axial ratio – This is the ratio of the ablation zone short axis diameter (radial) to the long axis diameter (longitudinal). An ideal MWA applicator would have an axial ratio approaching unity where the ablation zone is a sphere. Spherical ablation zones afford easier treatment

planning and are more likely to preserve more surrounding healthy tissue. Some current MWA applicators are able to achieve axial ratios near 1.0 at some time and power combinations, while most exhibit axial ratios of about 0.7 to 0.9 [34].

3. Shaft diameter – The smaller the diameter of the applicator, the less invasive the treatment. While 14-gauge (0.083" / 2.1 mm diameter) is widely considered the maximum desirable for minimally invasive use, clinical MWA applicators range from 13-gauge (0.095" / 2.4 mm diameter) to 17-gauge (0.058" / 1.5 mm diameter) [25]. Applicator diameter is also loosely correlated to stiffness and rigidity, a quality necessary for accurate applicator placement.

Furthermore, it is desirable to construct the applicator from materials that are echogenic, so the applicators can be readily visualized on ultrasound imaging, as well as have minimal streak artifact on CT imaging [35].

2.3 Clinical Shortcomings of current MWA applicators

The fundamental clinical limitation to broader MWA clinical use is that all currently available MWA systems can only produce a roughly spherical, ellipsoidal, or teardrop-shaped treatment zone centered on the axis near the tip of the applicator. This is not universally suitable for treating tumors with irregular shapes or those located near critical anatomy [25], [33].

To work around this limitation with current applicators, physicians must employ additional thermoprotective techniques, such as fluid or gas dissection, endoluminal heating/cooling, or balloon insertion to attempt MWA treatments near critical structures such as the stomach, colon, diaphragm, gall bladder, etc., increasing the difficulty of the procedure [36], [37]. Failure of these techniques, which can occur unpredictably as fluid, gas, or balloons tend to

move within the abdominal cavity, has the potential for serious and painful complications such as hemorrhage, pneumothorax, perforation of the gastrointestinal viscus, and biliary stricture, requiring additional emergent and extended medical care procedures [36], [37]. The presence of nearby heat sinks such as blood vessels or heterogenous tissue boundary layers can also skew the size and shape of omni-directional ablation zones in unpredictable ways. Ultimately, because the extents of the thermal treatment zone are often not known in real time, there is reduced certainty in the treatment outcome. As a result, and despite its potential, MWA is much less frequently employed for tumors in smaller organs with proximity to sensitive anatomy, such as the kidneys, due to the risk of complications from unintended overheating [36].

Finally, all existing MWA devices are configured to deliver maximum power and achieve as large of an ablation zone as possible. This complicates treatment of small targets surrounded by sensitive critical anatomy. Existing MWA systems are seldom considered for treating very small tumors in sensitive glands such as the adrenal or thyroid.

2.3 Directional MWA (DMWA) Applicators

Though there are no existing DMWA applicators in clinical use currently, a recent publication has highlighted the development and shown proof-of-concept for a new DMWA applicator [38]. This applicator is similar in form as existing clinical omni-directional MWA applicators but includes additional internal elements to shape the radiation pattern, limiting to approximately half the angular expanse. As illustrated in Figure 2-2, the resultant ablation zone is approximately a hemisphere.

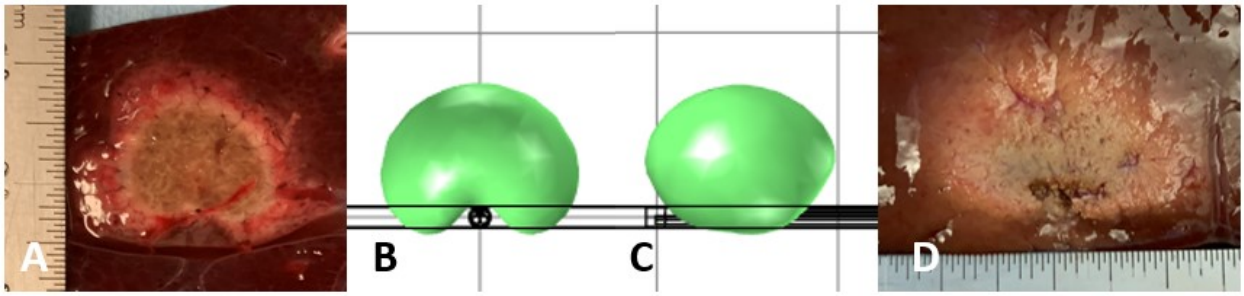

Figure 2-2: DMWA cross-sectional slice in *in vivo* liver (A) beside simulated 55 °C isothermal contour (B). DMWA longitudinal slice simulated 55 °C isothermal contour (C) beside *ex vivo* liver (D).

DMWA applicators can be evaluated based on shaft diameter, like existing MWA applicators, however, short-axis diameter and axial ratio metrics do not meaningfully describe the ablation zone shape. Additional criteria for comparison and evaluation of DMWA applicators include:

1. Forward ablation depth (d_f) – The maximal distance the ablation zone extends in the desired target (forward) direction measured perpendicular to the applicator. This measurement can be made from a cross section or longitudinal slice. For DMWA, care must be taken to slice experimental specimens and take measurements in the plane of maximal heating. Any slice not along the maximal plane will result in inaccurately small measurements – this contrasts to omni-directional ablation measurements where any longitudinal slice that follows the applicator tract will show equivalent ablation dimensions.
2. Backward ablation depth (d_b) – The maximal distance the ablation zone extends in the non-target (backward) direction measured perpendicular to the applicator. This measurement should be made from a cross sectional slice only to observe if the ablation zone extends further backward on either side of the applicator tract.

3. Directivity ratio (d_f/d_b)– The ratio of the forward ablation depth divided by the backward ablation depth. An ideal DMWA applicator would have an infinite directivity ratio.
4. Ablation width (w) – The maximum distance the ablation zone extends laterally. This measurement must be taken in the cross-sectional slice.
5. Ablation height (h) – The maximum distance the ablation zone extends from its distal end to its proximal end. This measurement must be taken in the longitudinal slice.
6. Shaft diameter – Similar to omni-directional applicators, diameter influences the invasiveness of the device which much be balanced with its rigidity and stiffness which influences usability. The importance of minimizing applicator diameter may change if a DMWA applicator is used during open surgery or laparoscopic procedures.

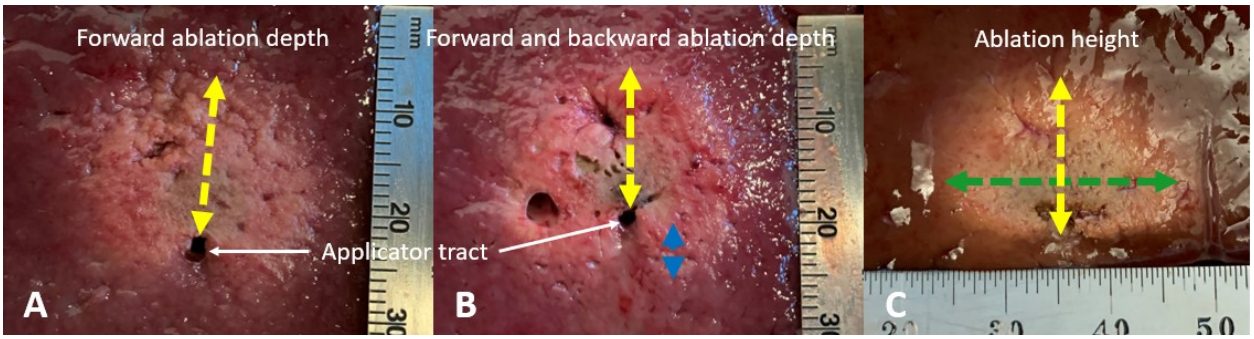

Figure 2-3: DMWA cross-sectional slice showing the forward ablation depth measurement (yellow dashed line) for an ideal directional ablation zone with zero backward heating (infinite directivity ratio) (A). DMWA cross-sectional slice showing the forward ablation depth (yellow dashed line) and backward ablation depth (blue dashed line) measurements (B). DMWA longitudinal slice showing forward ablation depth (yellow dashed line) and ablation height (green dashed line) measurements (C).

2.4 New DMWA-enabled Clinical techniques

The introduction of a DMWA applicator potentially offers many advantages and opportunities for new treatment techniques and approaches compared to existing omni-

directional applicators. As summarized in Figure 2-4, clinical value is offered by the ability to now treat a much wider variety of tumor shapes and tumors in areas where there is much more fragile healthy tissue.

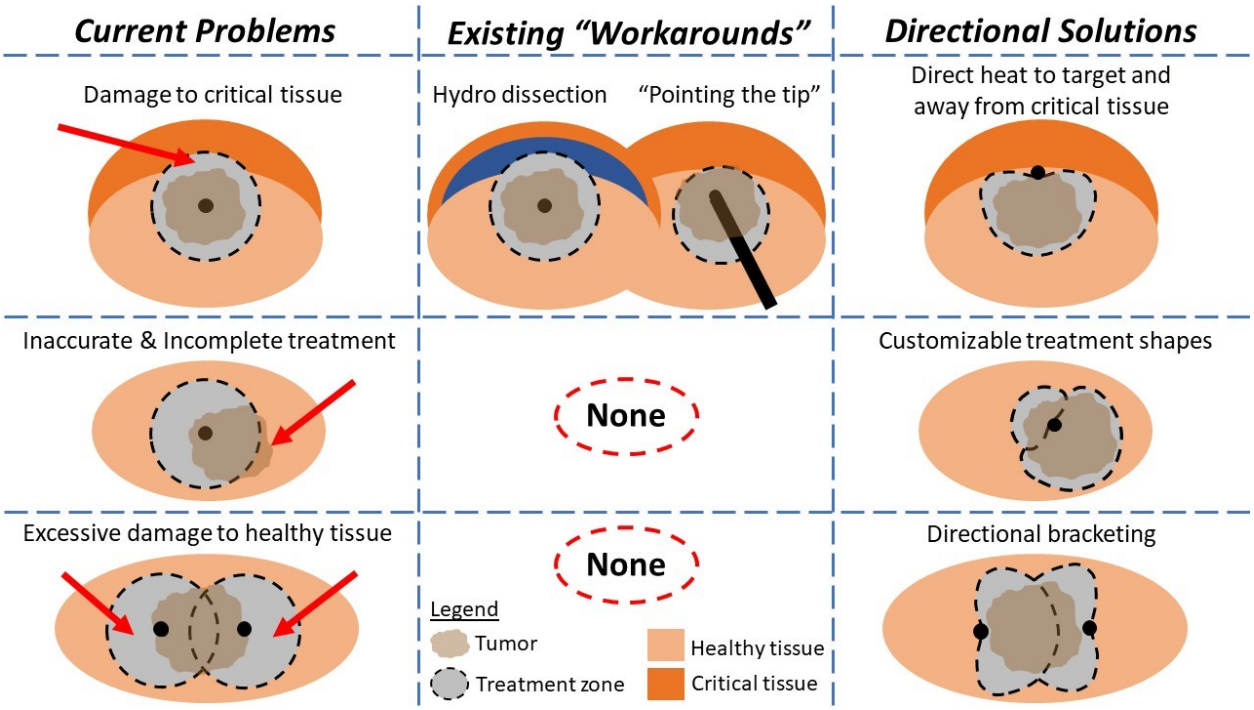

Figure 2-4: Illustrations of clinical challenges using current MWA systems with symmetric ablation patterns, "Workarounds" to attempt to address existing problems, and potential solutions provided by directional MWA.

2.4.1 "Outside-in" ablation

Rather than the "inside-out" treatment approach used by current omni-directional applicators, DMWA enables an "outside-in" approach which allows the physician to place the applicator alongside the tumor and direct energy toward the target and away from sensitive tissues. DMWA may enhance the effectiveness or reduce the dependence on thermoprotective techniques and may enable MWA treatment of tumors in more challenging locations. An "outside-in" approach may facilitate technically easier treatment of small lesions that are

displaced within the surrounding tissue when an applicator is inserted nearby (such as small lung nodules that may move within the elastic lung tissue, making them difficult to pierce) while preserving more surrounding healthy tissue than omni-directional applicators. An "outside-in" method potentially offers assurance of a treatment margin between the applicator and tumor. Finally, the ability to treat the tumor without penetrating through it may also reduce the risk of tumor seeding that could cause recurrence or new disease to develop [39].

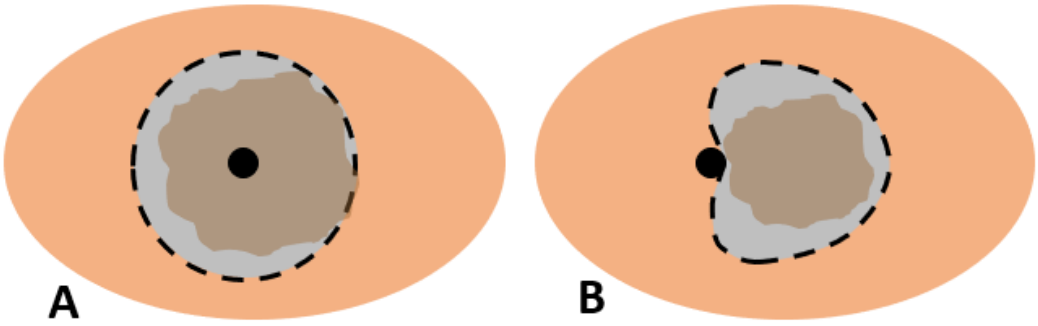

Figure 2-5: Illustration of conventional MWA approach where the applicator is centrally positioned within the target heating from the "inside-out" (A) compared to DMWA which enables heating via an "outside-in" approach with an applicator positioned adjacent to the target (B).

2.4.2 "Directional bracketing"

Multiple DMWA applicators could be used to "bracket" relatively larger tumors, treating them with a composite ablation zone, and providing assurance of clinical margin between the applicators and tumor. Bracketing is already a common technique to treat larger tumors with multiple omni-directional applicators [40], but directional bracketing may maximally preserve healthy surrounding tissue.

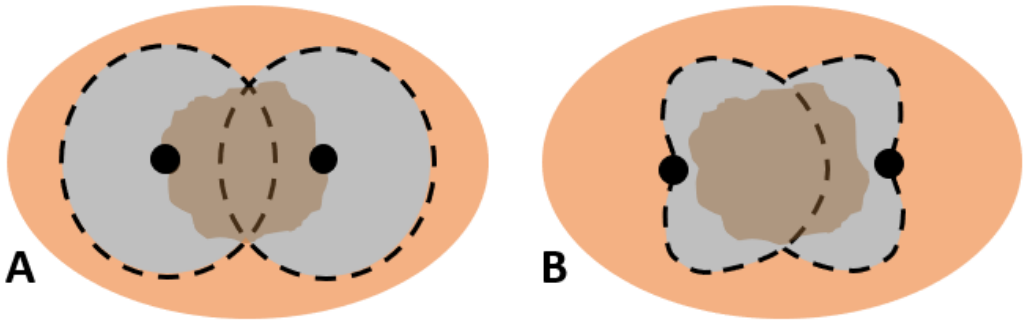

Figure 2-6: Illustration of conventional MWA two-applicator bracketing ablation approach (A) compared to "directional bracketing" ablation approach (B).

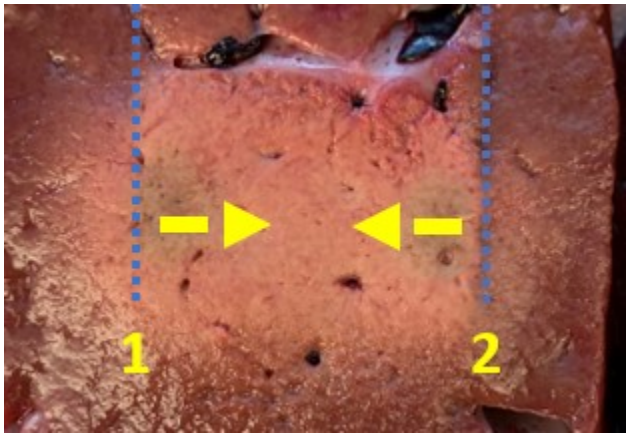

Figure 2-7: Image of two-DMWA applicator "directional bracketing" ablation approach in *ex vivo* liver. The section shown is a longitudinal slice parallel to the insertion axis of both DMWA applicators.

2.4.3 "Surface ablation"

Because DMWA applicators radiate in a specific direction, they may be placed on the surface of a target and could still heat it to ablative temperatures without penetrating it directly. While this may seem like only a subtle difference from the "outside-in" method of treating tumors within an organ, a non-penetrating approach may enable minimally invasive treatment for an entirely new range of difficult to treat conditions. For example, small organs or glands may be very difficult to pierce as they may be displaced rather than punctured by the applicator. Furthermore, the penetration of some glands, such as the adrenal gland, may severely damage

them and create dangerous complications. Positioning a directional MWA applicator alongside a gland, organ, or nerve could enable treatment of a shallow target zone within that structure without damaging the surrounding anatomy.

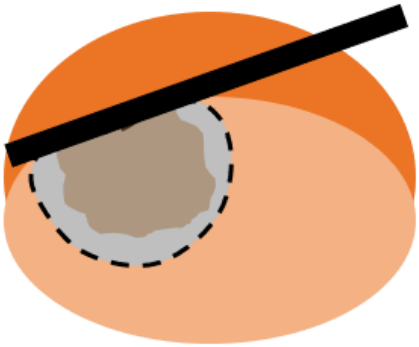

Figure 2-8: Illustration of DMWA "surface ablation" approach for targets near the organ surface (e.g subcapsular tumors)

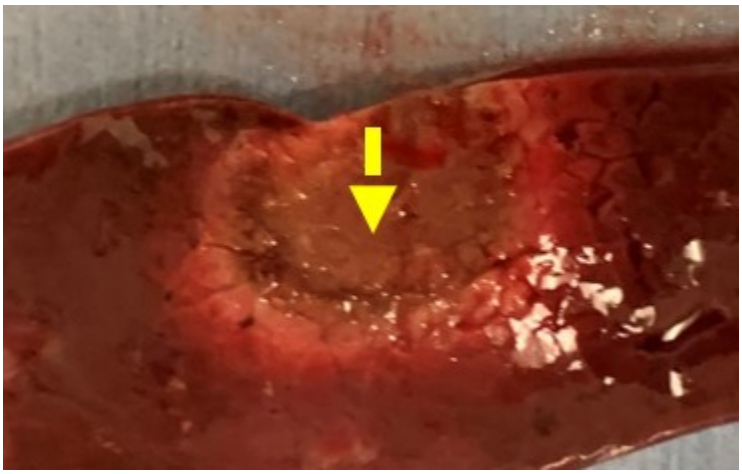

Figure 2-9: Image of "surface ablation" in porcine *in* vivo liver.

2.4.4 "Sector-sweep ablation"

If a DMWA applicator was inserted centrally into a tumor, it could be rotated to target multiple directions and sweep out a symmetric ablation zone similar in size and shape as capable of existing clinical applicators. Furthermore, directionality would enable targeted retreatment of

any regions of the tumor that may show viability on post-procedure imaging. Using a "sector-sweep" approach while varying generator power and time settings for treating different sectors of the tumor could create targeted, asymmetric ablation zones or compensate for inaccurate (off-center) placement of the applicator. However, this type of technique would likely require advances in imaging techniques to identify treatment extents and aid in determining when and by how much to rotate the applicator and which thermal dose should be used for subsequent sector re-treatment. It would be important to conduct imaging of the treatment zone extent with the DMWA applicator *in situ*.

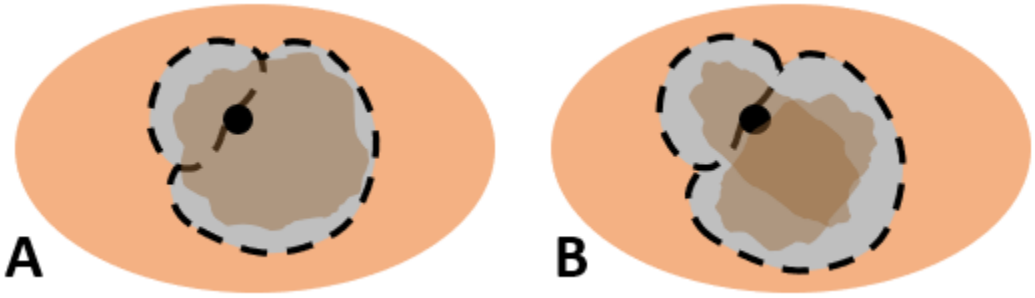

Figure 2-10: Illustration of "sector-sweep" ablation to compensate for off-center applicator placement.

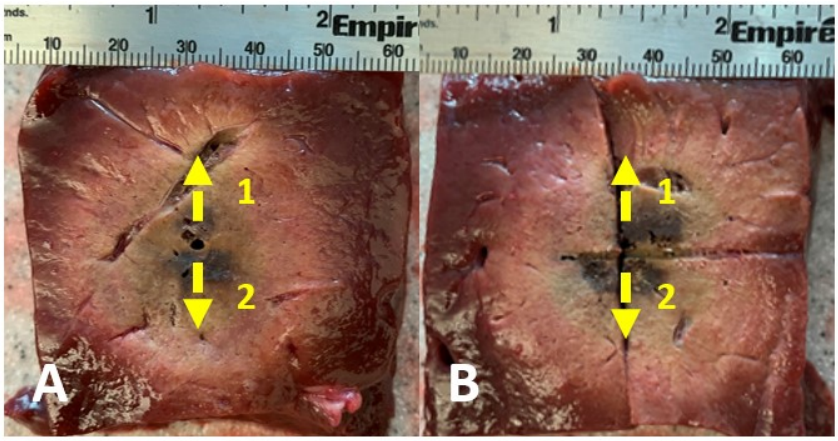

Figure 2-11: Images of "sector-sweep" DMWA used to create large (approximately 4 cm) spherical ablation in *ex vivo* liver shown in the cross-sectional (A) and longitudinal (B) planes (150 W generator setting for 10 min per direction).

2.4.5 "Offset ablation"

While the key benefit of DMWA is often from a controllable minimum or absence of any backward heating, enabling better spatial control of the thermal ablation zone. However, in some situations there may still be a need for some backward heating such as in a case when a MWA applicator could be inserted into a tumor, but not perfectly centrally due to interfering anatomy. In this case a higher power or longer duration DMWA procedure could be utilized to allow thermal conduction to cause ablation of some tissue in the backward direction, resulting in an approximately spherical ablation with its center offset from the applicator tract. The "offset" ablation zone could have a forward to backward depth directivity ration of approximately 2:1 compared to DMWA with reduced power or duration with directivity ratios exceeding 15.

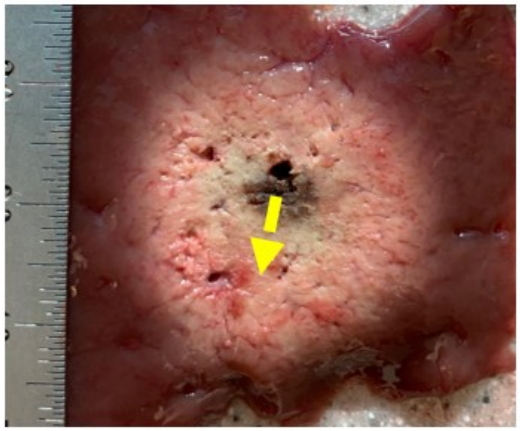

Figure 2-12: Image of "offset ablation" in *ex vivo* liver

2.5 DMWA applications in interventional oncology

2.5.1 Liver

Liver is the most common MWA clinical use site and there is substantial clinical experience and data for thermal ablation treatment of liver tumors [41], [42]. A primary driver

for the development of thermal ablation technologies to treat liver cancer is the fact that most liver cancer patients (up to ~80%) are ineligible for surgery due to poor liver function, advanced cirrhosis, co-morbid disease, or a challenging tumor location. Traditional chemotherapy and radiation therapy have historically not been effective for treating liver tumors, leaving these patients with few options beyond local interventions such as ablation and embolization. The relatively large physical size of the liver is also forgiving, often reducing the risk of thermal injury to adjacent healthy structures that normally accompanies overtreatment. Furthermore, the intense heating of MWA has the ability to overcome much of the "heat-sink" effect from highly perfused organs, such as the liver, much better than other ablation modalities [29]. Therefore, liver has been a favorable site to allow MWA to gain a clinical foothold, and the potential value has become clear despite the difficulty with precise spatial control of the treatment.

However, a meaningful minority of liver tumors (approximately 20-50%) are located near critical structures that would result in the need for further medical intervention if injured during MWA. As previously discussed, some of these critical structures such as the diaphragm, colon, or stomach, can be insulated or physically separated from the thermal ablation zone by thermoprotective techniques such as hydro or gas dissection or balloon insertion [36], [37]. However, the diffusion of fluid or gas or the movement of balloons within the abdominal cavity may limit the ultimate effectiveness of these techniques [36], [37]. Furthermore other structures, such as the gall bladder or bile ducts, cannot be insulated or separated from a nearby tumor by thermoprotective techniques and physicians must utilize the limited directionality with exiting applicators by "pointing at the vital structure" as the thermal ablation zone typically extends only a few millimeters past the distal tip of the applicator [37].

The use of a DMWA applicator may enhance the effectiveness or reduce the necessity of thermoprotective techniques or enable treatment of liver tumors near critical structures that cannot be otherwise thermally isolated. DMWA has been evaluated in *ex vivo* and *in vivo* liver [38].

2.5.2 Kidney

The kidney is a much smaller target site than liver with proximity to many more thermally sensitive critical structures such as the bowel and ureter [43]. Potential consequences of excessive thermal injury include pelvicalyceal/ureteric stricture, or bowl perforation [36]. Currently radiofrequency ablation (RFA) and cryoablation are the two most commonly used ablation techniques in the kidney [43]. This is likely because RFA heats less intensely than MWA, reducing the chance of excessive thermal injury and the resultant "oven effect" in the kidney [44], while the ice ball from cryoablation can be visualized on imaging, also reducing the chance of excessive thermal injury to non-target structures. However, similar to liver, the kidney is a highly perfused organ which restricts the ability of RFA and cryoablation to treating only small tumors [29]. However, the advent of directional MWA may provide the necessary spatial control of the thermal ablation zone to effectively treat renal tumors while maximally preserving renal function.

2.5.3 Lung

The lung is a common site to which cancer metastasizes , but only about 30% of lung cancer patients are considered surgical candidates due to co-morbidities, poor cardiopulmonary function, and age [45]. Like liver and kidney, lung is also a highly blood-perfused organ, but it is

also aerated, resulting in a very low electrical conductivity – making many types of thermal ablation challenging [46]. This low electrical conductivity reduces the rate of heating achievable by MWA, but also enables it to penetrate further [29]. However, the electrical and thermal properties of lung tumors may be more similar to those of solid tissues, suggesting MWA may have the ability to propagate further through healthy lung tissue while selectively heating tumor tissue more intensely, though more studies are needed to demonstrate this [29]. DMWA may provide the spatial control necessary to provide treatment of tumors near the heart, esophagus, or major airways.

However, with respect to lung tumor ablation, DMWA's most critical advantage may be its ability to utilize an "outside-in" treatment approach. Lung tumors that are solid or semi-solid may be displaced within the elastic lung parenchyma while targeting them with a rigid treatment applicator, making precise interstitial placement of a conventional thermal ablation applicator challenging. Conversely, placing a DMWA applicator beside a lung tumor, aiming towards it, may be technically favorable and provide better control or treatment margins. Incorporating directional MWA capabilities into flexible applicators suitable for bronchoscopic delivery of ablation may further broaden the use of this technology for treatment of pulmonary disease, although it is recognized that precise directional control of long, flexible catheter-based applicators may be technically challenging [47].

2.5.4 Bone

Similar to lung, bone is a common site of cancer metastasis. Should cancer develop in the vertebral body, pain or neurological problems may result. Possible treatments for primary bone cancer include surgery, chemotherapy, and radiation therapy, however, none of these typical

treatment options may be possible, effective, tolerable, or fast-enough acting for a very ill patient who had progressed to late stage metastatic cancer. Of thermal ablation options, RFA would have reduced heating ability in low-impedance bone tissues while cryoablation would require a prolonged wait time for thawing to allow backfill of the treatment zone with cement [48]. The use of high intensity ultrasound has also been proposed for treatment of tumors surrounded by bone, as the high acoustic absorption coefficient helps to confine the treatment zone primarily to the target, thereby protecting adjacent critical structures [49], [50]. The application of conventional omni-directional MWA in bone has not been studied in detail, with its potential use likely limited by concerns for the ability to provide sufficient spatial control of the treatment zone, especially for use near critical anatomy such as the spinal cord or other nerves. From a technical physics/engineering-based perspective, there have been few studies reporting on electromagnetic absorption and bioheat transfer dynamics in bone tissue, which has considerably different electromagnetic and thermal properties compared to soft tissue.

However, similar to treatment of lung tumors, DMWA may have significant advantages in its ability to less-intensely heat and propagate further through normal bone while more intensely heating soft tissue tumors and to also employ an “outside-in” approach to treat bone tumors which are otherwise difficult to access and penetrate directly.

2.5.5 Brain

When considering brain tumors, the need for precise spatial control of any treatment method is apparent. There has been some early development of lasers as a possible energy modality for brain tumor ablation [51]. DMWA may also offer a compelling minimally invasive treatment option for brain tumors. For use in brain, a DMWA applicator would need to be

constructed from with MRI-conditional materials to enable real-time temperature monitoring of the treatment zone with established MRI thermometry approaches [52]. Experimental MRI-compatible DMWA applicator have been successfully designed and experimentally evaluated previously in the high-field MRI environment [53].

2.6 DMWA applications outside interventional oncology

2.6.1 Functional glandular tumors

Benign, but functional tumors in glands, such as the adrenal or thyroid, can result in unregulated hormone production that leads to a variety of side effects including hypertension, irregular or rapid heartbeat, and weight loss, among many others [54]. Current treatment of these conditions includes surgical resection (only feasible for unilateral disease), which many times still requires chronic medication, or simply management of the symptoms with chronic medication. Current thermal ablation technologies optimized for large volume ablation in vascular organs do not provide the necessary spatial control to create localized ablation of small (~1cm^3) targets in glands such as the adrenal or thyroid which are not only delicate and susceptible to mechanical and thermal damage themselves, but are also in close proximity to many critical structures [54]. Thermal damage to the adrenal medulla during ablation may lead to hypertensive crisis due to catecholamine release [55]. However, DMWA has demonstrated an ability to provide precise spatial control while creating approximately 1 cm^3 lesions in an *in vivo* liver model [38] and has been used in an *in vivo* study to ablate porcine adrenal glands using a "surface ablation" technique to minimize collateral damage to the adjacent normal adrenal cortex [54].

2.6.2 Nerves transmitting chronic pain signals

Radiofrequency neurotomy is a procedure to ablate specific nerves to block their ability to transmit the signals that are the cause of chronic pain in the back, neck, or joints for up to 6 to 12 months [56]. The nerve targets are typically very small (a few millimeters across) and are in close proximity to many other critical structures, so similarly to glandular ablation, most thermal ablation systems designed for large volume ablation are poorly suited for these applications. Specially designed DMWA applicators may be able to provide more spatial control to access more potential nerve target sites than existing RF neurotomy systems.

2.6.3 Uterine Fibroids

Uterine fibroids can be a cause of heavy menstrual bleeding and pelvic pain or pressure among many other symptoms [57]. Various surgical treatments options are available with various risks of complications and many resulting in the inability to have children post-surgery [58]. While RFA ablation system have been demonstrated for the treatment of uterine fibroids [59], specially designed DMWA systems may have a better ability to treat a wider range of fibroids which are dense and difficult to penetrate by utilizing an “outside-in” treatment approach.

2.6.4 Benign Prostate hyperplasia

Benign prostate hyperplasia (BPH) is a common condition as men age resulting in a range of uncomfortable urinary symptoms [60]. However, the prostate is a very challenging target site surrounded by very sensitive anatomy including the ureter, nerves, and the rectum. Transurethral microwave thermotherapy (TUMT) is procedure which may serve as a minimally

invasive treatment option for BPH [60]. Specially designed DMWA systems may offer improved ability to debulk an enlarge prostate for symptom relief while minimizing the risk of thermal injury to surrounding anatomy.

2.6.5 Esophageal Varices

Esophageal varices are enlarged veins in the esophagus that occur when blood flow to the liver is blocked by a clot or scar tissue that can develop in patients with liver disease; they may leak blood and if they rupture may cause life-threatening bleeding [61]. Experimental results from a developmental system have shown proof-of-concept for employing DMWA to ablate esophageal varices [62].

2.7 DMWA current limitations

Currently, no DMWA applicators are available clinically and the experimental results from DMWA applicators under development were with applied time and power combinations selected to minimize backward heating, which resulted in overall ablation volumes substantially smaller than existing omni-directional devices [38]. Though further study of the ability to create larger “directional-bracketing” or “sector-sweep” composite ablation zones is necessary, omni-directional MWA applicators may still be best suited for delivering large volume ablation zones in short times where precise spatial control is not a significant concern. Shorter treatment times are valuable in the clinical setting so imaging scanners, and other critical resources, can be freed up for other procedures, and reduce cost. Additional animal studies will be necessary to fully characterize the directional applicators *in vivo* performance across a broader range of power levels and tissue types.

2.8 Conclusion

DMWA's ability to provide precise spatial control of the thermal ablation zone may be critical in the treatment of many challenging cases, and for expanding thermal ablation as a minimally invasive treatment option outside of interventional oncology. With further technical development and translation of this technology, it is anticipated that DMWA technology may be particularly well suited for non-penetrative treatment of small-targets – structures which are not currently well suited for treatment by existing MWA systems. Further development and evaluation of this technology in the clinical setting is warranted to determine the potential benefit of this technology.

Chapter 3 - Design of a DMWA applicator

3.1 Introduction

While insights into construction methods and evaluation criteria can be gained from proof-of-principle DMWA applicator designs proposed and tested experimentally in the literature, none these designs are currently available for clinical use [18]–[21], [38]. Thus, there remains a need to design, develop, and translate DMWA technology capable of meeting existing clinical needs. The design of a DMWA applicator still begins with many of the same design principles as omni-directional applicators but includes several more considerations to establish directivity. As antenna directivity is a function of size relative to wavelength, physically larger antenna assemblies provide enhanced directivity. However, there is an equally important need to minimize the outside diameter of a DMWA applicator to reduce its invasiveness. Furthermore, there are a number of additional clinical usability requirements to consider when optimizing the design for a DMWA applicator. This chapter reports on our experience designing a microwave ablation system incorporating DMWA applicators with technical capabilities suitable for use in the clinical setting.

3.2 Traditional MWA Applicator Design Priorities

The objectives of traditional MWA applicator antenna design are primarily twofold. First, is maximizing power transfer to the target tissue. This is accomplished by carefully matching the antenna's impedance (which is determined by the antenna dimensions and the electrical properties of materials surrounding the applicator, i.e., the combination of tumor, healthy tissue, cooling water, insulating catheter, etc.) to that of the feeding transmission line. A well-matched

antenna will enable the transfer of a large fraction of the incident power to the tissue with less power being reflected back to the source, allowing for shorter treatment times, lower applied powers, and less unwanted heating of the applicator or system cabling from attenuation (which may also alter the shape of the thermal ablation zone). A common way to evaluate antenna power transfer is through measuring the antenna's reflection coefficient at the input port, S_{11}:

Equation 3-1:

$$S_{11} = \frac{V_1^-}{V_1^+} = \frac{Reflected\ Voltage\ Wave}{Incident\ Voltage\ Wave}$$

In practice, antenna designs with a S_{11} of at least -10 dB or better (more negative) are desired for MWA applicators so 90% or more of the incident power is transferred to the target. Practically, the antenna length is one of the most sensitive parameters affecting S_{11}. However, optimizing antenna length to minimize S_{11} also relies on a detailed understanding of the electrical properties of the environment surrounding the applicator. Though the values of electrical properties at MWA frequencies and temperatures have been extensively studied in liver [63], they are less well known in most other tissue [64]. Furthermore, the electrical properties of the target tissue that affect impedance matching can vary between patients and tumor biology, and during the course of an ablation, the permittivity and conductivity of the surround tissue typically drops as the tissue is desiccated and dehydrated by heat, causing the impedance match to reduce over time. One method to establish a more stable reflection coefficient for MWA applicators which may be used in a wide range of tissues with varying electrical properties is providing dielectric loading of the antenna. This can be accomplished by encapsulating the antenna in a relatively high permittivity material such as water. Further, since the dielectric properties of

water are temperature dependent, circulating the water through the applicator ensures that water at a relatively stable temperature is delivered to the tip of the applicator, thus providing a stable electric load.

A second, easier to quantify but larger in magnitude, loss in a MWA system is the insertion loss or attenuation in the coaxial transmission lines which supply microwave power from the generator to the applicator and can be 2-2.5 m long in clinical systems. Some large diameter transmission lines may have minimal insertion loss (less than -0.5 dB/m); however, those low-loss options are heavy and stiff, making them impractical clinically. Smaller diameter, lighter, and more flexible transmission lines can have significantly more insertion loss (typically -1.0 to -2.0 dB/m). The very small diameter coaxial transmission cables used within the applicator itself also have significant insertion loss (typically -2.0 to -3.0 dB/m). Summed together, the insertion losses can be 30-50% of the generator output. Finally, if water is used to cool the applicator and surround the antenna, it will also absorb some of the radiated MW energy prior to transmission to the tissue. These water losses vary considerably based on the design of the applicator but can be in the order of 30-50% of the power radiated from the antenna.

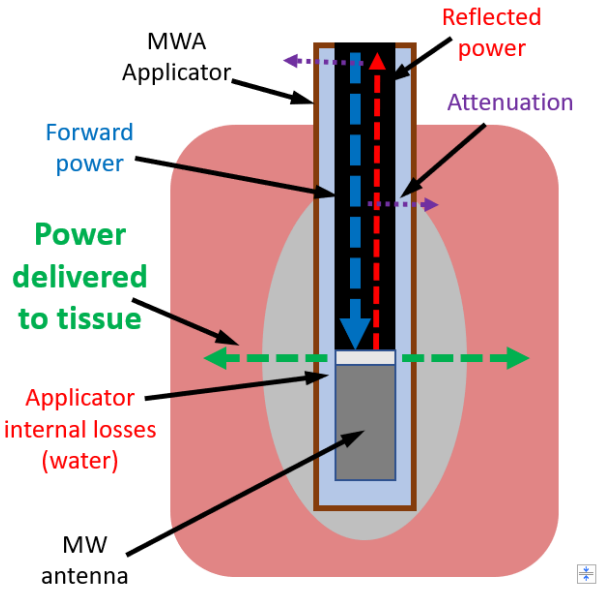

Figure 3-1: Illustration of MW power delivered to tissue and other losses during MWA.

The second goal of traditional MWA antenna design is to achieve a large, but spherical ablation zone. Larger ablation zones enable the treatment of larger tumors while still maintaining the desired clinical margin. More spherical ablation zones are desired for treatment planning since physicians can intuitively map spheres to target single small/medium tumors or overlap multiple spheres to target large tumors [65]. Also, many tumors generally have a near-spherical shape and therefore spherical ablation zones help spare more healthy surrounding tissue and avoid damage to nearby critical structures. Ideally, a MWA applicator could produce nearly spherical ablation zones with nearly constant dimensional ratios as applied power/time is scaled to treat targets of various diameters.

A first order method to evaluate the shape of an antenna's expected thermal ablation zone is through analysis of its electromagnetic specific absorption rate (SAR) profile in a multiphysics computational model of the target tissue. To do so, designers first determine the distribution of

the electric field generated by a MWA applicator by solving the Helmholtz electromagnetic wave equation:

Equation 3-2:

$$\nabla^2\mathbf{E} - k_0^2\left(\varepsilon_r - \frac{j\sigma}{\omega\varepsilon_0}\right)\mathbf{E} = 0$$

where, **E** [V/m] is the electric field, k_0 [m^{-1}] is the free-space wavenumber, ε_r is relative permittivity, σ [S/m] is effective conductivity, ω [rad/s] is anugular frequency, and ε_0 [F/m] is permittivity of free-space. The electromagnetic loss in the tissue depends on its conductivity and can be computed from the simulated electric field based on:

Equation 3-3:

$$\mathrm{Q}_{mw} = \frac{1}{2}\sigma \cdot \|\mathbf{E}\|^2$$

The SAR profile only gives the rate at which EM power is absorbed in the surrounding medium, and does not account for other thermal effects such as heat conduction, water vaporization in the surrounding tissue, or heat losses to blood perfusion, but has been shown to be an effective measure for optimizing ablation zone shape [66]. The normalized SAR profile for a simple insulated monopole MWA antenna design is shown in Figure 3-2 on the following page. In some cases, MWA antennas may include a balun or choke to reduce outer surface currents and improve on the typical SAR teardrop shape, however, in general these add complexity to the design and increase the overall device diameter [67], [68]. Another method to compensate for the

SAR tail or teardrop shape is to provide circulating cooling water within the applicator to actively cool the applicator shaft and reduce heating of the surrounding tissue.

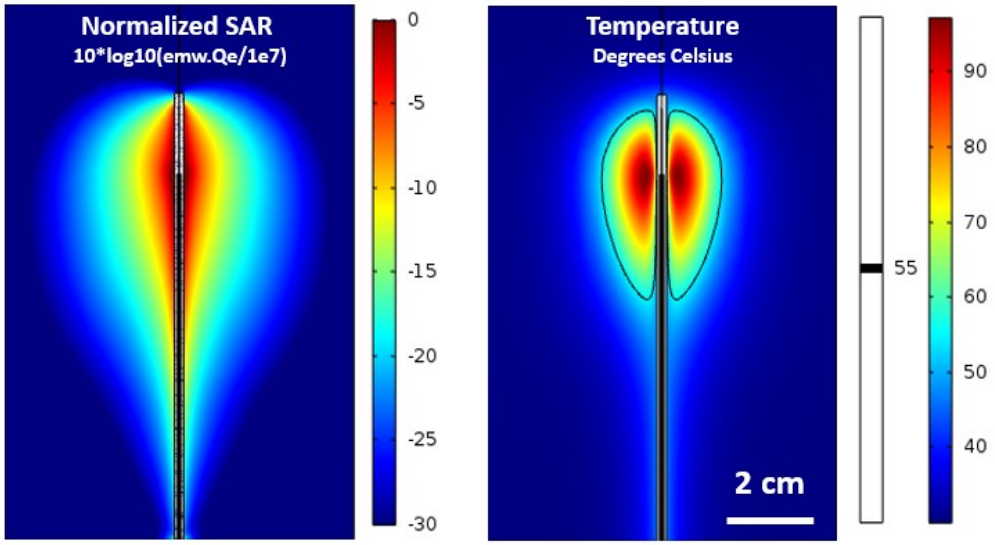

Figure 3-2: Simulated specific absorption rate (SAR) pattern for an insulated monopole MWA antenna (left) and temperature pattern of the same antenna with forced cooling of the applicator shaft (right) to reduce the thermal ablation "tail."

However, as previously mentioned, it is well established that electromagnetic properties of tissue (relative permittivity and conductivity) change substantially at elevated temperatures due to dehydration and protein conformation change during the course of thermal ablation [69]–[73]. Consequently, an antenna designed for optimal performance (based on initial reflection coefficient or simulated SAR pattern) in fresh, normal tissue, may quickly suffer degraded performance in practice as surrounding tissue is ablated. Therefore, it may be important to also consider the shape of the post-ablation SAR pattern or isothermal contours when optimizing prototype applicators.

Most MWA applicators aim to achieve large symmetric ablation zones through a combination of high-power direct MW heating that generates high central peak temperatures

near the applicator (within ~1-2 cm radius) that in turn develop thermal gradients that drive heat transfer through conduction to more peripheral regions. The ultimate ablation zone size and shape is eventually constrained by distributed and discrete cooling effects of blood perfusion in the surrounding tissue and nearby veins and arteries. To simulate the extent of a thermal ablation zone during the course of an ablation, designers typically start by building a computational model representative of the geometry and biophysical properties of the proposed target and surrounding anatomy. The Pennes' bioheat equation (Equation 3-4:) can be used to model the transient temperatures within tissues during MWA:

Equation 3-4:

$$\boldsymbol{\rho c}(\mathbf{T})\frac{\boldsymbol{\partial}\mathbf{T}}{\boldsymbol{\partial t}} = \boldsymbol{\nabla}\cdot\boldsymbol{k}(\boldsymbol{T})\boldsymbol{\nabla}\mathbf{T} + \mathbf{Q}_{\boldsymbol{mw}} - \boldsymbol{\omega}_{\boldsymbol{bl}}(\mathbf{T} - \mathbf{T}_{\boldsymbol{bl}})$$

where ρc is volumetric heat capacity [$Jm^{-3}K^{-1}$], T is temperature [K], k is thermal conductivity [$Wm^{-1}K^{-1}$], ω_{bl} is blood perfusion [$Wm^{-3}K^{-1}$], and T_{bl} is the temperature of blood. Figure 3-3 provides an illustration of Pennes' Bioheat equation and how each term contributes to influence the size and shape of the resultant ablation zone. Temperature dependence can be implemented for tissue electrical and thermal properties based on models developed from experimental measurements and updated in the coupled electromagnetic – heat transfer model at each timepoint.

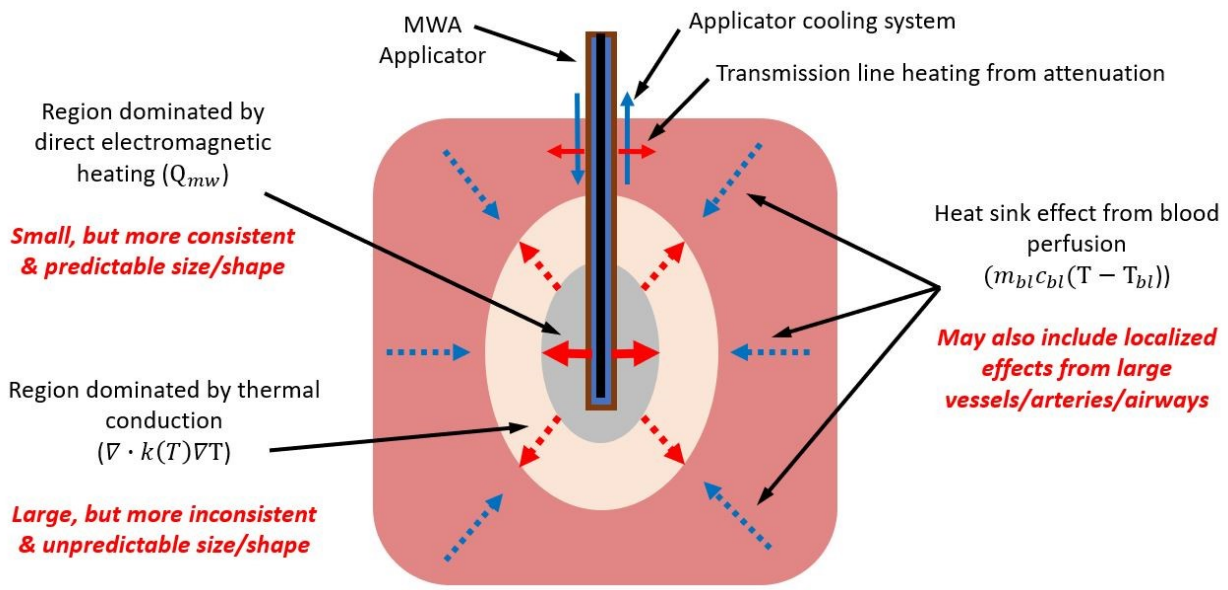

Figure 3-3: Illustration of the processes modeled with the bioheat transfer model used for microwave ablation simulation

Once a computational model representative of the target tumor, surrounding anatomy, and MWA system is complete, applicator designers utilize finite element method, or other numerical techniques, multi-physics modeling software to solve the coupled partial differential equations to develop simulations of the growth of thermal ablation zones during MWA procedures. Iterative design or parametric sweeps of specific applicator design elements, such as the antenna length, can be used to optimize new MWA designs for the proposed treatment.

One study has shown that of the options to optimize MWA antenna design based on best impedance matching, the most spherical SAR pattern, or the most spherical thermal ablation zone; optimization based on the most spherical SAR pattern produced the most spherical *ex vivo* ablation zones [66]. However, this may be due to current limitations in the accuracy and understanding of temperature-dependent tissue electrical properties changes during MWA.

3.3 DMWA Applicator Design Priorities

Although achieving efficient power transfer from the antenna to the surrounding tissue by developing a design with a S_{11} of at least -10 dB or better (more negative) is still desired, the radiation pattern and subsequent thermal ablation shape is significantly more important than for cylindrically-symmetric applicators given the intended use adjacent to and in close proximity to sensitive critical anatomy. Fortunately, SAR still provides a first order approximation of directivity during modeling and simulation. One method is to separate the forward and backward tissue regions into separate domains and then take the integral of the SAR in each domain which gives the total power deposited in that domain. Dividing the power in the forward domain by the power in the backward domain can give an approximate ratio of directivity which can be used to compare design alternatives. However, this method can give misleading results if a substantial amount of the SAR pattern is in undesirable areas, such as in a long tail along the front of the applicator, which results in power being deposited in the forward domain, but not in the target region near the applicator tip (see Figure 3-4, next page). A second approach is to normalize the SAR plots and measure the distance the specific contour levels extend into the forward and/or backward regions. However, either method still involves some subjectivity as to which portions of the SAR pattern would meaningfully contribute to the size and shape of an actual thermal ablation zone once other factors such as applicator cooling or blood perfusion are considered. For many designs, better directivity (as measured by SAR pattern techniques) is inversely correlated to better impedance matching. However, worse impedance matching results in less power deposition and ablation depth. This results in a tradeoff between maximum directivity and maximum thermal ablation zone volume.

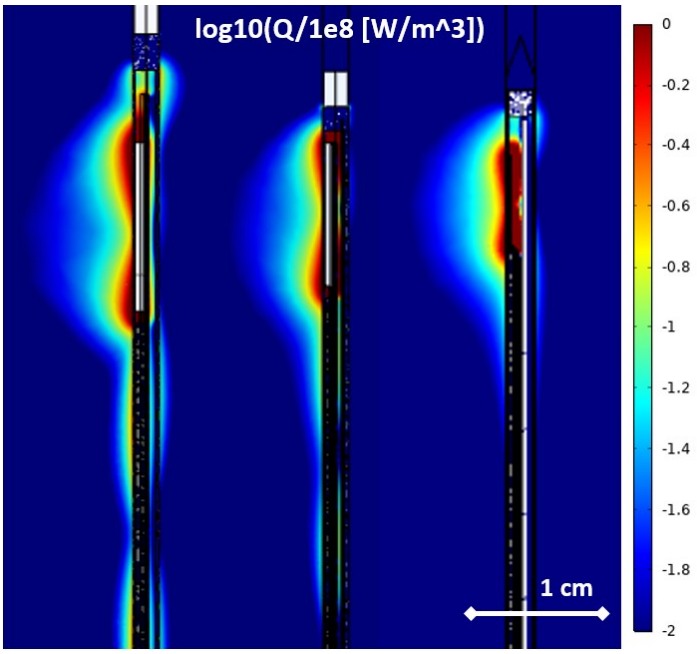

Figure 3-4:Specific absorption rate (SAR) patterns for various directional MWA applicator designs illustrating the challenge of using visual SAR patterns to optimize forward ablation depth and directivity.

A complete time-dependent, coupled electromagnetic and heat transfer multiphysics computational model is needed to truly compare the directivity of promising directional applicator designs. A multiphysics simulation can be used to illustrate the extents of a thermal ablation zone by displaying a 55 °C isothermal contour (see Figure 3-5, next page). However, this is computational resource intensive and time consuming, and still requires assumptions and simplifications of time and temperature dependent tissue electrical and thermal property changes and heat transfer due to the applicators cooling system.

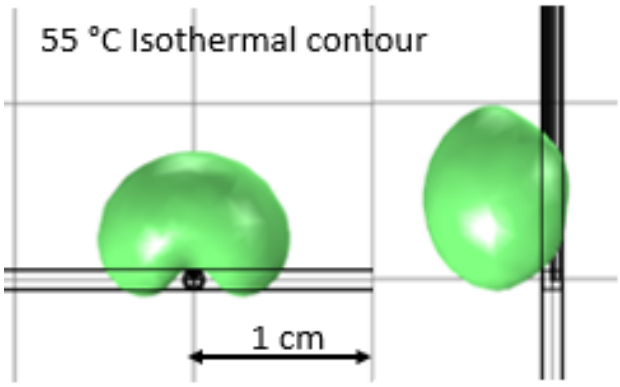

Figure 3-5: Simulated 55 °C isosurface indicating approximate shape of directional ablation zone based on a coupled electromagnetic-bioheat transfer computational model. 30 W, 5 min application.

A final directional MWA design consideration beyond modeling and simulation is that the fabrication and physical assembly of many potential directional antenna designs can be complex and difficult to accomplish reliably by hand, especially compared to omni-directional designs. Many omni-directional designs are concentric and can utilize easily obtainable cylindrical steel tubes, plastics, and/or ceramics to create applicators that have very small outside diameters but retain good rigidity and durability. Unfortunately, directional antenna designs require additional passive elements to shield and reflect the EM field. An ideal reflector element may be too small and complex to manufacture, conversely it may be too large for use in a practical minimally invasive design. Dedicating applicator cross-sectional area to these passive elements also reduces rigidity and durability.

Overall, imperfect simulation evaluation criteria combined with design considerations based on material availability and fabrication limitations demand the directional MWA design process be as much subjective as it is objective.

3.4 A Third Generation DMWA Applicator Design

Directional microwave ablation applicator designs using metallic hemispherical shield/reflector elements and operating at 2.45 GHz have been previously reported by McWilliams *et al.* [18] and Sebek *et al.*[19] and are considered the first and second generation designs from Kansas State University. Directional MWA applicator designs have also been previously reported by other groups including Berube *et al.* [74], whose design was intended for use in cardiac ablation and did not provide any cooling system, and Mohtashami *et al.* [20], whose design uses a hybrid slot/monopole design cut into the coaxial cable outer jacket and operates at 7.0 GHz. However, none are currently commercially available, nor in use in the clinical setting. Some limitations of these prior designs include a diameter too large for minimally invasive percutaneous use, complex fabrication techniques requiring hand-tuning, impractical operating frequencies, limited ablation volume, and limited directivity.

To develop a directional MWA applicator suitable for widespread use in the clinical setting, we used a simulation-based approach to optimize a third generation DMWA applicator design based on the following precedence of clinical requirements and performance goals:

1. Reduce overall diameter to ≤ 2.1 mm (14-gauge) to enable minimally invasive use
2. Minimize backward ablation depth; ideally zero for use near critical sensitive anatomy
3. Improve device rigidity and durability to enable percutaneous use
4. Maximize forward ablation depth to treat larger lesions
5. Simplify fabrication and construction methods for ease of industrialization and mass production

After several iterations, a design consisting of two co-linear metal tubes laid alongside a coaxial transmission cable in a triangular arrangement shown in cross-section (see Figure 3-6, next page) was selected as optimal. The transmission cable was made from 0.034” semi-rigid coaxial cable. The metal tubes form a shield to prevent EM radiation in the undesired sector. The tubes are glued to the outer conductor of the coaxial cable to improve applicator stiffness and rigidity. With advanced manufacturing techniques, fusing the tubes and cable together by welding or soldering may add stiffness to the device, and if done in a way to act as a choke/balun may also restrict surface currents along the outer surface of the cable and tubes. These tubes also provide an inflow path for circulating cooling water. At the distal end of the coaxial transmission cable, the outer conductor is stripped away to expose a small length (0-1 mm) of dielectric material and a length of center conductor (5-10 mm) to form a linear antenna. The center conductor is bent and offset near the exposed dielectric to position the antenna element further away from the conductive tubes and closer to the outer wall of the applicator. The coaxial cable and metallic tube assembly is housed in a non-conductive extruded polyimide tube. The overall outer diameter of the current configuration is 0.0845” (14 gauge) but could be adapted for devices as small as 0.053” (17 gauge)

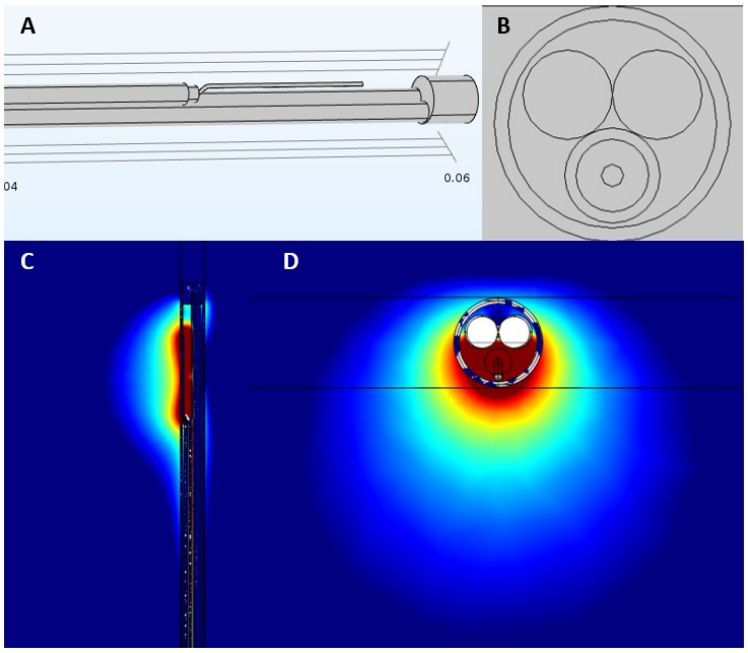

Figure 3-6: (A) Perspective view of the directional applicator internal structure. (B) Cross section view of the applicator structure showing the two metallic flow tubes on top of the coaxial cable. (C) Longitudinal view of the applicators simulated EM specific absorption rate (SAR) pattern. (D) Cross sectional view of the applicator SAR pattern.

In the current design, the metallic tubes are extended into a non-conductive epoxy plug at the very distal end of the device 1-5 mm beyond the distal tip of the antenna. This allows the metallic tubes to provide axial rigidity since they are fixed in place at both the distal and proximal ends. A small notch is cut in each tube slightly proximal from the distal epoxy plug to provide a path for circulating water. The distal end of the device can be terminated in a trocar tip or other type of pointed tip for easier insertion into tissue.

The void space between the polyimide tube housing and the triangular configuration of the coaxial cable and metallic tubes forms the outflow path for circulating water. In the current configuration, the antenna element is unsupported on the distal end and is surrounded by circulating water (see Figure 3-6). The high relative permittivity of the surrounding water contributes to proper antenna impedance matching.

However, since water also has a significant electrical conductivity, filling some or all of the space between the antenna element and the metallic flow tubes with a low-loss, high-dielectric material, such as TiO_2 ceramic, could reduce internal MW energy loss and improve efficiency. Furthermore, since MW loss within the applicator raises the applicators internal temperature, including low-loss material may enable higher applicator operational power levels. Unfortunately, although TiO_2 is very common in powder form, we have been unable to procure a small enough diameter TiO_2 ceramic cylinder to position between the antenna element and the metallic flow tubes and displace lossy water in that region.

The third-generation directional MWA prototype can be fabricated by hand by a practiced person in less than two hours and at a cost of less than $75. The third generation Directional MWA applicator has been tested extensively in *ex vivo* and *in vivo* tissue samples as discussed in Chapter 4.

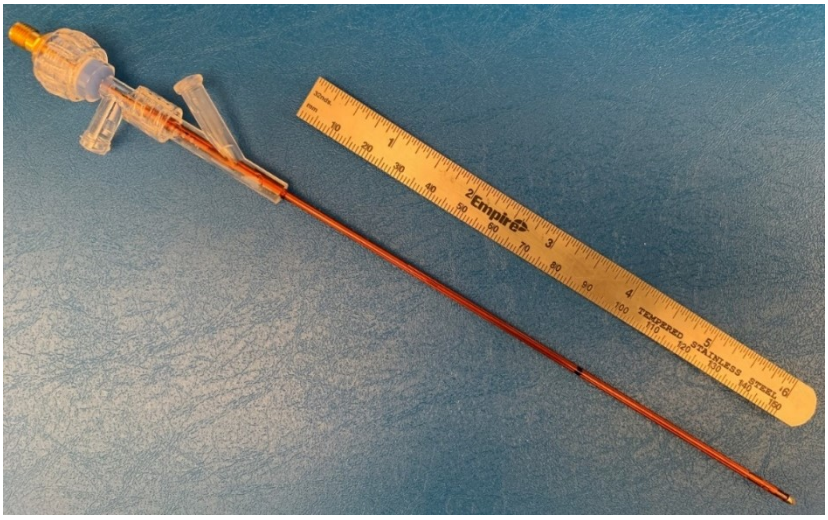

Figure 3-7: Third-generation directional MWA applicator.

3.5 DMWA Commercialization efforts

In general, it seems the current DMWA design may be limited to producing a maximum of only 10-15 mm deep ablation zones before developing substantial backward heating. Further modeling and simulation results indicate planned incremental improvements are not expected to dramatically improve applicator performance. However, significant study of the clinical environment and many discussions with clinical end users have indicated the current directional ablation applicator design may still serve a compelling need for treating malignant tumors near critical sensitive anatomy, treating benign disease in small targets such as glands, and providing new options for palliative care. As such, the DMWA applicator is currently the subject of intensive commercialization efforts supported by National Science Foundation (NSF) Innovation Corps (I-Corps), Small Business Technology Transfer (STTR) Phase I, and Small Business Innovation Research (SBIR) Phase II grants.

With satisfactory electromagnetic and thermal performance of the third-generation DMWA applicator demonstrated in a clinically-relevant environment (Chapter 4), focus shifted to: (1) improving the stiffness/rigidity of the applicator to make it suitable for percutaneous use, (2) modifying the applicator internal design to facilitate mass production, and (3) completing the remaining elements needed for clinical use including the applicator hub/handle and transmission and cooling line bundle. As development of the third-generation applicator already represented the limits of our production capabilities locally, we initiated a collaboration with a third-party original equipment manufacturer (OEM) with specific microwave experience to help develop fabrication procedures and techniques for the DMWA design suitable for industrialized manufacturing at scale.

To improve the stiffness/rigidity, variants of the applicator have been built using either a fiberglass tube outer shaft or steel tube with transition to PEEK outer shaft. A fiberglass shaft required a minimum wall thickness almost twice as thick as the original polyimide wall; however, due to the assumed relative permittivity of fiberglass (~4.15-4.3) being about 40-50% higher than polyimide (~2.9), antenna impedance matching and the subsequent optimal antenna length was mostly unaffected. However, the thicker wall fiberglass design did require use of smaller flow tubes that resulted in reduced electromagnetic directivity and reduced coolant flow, both of which contributed to increased backward heating. Furthermore, producing fiberglass tubes in the necessary custom dimensions requires expensive tooling. Samples ground-down to the appropriate dimensions from larger stock showed potential for acceptable electrical and mechanical performance, but the grinding process caused approximately half of the samples to weep water through microfractures in the thin fiberglass walls. A steel shaft with a transition to PEEK near the MW antenna offered even more stiffness/rigidity than the fiberglass option, but required a steel to PEEK transition near the antenna that could leak and its junction, is more difficult to manufacture, and seems to contribute to extended lengthwise heating (ablation tail) from MW inducing surface currents in the steel despite the PEEK transition. Both design variants are still under consideration with early indications suggesting the fiberglass shaft is the preferred option.

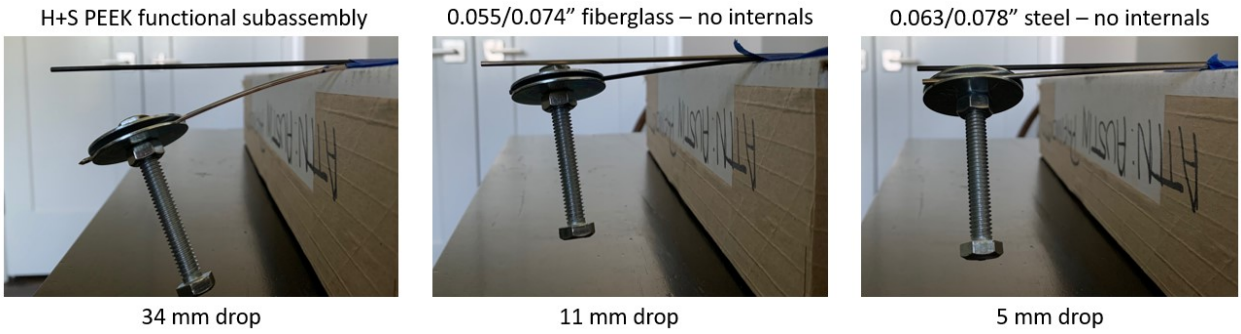

Figure 3-8: PEEK (left), fiberglass (middle), and steel (right) shaft stiffness testing using an approximately 50 gram weight attached to the end of the shaft cantilevered 10 cm, illustrating varying rigidity of different designs.

Figure 3-9: DMWA applicator variant with steel outer shaft and PEEK "window" surrounding the MWA antenna

To ready the applicator internal design for mass production, the hand-cut and notched flow tubes were replaced with steel tubes with laser cut holes to return coolant flow though the inside of the applicator outer shaft. A custom tool was built to bend the monopole in a consistent and controlled manner. Furthermore, a PEEK endcap/spacer was designed to align and case the distal tips of the flow tubes, anchor a steel trocar point, and support the distal end of the previously unsupported monopole antenna. However, displacing a portion of the water surrounding the monopole antenna with a low-permittivity plastic material has resulted in a 10-15% reduction in energy transfer to the tissue in the forward direction. Options are being investigated to leave the antenna monopole unsupported or provide a support made of a higher

permittivity material such as titanium dioxide (TiO_2) though no manufacturers who can produce this material in such small dimension and tolerances have been identified (minimum TiO_2 cylinder diameter achievable from known sources is 0.9 mm).

To complete the integrated design of a clinical DMWA applicator, a custom manifold was designed for the proximal end of the applicator shaft where the water inflow and outflow and the internal microwave transmission cable diverge. A 2.5 meter longer transmission bundle, which connects the DMWA applicator to the MW generator and coolant pump was developed which housed a larger diameter, flexible, coaxial MW transmission cable, inflow and outflow coolant lines, and auxiliary DC conductors. Substantial effort was invested to balance weight, flexibility, and attenuation (heating) with the MW transmission cable selection to provide the most usable clinical solution. A custom cover with integrated LED to indicate MW power-on status was also developed to protect and provide thermal insulation for the manifold and the external water and power connections. As a safety feature, a thermocouple probe was included within the shaft on the opposite side of the flow tubes as the coaxial transmission cable to monitor internal return flow coolant temperature. However, the relatively large diameter of the current thermocouple probe has required reduced flow tube dimensions, negatively impacting directional electromagnetic performance, and has reduced the achievable coolant flow rate – raising internal operating temperatures. Alternatives are being investigated to reduce the dimensions of this thermocouple or move it out of the applicator shaft. A new combined RF/DC connector for MW power, thermocouple leads, and LED power within a single connection was also developed for this project to simplify clinical setup and use. The current (October 2020) industrialized DMWA functional prototype design is show in Figure 3-10.

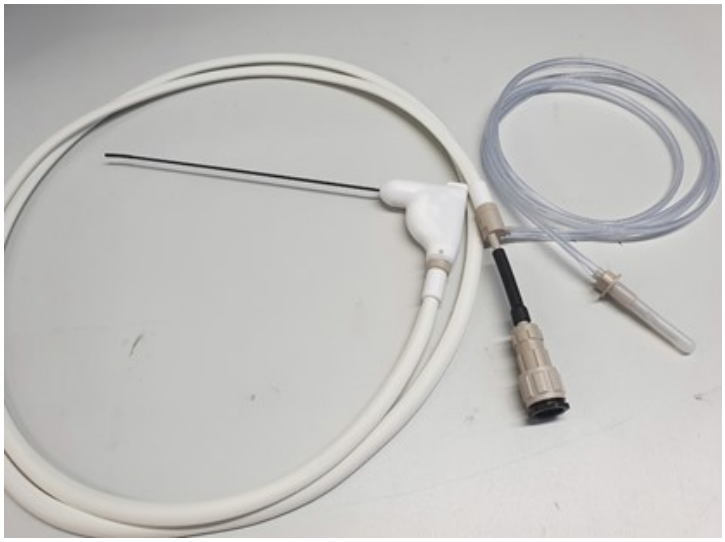

Figure 3-10: Industrialized DMWA applicator prototype with flexible interconnecting RF cables and fluid lines for connections to the MWA generator and peristaltic pump

To provide a complete clinical system, we partnered with another experienced engineering OEM and design firm to adapt a version of their commercially available radiofrequency generator platform to power the DMWA applicator at 2.45 GHz. Future versions of this MW generator platform are expected to support up to 4x MW channels. Early functional subassemblies (not pictured) of the industrialized DMWA applicators were used in combination with the new MW generator platform for the *ex vivo* and *in vivo* testing described in Chapter 5.

Figure 3-11: Early-build microwave generator platform, including a high power generator and peristaltic pump

The complete industrialized DMWA applicator prototype shown in Figure 3-10 paired with the prototype MW generator platform shown in Figure 3-11 was recently used in 4 *ex vivo* muscle and 20 *ex vivo* liver ablations without failure or any indication of performance degradation. Table 3-1 lists the performance of the early industrialized DMWA system showed compared to the experimental DMWA applicator designs tested in Chapter 4.

Table 3-1: Industrialized DMWA system performance in *ex vivo* liver compared to DMWA results presented in Chapter 4

App #	P_{GEN} (W)	Duration (sec)	Pump (mL/min)	Fwd (mm)	Bkwd (mm)	DR	Width (mm)	$T_{internal}$ °C	T liver C °C	$P_{reflected}$ (W)
Original [38]	80	300	~60-100	**13.3** ± 1.0	**2.3** ± 0.5	**5.8**	17.8 ± 0.5			
Original [38]	100	300	~60-100	**13** ± 0.8	**2** ± 0.0	**6.5**	19.8 ± 0.5			
F2.1	100	300	100	**12.3** ± 1.3	**1.0** ± 0.0	**12.3**	21.0 ± 1.4	11.8 ± 3.5	35.9 ± 0.8	1.0 ± 0.0
F2.1	100	300	50	**12.8** ± 0.5	**2.3** ± 0.5	**5.7**	22.0 N/A	23.0 ± 1.0	35.8 ± 1.5	3.5 ± 0.0

These recent *ex vivo* results show perhaps a 4-8% reduction in forward ablation depth performance while a potential 50+% improvement in backward depth at the highest coolant pump setting. This suggests the ultimate directivity ratio achievable may be driven more by the forced cooling of the applicator than any changes in the electromagnetic performance. Further examination of the applicator internal design to determine any opportunity for performance improvement as well as high repetition testing of multiple completed industrialized DMWA is ongoing.

Chapter 4 - Directional microwave ablation: Experimental evaluation of a 2.45 GHz applicator in ex vivo and in vivo liver[1]

4.1 Introduction

All commercially available microwave ablation (MWA) devices produce only near-spherical or ellipsoidal treatment zones cylindrically symmetric around the axis of the applicator [25], [33], [75]. These devices may not always be suitable for conformal heating of tumors across a wide range of shapes and anatomical locations, and place constraints on the positioning of the applicators within the body. Current MWA systems also have limited ability to reliably predict or control the extent of the thermal treatment zone to ensure the tumor and a surrounding margin receive the proper thermal dose without also damaging critical surrounding anatomy [76]. Efforts to minimize the thermal damage to non-target tissue risk incomplete thermal coverage of the target, potentially leading to disease recurrence. Conversely, excessive energy delivery may risk the thermal damage zone extending beyond the target boundary and damaging critical structures. Thermoprotective techniques, such as fluid or gas dissection, balloon interposition, or endoluminal cooling/warming offer some ability to isolate and insulate critical structures from the thermal ablation zone [77]. However, these techniques have limitations and are not universally applicable for all challenging cases, especially if the target tissue and critical structures are integral within the same organ (e.g. the gall bladder or bile ducts).

[1]This chapter was reproduced/adapted from A. Pfannenstiel, J. Sebek, H. Fallahi, W. Beard, C. Ganta, D. Dupuy, and P. Prakash, "Directional Microwave Ablation: Experimental Evaluation of a 2.45-GHz Applicator in Ex Vivo and In Vivo Liver," *Journal of Vascular and Interventional Radiology*, vol. 31, no. 7, pp. 1170-1177.e2, Jul. 2020, doi: 10.1016/j.jvir.2020.01.016, https://www.sciencedirect.com/science/article/pii/S1051044320300312, with permission from Elsevier.

Directional microwave ablation applicators limit the microwave radiation to a fraction of the angular expanse around the axis of the applicator and offer the ability to direct energy towards a target and away from critical healthy tissue. This feature has the potential to reduce the burden on separation techniques or offer a treatment option when separation is not feasible. Directional applicators also have the potential to enable treatment of tumors in organs or small glands that are difficult to safely penetrate and ablate with existing cylindrically symmetric devices. Prototype designs for directional MWA have been reported, but none are commercially available yet [18], [19]. The purpose of this study was to characterize performance of an experimental 14-gauge, 2.45 GHz, water-cooled, directional microwave applicator which produces an approximately hemispherical ablation zone.

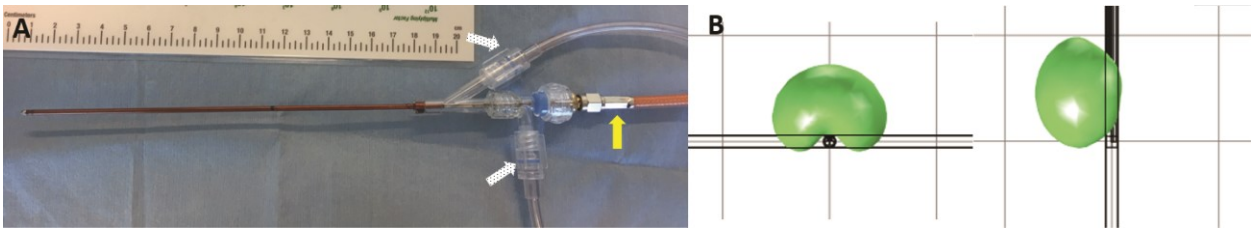

Figure 4-1: Third-generation prototype directional MWA applicator, with arrows indicating connections to microwave power (yellow) and coolant flow lines (white dotted) (A). Simulated 55 °C isosurface indicating approximate shape of directional ablation zone based on a coupled electromagnetic-bioheat transfer computational model (B).

4.2 Materials and Methods

The MWA applicator used in this study was developed using a simulation-based approach to revise and optimize the directional MWA applicator designs originally reported by McWilliams *et al.* [18] and Sebek *et al.*[19] for minimally invasive percutaneous clinical use. The applicator consists of a water-cooled coaxial antenna augmented with metallic reflector elements to restrict microwave radiation to a preferred lateral direction. The prototype applicator, shown in Figure 1,

has an outer diameter of 2.1 mm and shaft length (tip to bottom of hub) of 15 cm. Directional MWA applicators based on this design with smaller diameters may be technically possible with improvements in fabrication methods.

The applicator's 3D thermal ablation zone profile was experimentally evaluated in fresh *ex vivo* bovine liver, using a previously described protocol [19]. Liver tissue was sectioned into approximately 6 × 6 × 6 cm^3 blocks and warmed to ~37 °C in a temperature-controlled water bath while sealed in water-tight plastic bags. A custom 3D printed fixture facilitated consistent applicator insertion angle and depth into the tissue samples. A peristaltic pump (Cole-Parmer, Vernon Hills, IL) was used to circulate ice water (3-5 ºC) through the applicator at a flow rate of approximately 100 mL/min. Microwave power was supplied to the applicator using an industrial 2.45 GHz microwave generator (Sairem, Neyron, France). Forward and reflected power were monitored with a Bird 7022 power sensor (Bird Technologies, Solon, OH). Experimental ablations were performed at 60 W, 80 W, and 100 W (generator setting) for 3, 5, and 10 minutes each; experiments were repeated n = 4 times at each power and time combination, for a total of 36 ablations. Tissue samples were sliced perpendicular to the axis of the applicator to measure and document the forward and backward depth, width, and shape of the ablation zone based on the extent of tissue whitening. Forward depth was measured to include only brown or white regions whereas backward depth was measured to include any visible zones, including light pink, thus providing the most conservative (i.e. lower bound) measure of directivity. Figure 4-2 provides an example of how measurements were taken. Ablation shape was characterized by the directivity ratio, defined as the ratio of the forward depth to the backward depth. Although not used to define applicator directivity, a supplemental set of nine *ex vivo* ablations (n = 1 at each power and time

combination) was performed in which the tissue sample was sliced along the longitudinal axis of the applicator to observe and measure the height of the ablation zone.

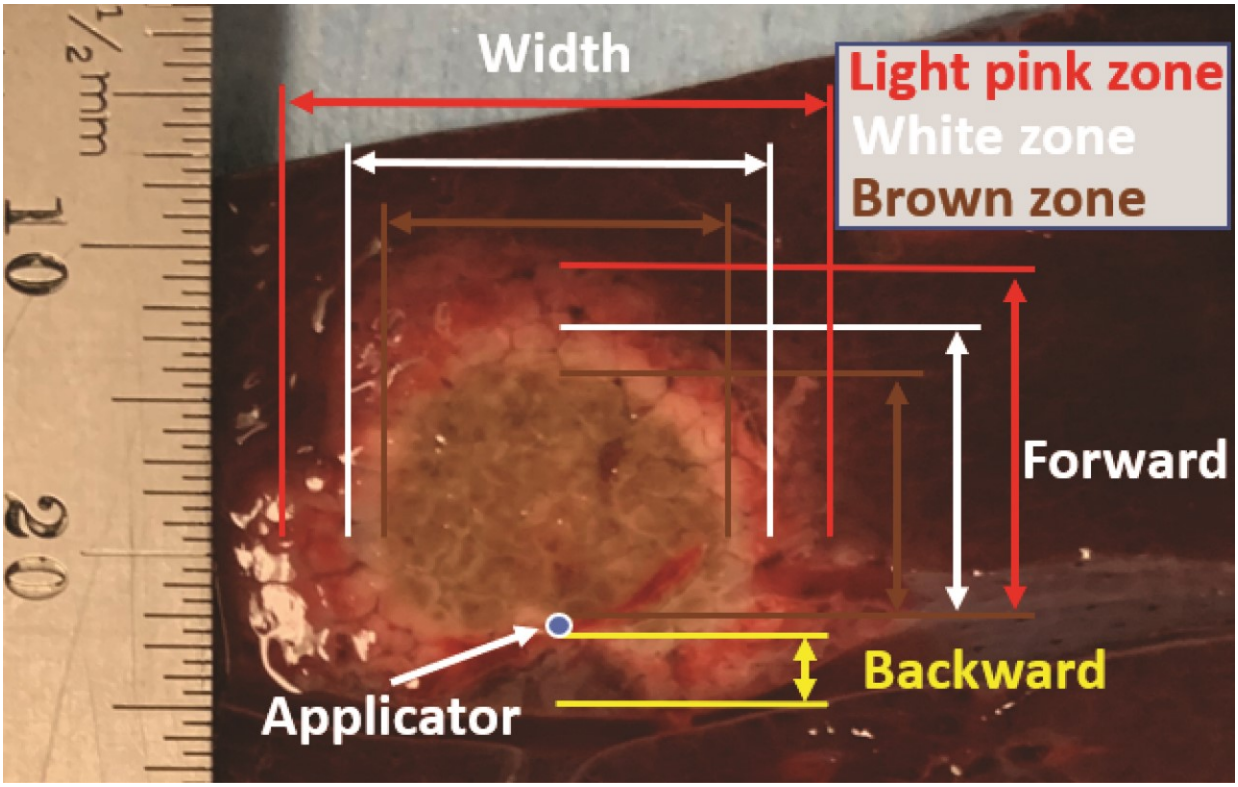

Figure 4-2: Representative image of how ablation zone measurements were taken for an *in vivo* ablation zone stained with TTC. Data presented for forward ablation zone depth was conservatively reported based on measurements taken of the brown and white zones as these regions are the most likely to represent complete ablation. Data presented for backward ablation zone depth was conservatively reported to include any visible ablation zone, including any light pink zones. *Ex vivo* ablation zones typically did not display as clearly pronounced transitions between zones as *in vivo* samples.

All *in vivo* experiments were carried out under an experimental protocol approved by the local Institutional Animal Care and Use Committee. Experiments were conducted in two 45 – 50 kg, female domestic swine. Pigs were premedicated with Atropine (0.05 mg/kg, IM) and anesthesia was induced by an intramuscular injection of 4.4 mg/kg Telazol, and 2.2 mg/kg Xylazine. Pigs were orotracheally intubated and anesthesia was maintained by isofluorane in O_2. Anesthetized pigs were positioned in dorsal recumbency and a ventral midline incision was made from the

umbilicus extending cranially to the xyphoid. The directional microwave ablation applicator was serially inserted into each of the liver lobes to induce thermal ablation. In each of the two animals used in the study, up to four ablations were performed in each of the four liver lobes that could be accessed via the laparotomy approach.

The *in vivo* MWA procedures were divided into two experimental groups. The objective of the first group, referred to as "insertional" ablations, was to test a subset of the time and power combinations previously used in *ex vivo* experiments to determine the effects of blood perfusion on the resulting ablation zone size and directivity. The MWA applicator was inserted directly into the approximate center of mass of a liver lobe with the goal of ablating a homogenous section of the lobe, similar to how *ex vivo* ablations were conducted. Ablations were conducted at 80 W for 5 minutes (n = 3), 100 W for 5 minutes (n = 3), and 100 W for 10 minutes (n = 2). 60 W was not considered for *in vivo* use as the effects of blood perfusion were expected to result in excessively small ablation zones. 5 minute ablations were generally preferred over 10 minutes to avoid ablating completely through the relatively small cross-sectional area of the accessible sections of porcine liver lobes and to minimize the chance of operator fatigue causing inadvertent movement of the applicator relative to the target during the open laparotomy approach. In one ablation per animal, the applicator was inserted near (approximately 2-3 mm) but aimed away from the gall bladder to also opportunistically test the ability to avoid collateral damage to the gall bladder. Upon completion of each ablation the applicator was removed and a wooden dowel, marked with a color corresponding to the ablation number, was inserted along the applicator track to enable proper localization and identification of the thermal lesion post-procedure.

The objective of the second group, referred to as "surface" ablations, was to determine if a non-penetrating approach could ablate into the liver while non-target structures adjacent to the

liver could be spared from thermal damage. The MWA applicator was placed on the surface of the liver capsule, directing power into the liver, while another organ was placed directly on the backside of the MWA applicator to model an applicator placed between and directly in contact with both target and non-target tissues. Non-target tissues used included spleen (n = 3), large intestine (n = 2), and small intestine (n = 1). Applied power was limited to 80W to reduce the risk of ablating entirely through the relatively thin areas of the liver lobes where these ablations were performed and duration was limited to 5 minutes to avoid operator fatigue inducing inadvertent movement and slippage of the applicator relative to the surrounding tissues which would skew the experimental results.

Pigs were euthanized at the conclusion of the ablation procedure while still under anesthesia. Euthanasia was performed by intravenous injection of sodium pentobarbital 390 mg/ml at a rate of 0.2 ml/kg of body weight. Following euthanasia, the livers were harvested, sectioned in ~5 mm thick axial slices, and stained for viability with triphenyltetrazolium chloride (TTC), enabling more accurate identification of ablation zone extents [12]. The sections were then fixed in 10 % buffered formalin and embedded in paraffin blocks. Approximately 5 μm thick hematoxylin and eosin (H&E) stained sections were obtained from the paraffin embedded samples for histologic examination.

4.3 Results

The attenuation losses for the interconnecting cables were experimentally measured, and the power delivered to applicator input was determined to be 40, 52, and 62 W, for generator settings of 60 W, 80 W, and 100 W. Table 4-1 provides the forward depth, backward depth, directivity ratio, and width of the experimental *ex vivo* ablation zones; data are presented as the

mean ± standard deviation of $n = 4$ experimental ablations at each power/time combination. Mean forward ablation depth ranged from 8.3 – 15.5 mm, mean backward depth ranged from 0.0 – 3.5 mm, and directivity ranged from 4.7 – infinite (no observable backward heating). Figure 4-3 shows a scatter plot of ablation zone forward and backward measurements vs. applied energy. Table 4-1 and Figure 4-3 show that although increasing power and duration yields increased forward ablation zone depth, an accompanying greater increase in backward ablation zone depth reduces the overall directivity ratio. Figure 4-4 shows a matrix of example *ex vivo* ablation zones in the axial plane (i.e. perpendicular to the applicator insertion axis) across the range of experimental power/time combinations investigated in this study. Figure 4-5 shows the height of the ablation zone along the longitudinal axis of the applicator ranges from 13 - 25 mm.

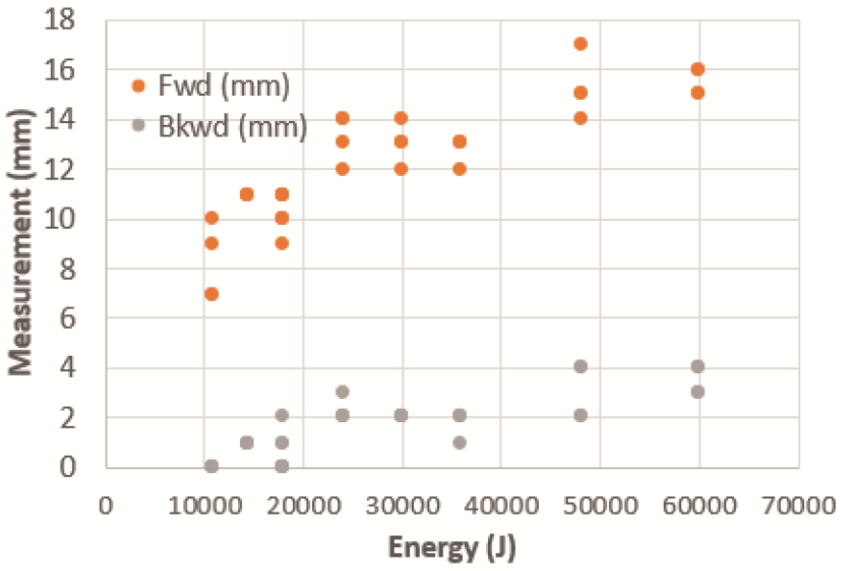

Figure 4-3: Scatter plot of forward and backward ablation zone depths (axial plane) measured in *ex vivo* bovine liver tissue as a function of applied energy at the microwave generator (some points represent multiple repeated data points).

Table 4-1: Dimensions of ablation zones measured following experiments in *ex vivo* bovine liver. Results are presented as the mean ± standard deviation of $n = 4$ experiments per row.

Power [W]	Time [min]	Energy (J)	Fwd [mm]	Bkwd [mm]	Directivity	Width [mm]
60	3	10,800	8.3 ± 1.5	0.0 ± 0.0	∞	10.5 ± 1.7
60	5	18,000	10.8 ± 0.5	0.0 ± 0.0	∞	14.5 ± 1.7
60	10	36,000	12.8 ± 0.5	1.8 ± 0.5	7.1	20.0 ± 2.2
80	3	14,400	11.0 ± 0.0	1.0 ± 0.0	11.0	14.0 ± 0.8
80	5	24,000	13.3 ± 1.0	2.3 ± 0.5	5.8	17.8 ± 0.5
80	10	48,000	15.3 ± 1.3	3.0 ± 1.2	5.1	23.3 ± 1.0
100	3	18,000	10.0 ± 0.8	1.0 ± 0.8	10.0	15.0 ± 1.4
100	5	30,000	13.0 ± 0.8	2.0 ± 0.0	6.5	19.8 ± 0.5
100	10	60,000	15.5 ± 0.6	3.5 ± 0.6	4.7	24.3 ± 1.5

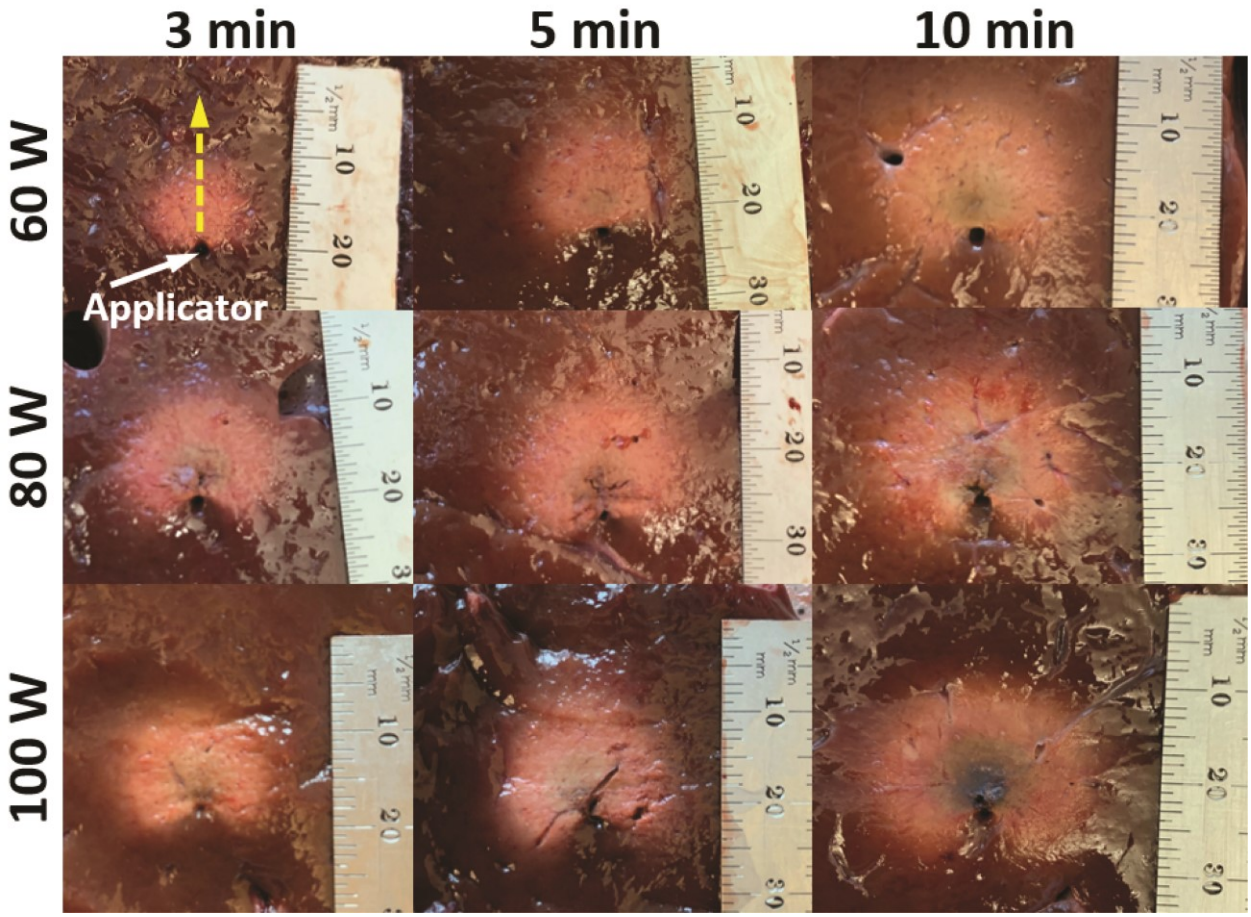

Figure 4-4: Matrix of images showing *ex vivo* bovine liver ablation zones (axial section) across all combinations of time and power settings tested. The applicator insertion track is indicated with a white arrow and direction indicated with a dashed yellow arrow in the top left image. Although increasing power or duration increases the depth of the forward ablation zone, beyond 80 W or 5 minutes sidelobes begin to form and extend into the backward region, reducing the overall directivity of the ablation zone.

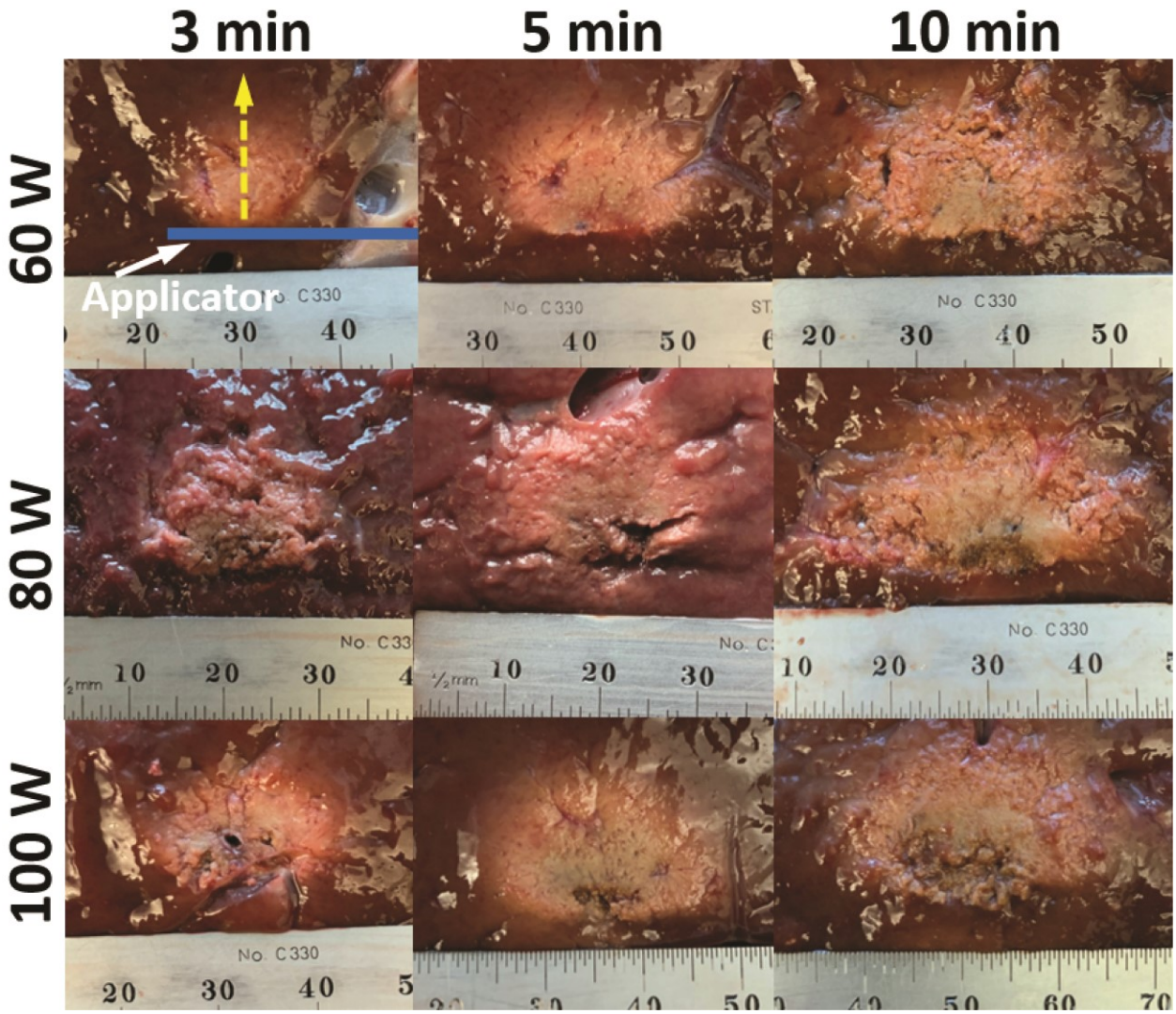

Figure 4-5: Matrix of images showing the *ex vivo* bovine liver ablation zone (longitudinal section) across all combinations of time and power settings tested. The applicator orientation is indicated with a blue line and direction indicated with a dashed yellow arrow in the top left image. The directional MWA applicator demonstrated a constrained ablation height along the longitudinal axis and did not display a tail or teardrop shape.

Table 4-2 lists the mean ablation zone dimensions and directivity ratios following *in vivo* ablation. Of the ablations in the "insertional" experimental group (n = 8), mean forward ablation depth ranged from 10.3 – 11.5 mm, mean backward ablation depth ranged from 0.7 – 1.0 mm, and directivity ranged from 11.5 – 14.7. Compared to *ex vivo* ablation zones, the forward ablation depth following 80 W, 5-minute heating was reduced by 23%, the backward ablation depth was reduced by 70%, and the directivity ratio increased by 153%. For 100 W, 5-minute ablations, forward

ablation depth was reduced by 13%, the backward ablation depth was reduced by 65%, and the directivity ratio increased by 148%. Figure 4-6 provides TTC and H&E stained axial slice images of a directional ablation performed near, but aimed away from the gall bladder. No gross or microscopic thermal damage to the gall bladder was observed.

Table 4-2: Dimensions of ablation zones measured following experiments in i*n vivo* porcine liver.

Power [W]	Time [min]	Samples	Fwd [mm]	Bkwd [mm]	Directivity	Width [mm]
Direct insertion						
80	5	$n = 3$	10.3 ± 2.1	0.7 ± 0.6	14.7	10.3 ±2.5
100	5	$n = 3$	11.3 ± 2.9	0.7 ± 0.6	16.1	14.3 ± 1.2
100	10	$n = 2$	11.5 ± 0.7	1.0 ± 1.4	11.5	16.5 ± 2.1
Surface ablations						
80	5	$n = 5$	7.8 ± 1.1	N/A	N/A	12.8 ± 1.1

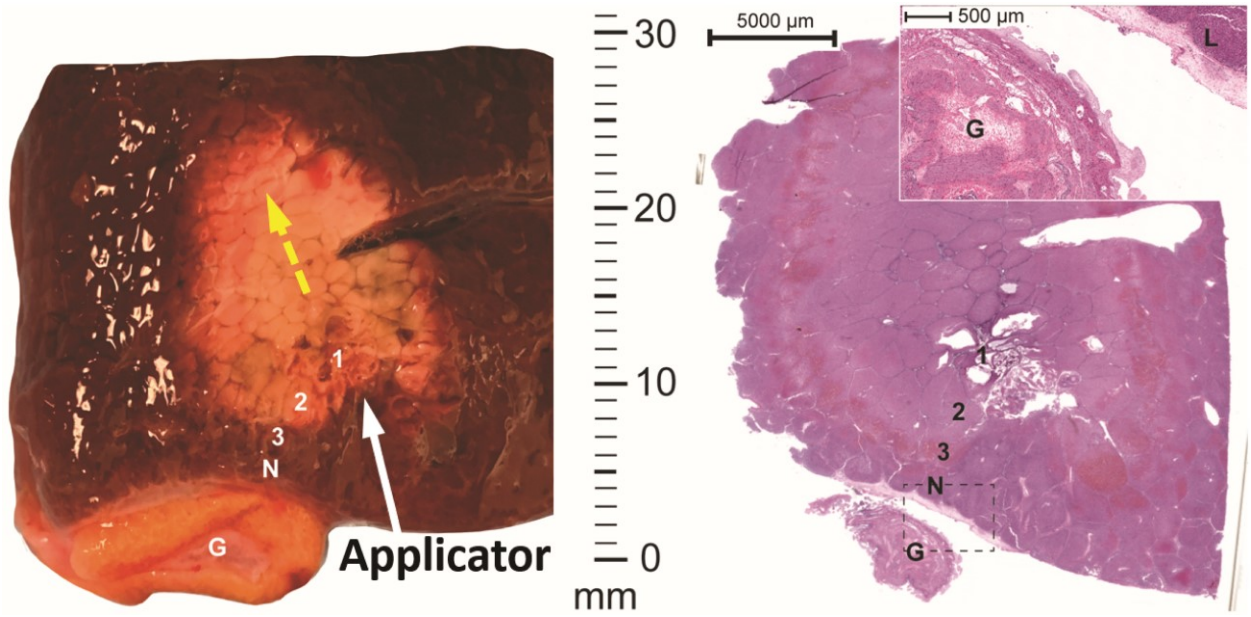

Figure 4-6: Gross image of ablation zone (axial section) after TTC staining, illustrating viable liver tissue between the directional applicator, and the gall bladder (Left). The applicator insertion point is indicated with a white arrow and direction indicated with a dashed yellow arrow. Associated image of H&E stained section (Right) illustrating unaffected gallbladder (G) and normal liver tissue (N) between the gall bladder and zones 1-3 of the ablation zone. The scale bar represents 5000 µm for the large image and 500 µm for the inset image showing gall bladder (G) and normal liver tissue (L).

Histological examination of *in vivo* liver ablation sections showed three distinct changes represented as zones 1-3 (Figure 4-6 and Figure 4-7 provide example images illustrating these zones). The central area near the MWA applicator probe was zone 1; there was complete loss of hepatic sinusoidal architecture with marked dilation of interstitial spaces which were filled with eosinophilic material (edema and cellular debris) admixed with hemorrhage. The hepatocytes in this zone were markedly shrunken and the nuclei were often pyknotic and were often elongated (streaming). The hepatocytes in zone 2 were moderately shrunken with dense eosinophilic cytoplasm and nuclei were often deeply basophilic with loss of chromatin detail. The interlobular collagen bundles in this zone showed loss of normal architecture and often acquired deep pink staining (H&E) compared to the normal bright pink staining (Zone N). In zone 3 there was marked interstitial sinusoidal congestion with dilation of sinusoidal spaces (edema). The hepatocytes were slightly shrunken with mild loss of chromatin detail in the nuclei and the interstitial collagen bundles showed no significant changes. Zone 3 was within the transition between non-viable and viable tissue observed on TTC staining. Zone N represents liver area showing normal hepatocytes. The gall bladder sections adjacent to the ablation zone showed no significant microscopic lesions (Figure 4-6).

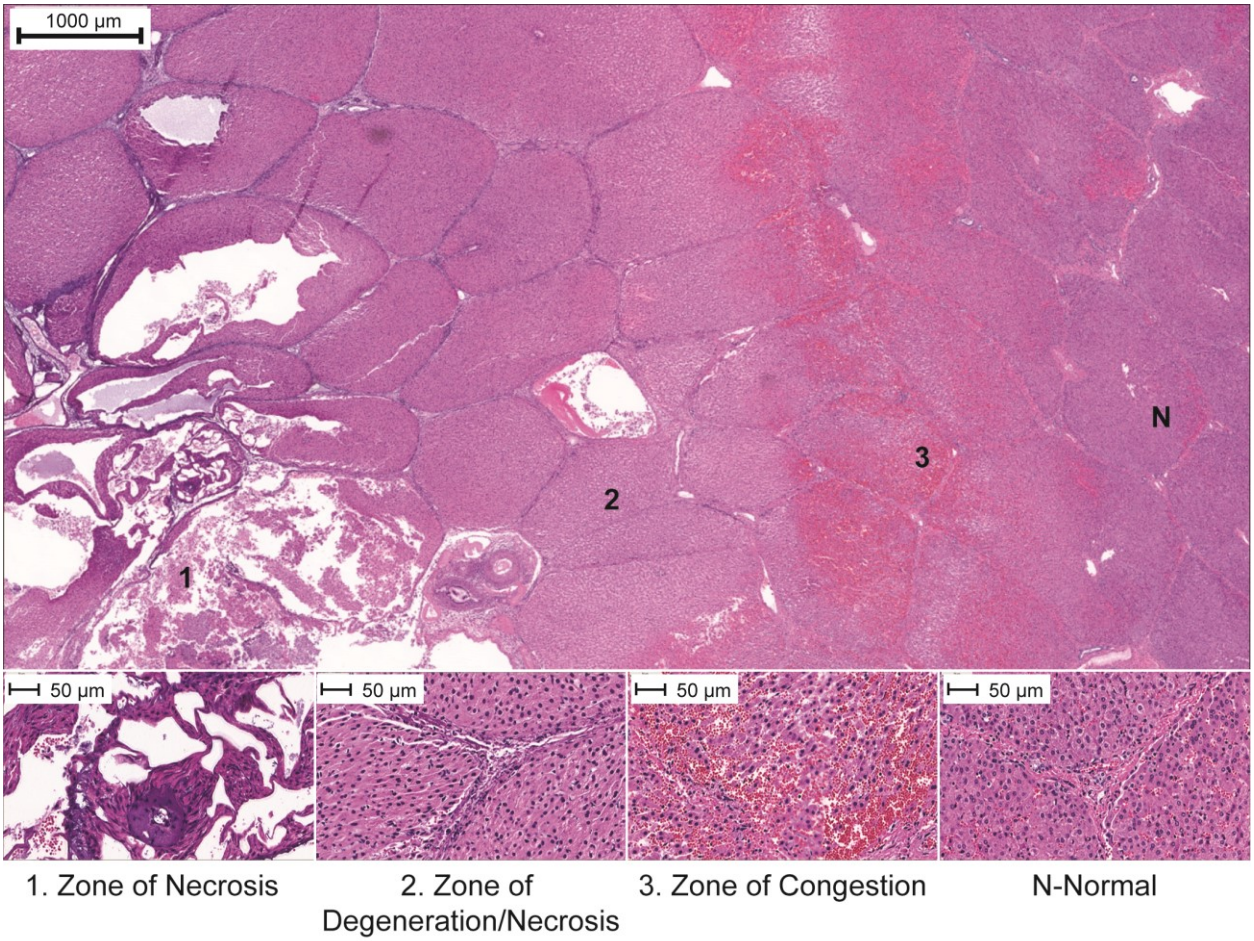

Figure 4-7: Example H&E stained liver ablation section showing three distinct zones of histological tissue morphology. The scale bar in the top image represents 1000 µm while the zoomed-in lower sub-images has a scale bar of 50 µm each. Zone 1 was the central area near the MWA applicator; there was complete loss of hepatic sinusoidal architecture with marked dilation of interstitial spaces which were filled with eosinophilic material (edema) and cellular debris admixed with hemorrhage. The hepatocytes in this zone were markedly shrunken and the nuclei were often pyknotic (necrosis) and elongated (streaming). In zone 2, the hepatocytes were moderately shrunken with dense eosinophilic cytoplasm and nuclei were often deeply basophilic with loss of chromatin detail (degeneration/necrosis). The interlobular collagen bundles in this zone showed loss of normal architecture and often acquire deep pink staining (H&E) compared to the normal bright pink staining (Zone N). In zone 3 there was marked interstitial sinusoidal congestion with dilation of sinusoidal spaces admixed with RBCs (edema and congestion). The hepatocytes were slightly shrunken with mild loss of chromatin detail in the nuclei and the interstitial collagen bundles showed no significant changes. Zone N represents liver area showing normal hepatocytes and connective tissue architecture.

Five 80 W, 5 minute “surface” ablations were performed and exhibited a mean depth of 7.8 ± 1.1 mm. The mean width was 12.8 ± 1.1 mm. In one procedure, the spleen and liver were held together with a light force of the physician’s hand to keep the experimental arrangement in place. A slight darkening of the surface of the spleen opposite the ablation zone was visible immediately post-procedure. Post-excision, the darkened region on the spleen’s surface was only faintly visible and no damage was noted once the tissue was sectioned and stained. For all other ablations of this type, no pressure other than the weight of the tissue was applied between the target and non-target tissues and there was no visible thermal damage to any non-target tissue post-procedure, post-excision, or post-staining. A sixth ablation was attempted using large intestine as the non-target tissue, but accidental relative motion between the applicator and tissue was observed during the procedure, resulting in two discontiguous and atypically small and shallow ablation zones in the liver and one small ablated region on the large intestine where the applicator had rotated to slightly aim towards the large intestine. Figure 4-8 provides a panel of images showing an experimental setup and post ablation results for the target and non-target tissues.

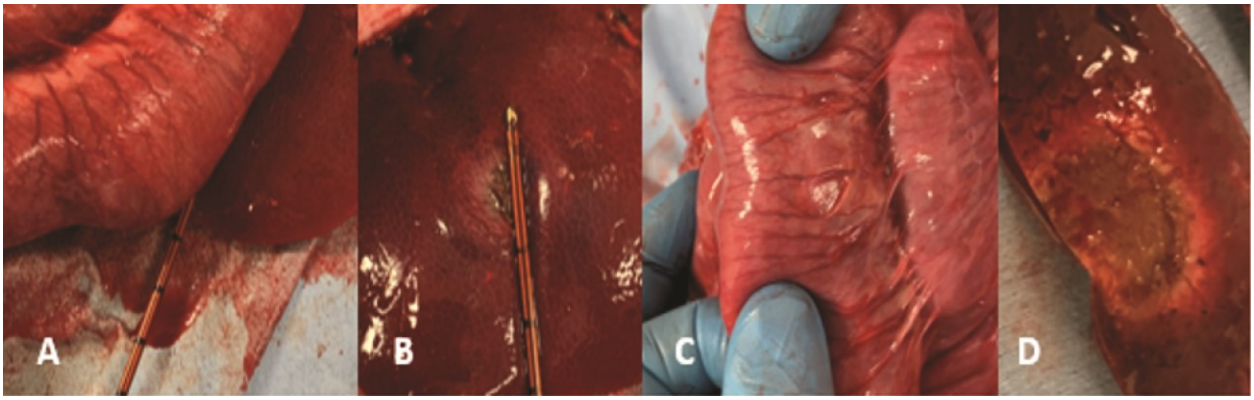

Figure 4-8: Experimental *in vivo* "surface ablation" setup with directional MWA applicator aimed at the liver and directed away from the large intestine (A). Post-procedure image showing a visible ablation zone on the surface of the liver. (B). Image of the section of large intestine in contact with directional MWA applicator spared free from any thermal damage (C). Cross-sectional slice showing the ablation zone extending into the liver (D).

4.4 Discussion

The ideal directional MWA applicator would have a directivity ratio approaching infinity (ablation of only the forward direction with no ablation in the reverse direction) to provide surety of protection of tissues in the backward direction. However, directional MWA is challenging to implement in a practical form. Directivity from microwave antennas is a function of the antenna size relative to the wavelength, with larger antennas dimensions affording enhanced directivity. Since applicators with diameter 14-gauge or smaller (< 2.1 mm) are desirable for minimally invasive percutaneous use, but wavelengths at microwave frequencies in tissue are ~2-4 cm, designing minimally invasive antennas with directional radiation patterns is technically challenging. Tissues also have non-zero thermal conductivity which means even if MW energy is radiated exclusively in the desired direction, the resulting temperature rise in the target sector will create a thermal gradient that could heat non-target sectors.

This study demonstrated the technical feasibility of designing directional MWA applicators with a small diameter (14-guage, 2.1 mm) and that using relatively lower power (60 – 80 W) and durations (3 – 5 minutes) improved directivity. Omni-directional MWA applicators commonly utilize high power and time settings to create high central peak temperatures that drive thermal conduction in all directions to achieve large ablation zones. However, for directional MWA, restricting power and duration leverages relatively more direct MW heating (vs. thermal conduction), reducing the magnitude and duration of the thermal gradient that drives conductive heating of surrounding non-target tissues. Due to the low power and duration strategy used in this study, experimental ablation zones had relatively small depths (8.3 – 15.5 mm *ex vivo*) but were remarkably consistent (standard deviations 0.0 – 1.5 mm in *ex vivo* tissue). In addition to directionality in the cross-sectional axis, the directional MWA applicator also demonstrated a very constrained ablation height along the longitudinal axis and did not display a long tail or teardrop shape.

Pilot animal studies showed improved directivity ratios over *ex vivo* results (increase of 148-153%) since the cooling effect of blood perfusion counteracts thermal conduction from the ablation zone hot spot and reduces unintended heating of non-target tissues. Furthermore, when the directional MWA applicator is placed between two distinct and separate tissue structures, the present pilot studies show a strong ability to heat only the target tissue while preserving the surrounding tissue. In addition to the applicator's directional radiation profile, this may also be due to the boundaries between heterogeneous tissue creating an "oven effect" which retains heat and reduces thermal transfer out of the target organ [44]. This effect may also amplify the ability of the applicator's circulating cooling water to conductively cool the non-target tissue.

A MWA applicator with directional control of the radiation pattern could simplify treatment of challenging tumors located near critical healthy tissues by directing heat away from sensitive anatomy such as the stomach, diaphragm, and colon with less need for additional thermoprotective techniques such as hydrodissection or balloon insertion. Directional MWA applicators could be enabling for the treatment of some tumors near other sensitive structures that are difficult to move or insulate with existing techniques, such as the bile ducts or gall bladder. Placing one or more directional MWA applicators beside and aiming towards a target (rather than central placement) could provide for a technically easier approach, reduce the risk of tumor seeding [39], and facilitate targeting of lesions that are difficult to pierce (such as small lung nodules that can be easily displaced in the relatively elastic parenchyma). Finally, placing a directional MWA applicator beside a small organ or gland, without penetrating it, to treat a shallow lesion with a "surface" ablation technique could enable treatment in glands or organs that are challenging or potentially risky to puncture, such as the adrenal gland. This method has been previously investigated *in vivo* to ablate porcine adrenal gland, where the ability to achieve subtotal ablation of the adrenal cortex, with minimal damage to the adrenal medulla, was demonstrated using a directional MWA applicator placed on the surface of the gland and delivering up to 70 W for 60 seconds [54]. Figure 4-9 provides example illustrations of how directional MWA could be utilized over existing techniques to treat challenging cases.

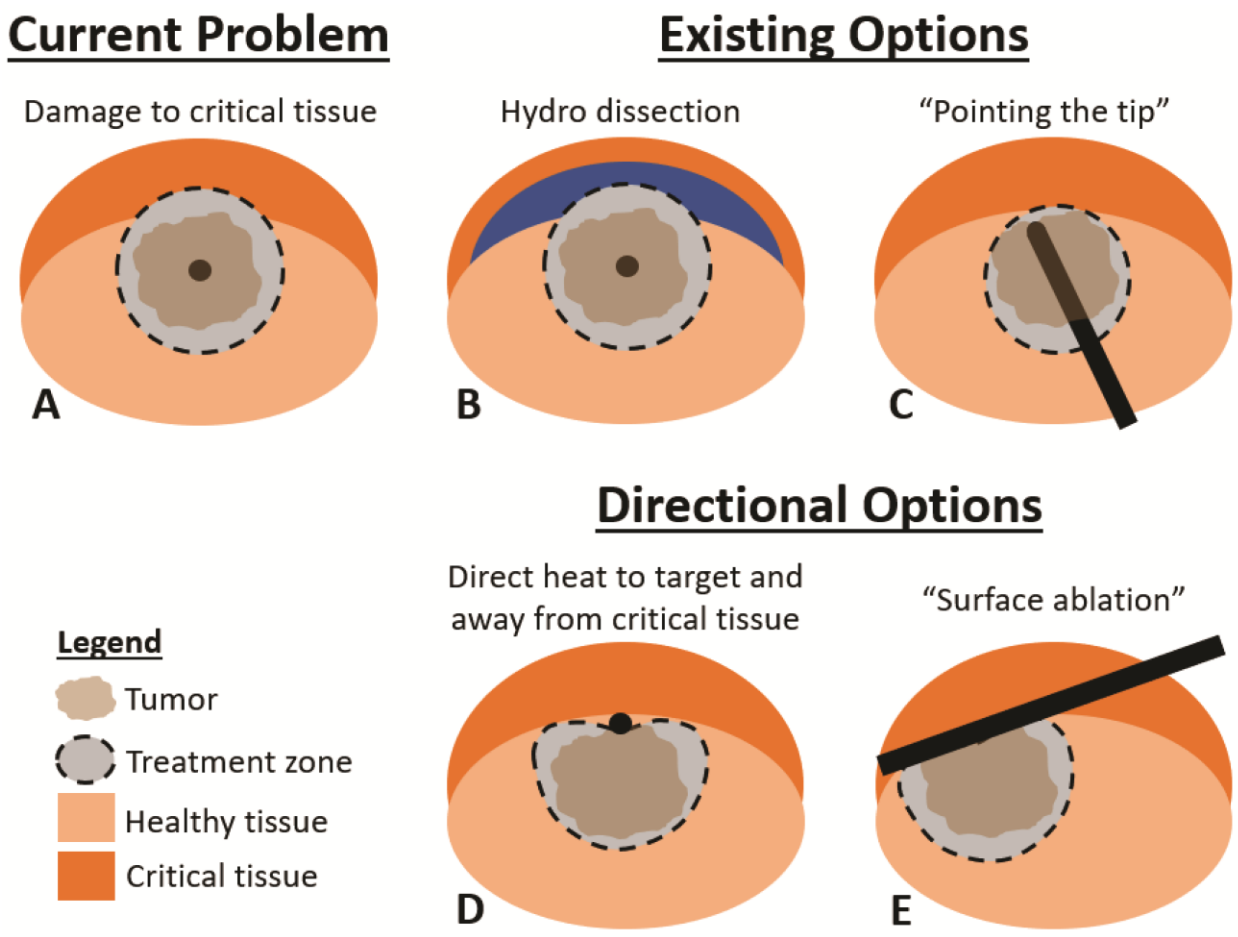

Figure 4-9: Use of cylindrically symmetric microwave ablation (MWA) applicators to attempt treatment of challenging tumors near critical tissue may cause inadvertent damage to that critical tissue. Existing techniques such as hydrodissection (B) can attempt to isolate and insulate the target from critical tissue through fluid injection while "pointing the tip" (C) leverages the idea that the thermal ablation zone typically does not extend very much past the tip of existing MWA devices. A Directional MWA applicator could enable procedures where energy is specifically directed toward the target and away from critical tissue (D) or "surface" ablation where the applicator does not have to penetrate the targeted organ or gland (E).

This study had some limitations. This was an acute study, with animals euthanized and tissue samples harvested within an hour after completion of all ablations. The microscopic changes in the liver are the result of acute injury secondary to microwave ablation. As is well established in the literature, assessment of thermal damage with H&E staining on tissue excised acutely (< 3 h) following thermal ablation does not provide conclusive evidence of the ultimate size of the

ablation zone, as the morphologic features of thermal injury will have had inadequate time to accrue and become microscopically visible [78]. Therefore, TTC viability stain was employed to assess the extent of the microwave ablation zone, similar to other acute studies. [79]–[81]. A long-term *in vivo* follow up study would be required to more clearly understand the significance of morphological changes in zones 2 and 3, and to conclusively determine the extent of complete cell death and necrosis in these zones. The applicator used in this study was developed to show proof of concept of an improved design, and the applied time and power combinations examined were selected to minimize backward heating, which resulted in overall ablation volumes substantially smaller than existing omni-directional devices. Additional animal studies will be necessary to fully characterize the directional applicators *in vivo* performance across a broader range of power levels and tissue types.

This study was undertaken to determine and characterize the ability of an experimental 14-guage, 2.45 GHz, water-cooled, MWA applicator to produce directional ablation zones in *ex vivo* and *in vivo* liver tissues. Directional MWA has the potential to reduce the need for thermoprotective techniques, enable treatment of challenging tumors near critical structures, and enable treatment of small tumors in challenging locations such as the lungs or adrenal glands. Further development is ongoing to increase the applicator's ablation volume while preserving directionality, and thereby expand the potential range of applications.

Chapter 5 - Investigation of power pulsing on a DMWA applicator's ablation zone size and directivity

5.1 Introduction

One of the advantages of MWA over other thermal therapy energy modalities is that the MW heating process can quickly achieve very high (>100 °C) central peak temperatures [82]. The high peak temperatures establish a steep thermal gradient that helps grow and expand the size of the ablation zone beyond the relatively small region of intense electromagnetic heating through thermal conduction. With conventional cylindrically-symmetric applicators, the thermal gradient expands the ablation zone in all directions and enables MWA to create larger treatment zones than competing energy modalities.

However, for directional MWA (DMWA) applicators that are designed to radiate MW energy in a preferred direction and develop directional ablation zones, excessive thermal conduction can be counterproductive. In this case, heat transfer through thermally conductive biological tissues can detrimentally expand the ablation zone into the non-target direction, causing an overall reduction in the directivity ratio (defined as the forward ablation depth divided by the backward ablation depth). When considering the anticipated clinical use of DMWA is to direct heat towards a target tumor while avoiding thermal injury to nearby critical anatomy, the necessity of limiting undesired thermal conduction in the backward direction is evident.

Reducing the applied power level would reduce the magnitude of the peak temperature driving the thermal gradient causing backward heating. Reducing the ablation duration would reduce the time thermal gradients are heating non-target sectors. However, with respect to

DMWA, a careful balance must be struck as excessive limitations on power and duration would also limit the forward ablation depth and total ablation volume, reducing the clinical utility.

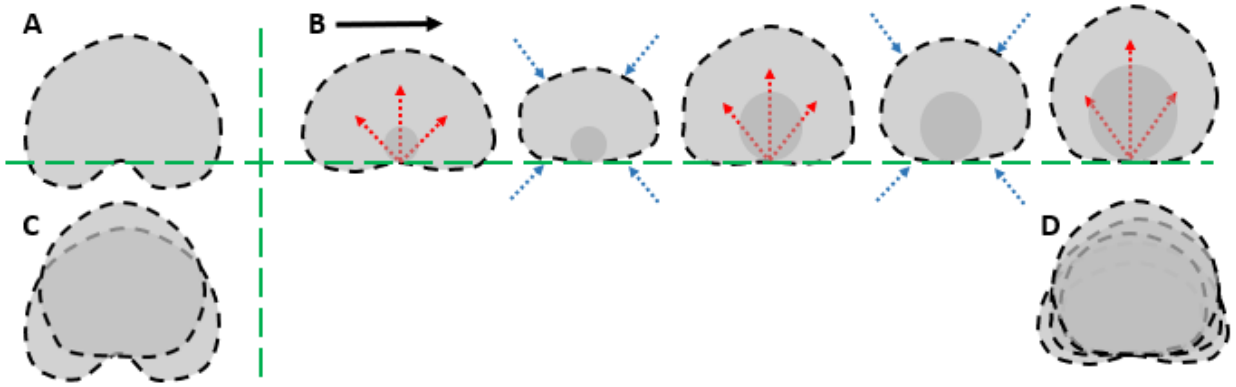

Figure 5-1: (A) Example ablation zone shape created by constant power level application. (B) Illustration of the changes in ablation zone shape as it grows when power is cycled on and contracts as power is cycled off and the effects of blood perfusion dominate. (C) Example overlay of equivalent energy constant power and modulated power ablation zones showing improved directivity of a modulated power approach. (D) Overlay of all modulated power cycle ablation zones showing a continual improvement in directivity.

One hypothetical method to balance the need to produce clinically useful ablation zone volumes with maintaining directivity could be controlling the duty cycle of the DMWA applicator's applied power. During the "on" portion of the cycle, MW energy would be radiated and deposited in the tissue region dictated by the design of the directional antenna. This region would rapidly heat, modifying the electrical and thermal properties of the tissue through desiccation and dehydration; at ~55-60 °C the tissue would coagulate, shutting off the heat sink effect of blood perfusion [83]. During the "off" portion of the cycle, excessive rise of the central peak temperature would be halted; blood perfusion in the surrounding tissue would cool the ablation zone margin, particularly in the non-target sectors to the side and behind the applicator. When the "on" portion of the cycle returns, the MW energy would be absorbed incrementally

less in the previously heated and partially desiccated tissue and radiate incrementally further in the forward direction. This could shift the thermal "hot spot" of the ablation more toward the desired direction and further from the undesired direction, reducing thermal gradients driving heat transfer to the non-target sectors and improving ablation directivity.

Past studies have shown ramped and pulsed power protocols appear to have limited or no benefit compared to continuous power for ablation size or sphericity, with higher applied power being the most significant factor for creating larger omni-directional ablation zones [22], [84], [85].

However, the unintended backward heating during DMWA is mostly a consequence of thermal conduction rather than direct electromagnetic heating, and it may be better controlled by a power pulsing protocol rather than continuous high power application. Furthermore, as limiting backward heating would be of high importance for clinical users who are concerned with precision control of the treatment zone and avoidance of thermal damage to non-target nearby critical anatomy, marginal improvements in directivity during DMWA may be still clinically significant. In this study, computational modeling and simulation were conducted to determine the impact of duty cycle and cycle period on backward ablation depth, forward ablation depth, and directivity ratio when controlled for total energy delivery. *Ex vivo* and *in vivo* experimentation was conducted to validate the modeling.

5.2 Methods

5.2.1 Directional Microwave Ablation Applicator

The DMWA applicator design considered for this study is an experimental 2.45 GHz, , water-cooled, 14-gauge design which has been previously characterized in *ex vivo* and *in vivo*

liver tissues [38]. Specifically, ablation zone extents following 100 W, 5 min heating provided by Pfannenstiel *et al.* were used as experimental baselines to develop and validate *ex vivo* and *in vivo* computational models [38]. The applicators used in experimental testing were variants of the above mentioned design with very similar internal structure, but either fiberglass (F1.1 with raw fiberglass shaft and F1.2 with fiberglass coated in Loctite 4011) or steel with a PEEK transition near the antenna (S2.1 and S 2.2) outer shafts.

5.2.2 Computational Model

A 3D finite element method (FEM) solver (COMSOL Multiphysics v5.5, COMSOL, Inc. Burlington, MA) was used to model the electromagnetic radiation pattern and subsequent heat transfer from the MWA applicator in a manner similar to that reported by McWilliams et al. and Sebek et al [86], [87]. The model was used to solve the Helmholtz electromagnetic wave equation:

Equation 5-1

$$\nabla^2\mathbf{E} - k_0^2\left(\varepsilon_r - \frac{j\sigma}{\omega\varepsilon_0}\right)\mathbf{E} = 0$$

where, **E** [V/m] is the electric field, k_0 [m^{-1}] is the free-space wavenumber, ε_r is relative permittivity, σ [S/m] is effective conductivity, ω [rad/s] is anugular frequency, and ε_0 [F/m] is permittivity of free-space. The distal 6 cm of the applicator was modeled inserted into an 8 x 8 x 8 cm cube of homogenous liver tissue. The electrical properties of the liver tissue are provided in Table 5-1. Scattering boundary conditions were applied at the extents of model. All metallic elements were modeled as perfect electrical conductors with infinite conductivity. A coaxial port

boundary condition was established at the proximal of the coaxial cable dielectric and used to set the applicator's forward power of 53.7 W. This power level corresponds to a 100 W generator output after accounting for the sum of insertion losses in the transmission lines and connectors [-1.54 dB from 2.5 m of Succoform 141 (measured) + -0.17 dB from QMA to SMA adapter (datasheet) + -0.73 dB from 0.25 m of UT-034 (extrapolated from datasheet) + and -0.20 dB from SMA connector (estimated) = -2.64 dB].

Table 5-1 Material Electrical/Thermal Properties

Parameter	Value	Unit	Temperature Dependency
Water relative permittivity, ε_r	77.6	-	Constant
Water electric conductivity, σ	1.32	S/m	Constant
FEP, ε_r [88]	2.1	-	Constant
Polyimide, ε_r [88]	3.4	-	Constant
Liver relative permittivity, ε_r [89]	43.0	-	Smoothed Step [90], [91]
Liver electric conductivity, σ [89]	1.69	S/m	Smoothed Step [90], [91]
Liver density, ρ [92]	1079	kgm^{-3}	Constant
Liver specific heat capacity, c [92]	3540	$Jkg^{-1}K^{-1}$	Piecewise Constant [92]
Liver thermal conductivity, k [92]	0.52	$Wm^{-1}K^{-1}$	Smoothed Step [92]
Liver blood perfusion rate, ω_{bl} [92]	40,000	$Wm^{-3}K^{-1}$	Smoothed Step [92]

The electromagnetic loss in the tissue domain was computed from the simulated electric field based on:

Equation 5-2

$$Q_{mw} = \frac{1}{2}\sigma \cdot |\mathbf{E}|^2$$

which was then coupled with Pennes' bioheat equation to compute the transient temperature profiles within the tissue:

Equation 5-3

$$\rho c(\mathrm{T})\frac{\partial \mathrm{T}}{\partial t} = \nabla \cdot k(T)\nabla \mathrm{T} + \mathrm{Q}_{mw} - \omega_{bl}(\mathrm{T} - \mathrm{T}_{bl})$$

where ρc is volumetric heat capacity [$Jm^{-3}K^{-1}$], T is temperature [K], k is thermal conductivity [$Wm^{-1}K^{-1}$], ω_{bl} is blood perfusion [$Wm^{-3}K^{-1}$], and T_{bl} is the temperature of blood. Table 5-1 lists the tissue thermal properties used in simulation including their type of temperature dependence. The initial temperature of the tissue domain was set to 37 °C to mimic living tissue. To simulate the forced cooling of the applicator, a 30 °C isothermal boundary condition was applied to the outer surface of the applicator. This was based on preliminary data from steady-state readings of 26-28 °C from an internal thermocouple of an early industrialized DMWA applicator prototype operated at 80W (lower cooling flow rate, but reduced insertion losses). The use of isothermal boundary conditions to model forced cooling of the applicator is a substantial simplification of multiple complex heat exchange processing including microwave heating of the chilled cooling water near the antenna, heat transfer from attenuation losses in the applicator transmission cable, and heat transfer between the surrounding tissue and the applicator surface and has been previously proposed in literature [93]. In reality, these heat transfer effects almost certainly contribute to a temperature gradient along the outer surface of the applicator which likely approaches 100 °C near the applicator distal tip and then reduces to approximately the cooling water inflow temperature several cm proximal from the antenna element. For a DMWA applicator design, there would also be a temperature gradient from the front to backside of the applicator. However, this temperature gradient is difficult to measure directly and computationally intensive to model due to its dependence on several independent variables.

Temperature dependence was implemented for tissue relative permittivity and conductivity to account for changes as tissue is heated and desiccated [90], [94]. Temperature dependence was also implemented for tissue specific heat capacity to account for the latent heat of vaporization of the water in the tissue and for thermal conductivity to reflect a slight increase at elevated temperatures. Finally, temperature dependence was also implemented for *in vivo* simulations to account for the increased cooling effect of blood perfusion as tissue temperature increases until approximately 60 °C when blood coagulation causes perfusion to permanently cease. An additional step was included in the computational model to integrate the time when a tissue element first exceeded 60 °C, in order to prevent the perfusion from returning in that element even if temperature reduced below 60 °C during the power-off portion of the cycle.

An implicit transient solver was used with a maximum time step of 1 s where at each step temperature dependent thermal and electrical properties were updated. A non-uniform tetrahedral mesh was constructed with maximum edge size of 0.01 mm at the port boundary, 0.2 mm throughout the applicator, and 5 mm in the tissue domains. Additionally, a 1 cm^3 cube with a mesh maximum edge size of 1 mm and growth rate of 1.3 with its face centered on the applicator at the midpoint of the antenna was included to improve resolution in the region of most intense electromagnetic heating. With the above mesh settings, a coupled electromagnetic heat transfer 600 s duration, 50 % duty cycle, 20 s period simulation took 44 hours to compute with an Intel Xeon W-2225 CPU @ 4.1 GHz and 64 GB of memory.

Ex vivo ablations were simulated by setting $\omega_{bl} = 0$. The forward and backward *ex vivo* ablation zone dimensions were measured at the extent of the 55 °C isothermal contour plot and compared to the *ex vivo* experimental 100 W, 5 min data presented in [38] to validate the electrical and most of the thermal aspects of the model. *In vivo* ablations were modeled by

setting a non-zero value for the blood perfusion coefficient, ω_{bl}. Several values of ω_{bl}, ranging from 10,000 to 68,298 W/m^3/K were evaluated for a best match of simulated results to prior *in vivo* data. While 10,000 W/m^3/K provided the best match of simulated to prior experimental results, the calculated blood perfusion coefficient for normal human hepatic blood flow is 68,298 W/m^3/K. To provide a suitable balance between theoretical calculations and experimental data, ω_{bl} was set at 40,000 W/m^3/K for all simulated *in vivo* ablations.

To test the effect of adjusting the duty cycle and period of applied MW power on ablation size and directivity, a square wave with amplitude ranging from 0.01 to 1.01 was multiplied with the Q_{mw} term in the heat source equation in the computational model. A range of periods (T = 20, 10, 5) and duty cycles (50% and 75%) were examined. Simulation duration was adjusted as necessary to deliver an equivalent power as experimental ablations at 53.7 W (applicator) continuous power for 5 min (300s) = 16,110 J. To investigate how variability in the blood perfusion rate may impact power pulsing's ability to affect the ablation zone size and directivity, ω_{bl} values of 0, 20,000, 40,000, and 60,000 W/m^3/K were simulated for a pulsed power with a 75% duty cycle and 10 second period.

Simulated ablation zone forward and backward depths were measured as the distance extending from the DMWA applicator outer wall to the 55 °C contour – forward ablation depth was refenced to the posterior face of the applicator while backward ablation depth was referenced to the anterior face of the applicator. Positive backward depths indicate the simulated ablation zone extended behind the applicator while negative backward depths indicate the simulated ablation zone did not extend behind the applicator.

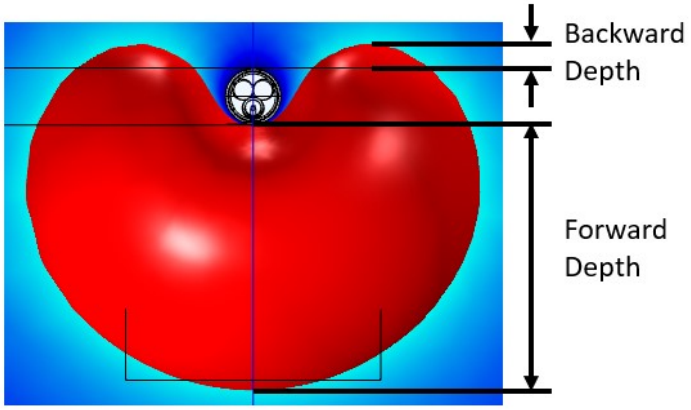

Figure 5-2: Measurement method for quantifying the size and shape of simulated DMWA zones

Although *ex vivo* tissues do not have blood perfusion and therefore do not provide any direct cooling affects, *ex vivo* ablations were performed as validation testing for the prototype industrialized DMWA applicators and to investigate if power pulsing would have any observable effect on ablation size and directivity if only losses to ambient were present. Bovine liver was sectioned into 6 x 6 x 6 cm cubes, sealed in plastic bags, and warmed to approximately 37 °C in a temperature-controlled water bath. A custom 3D printed fixture facilitated consistent applicator insertion angle and depth into the tissue samples. A peristaltic pump (Energize Medical, Lenexa, KS) was used to circulate ice water through the applicators at a flow rate of approximately 30-50 mL/min. Microwave power was supplied to the applicator using a developmental microwave generator (Energize Medical, Lenexa, KS) capable of operating in continuous or pulsed output modes. Experimental ablations were performed at 80 W (generator setting) for 5 minutes in continuous operation or 80 W for 7 minutes 9 seconds in pulsed (7 seconds on , 3 seconds off) mode; continuous and pulsed output experiments were each repeated $n = 4$ times for 4 applicators, for a total of 32 ablations. The pulse timing of 7 seconds on and 3 seconds off, resulting in a 70% duty cycle, was used instead of the 75% duty cycle simulated because the

generator used could only select the on and off time in whole seconds. Furthermore, 80 W generator power was used instead of 100W as simulated to limit potential fatigue on these first-use experimental applicators before follow-on *in vivo* testing. Applicator internal temperature was measured by a thermocouple probe inside the applicator shaft and monitored by a Fluke 52 II digital thermometer. Applicator temperature was not logged, and fluctuated during an ablation, but a single value approximately representative of the average temperature was recorded. Liver surface temperature was also recorded immediately prior to the commencement of an ablation experiment using a thermocouple probe and the same Fluke 52 II thermometer. Reflected power was displayed on the MW generator and a single value approximately representative of the average reflected power was also recorded.

Tissue samples were sliced perpendicular to the axis of the applicator to measure and document the forward and backward depth, width, and shape of the ablation zone based on the extent of tissue whitening. Forward depth was measured to include only brown or white regions whereas backward depth was measured to include any visible zones, including light pink, thus providing the most conservative (i.e. lower bound) measure of directivity. Figure 5-3 provides an example of how measurements were taken. Ablation shape was characterized by the directivity ratio, defined as the ratio of the forward depth to the backward depth.

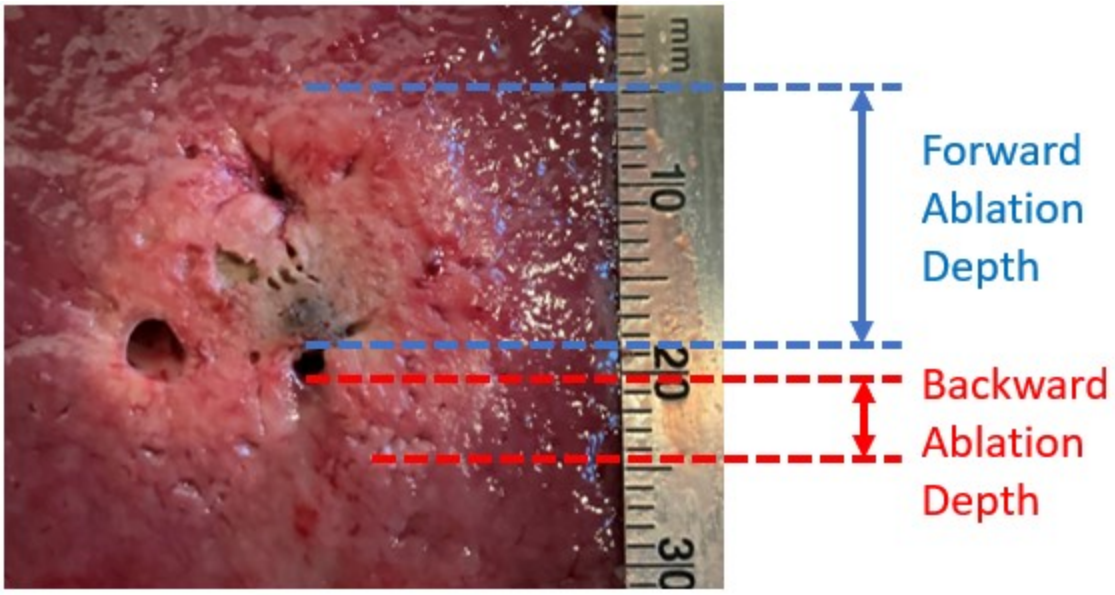

Figure 5-3: Representative image of how directional ablation zone extents were measured in *ex vivo* liver

In vivo experiments were conducted using two of the industrial DMWA applicator variants. All *in vivo* experiments were carried out under an experimental protocol approved by the local Institutional Animal Care and Use Committee. Experiments were conducted in two 45 – 50 kg, female domestic swine. Pigs were premedicated with Atropine (0.05 mg/kg, IM) and anesthesia was induced by an intramuscular injection of 4.4 mg/kg Telazol, and 2.2 mg/kg Xylazine. Pigs were orotracheally intubated and anesthesia was maintained by isofluorane in O_2. Anesthetized pigs were positioned in dorsal recumbency and a ventral midline incision was made from the umbilicus extending cranially to the xyphoid. The MWA applicator was inserted directly into the approximate center of mass of a liver lobe with the goal of ablating a homogenous section of the lobe. Continuous power ablations were conducted at 100 W for 5 minutes (n = 8) and pulsed power ablations were conducted at 100 W for 7 minutes 9 seconds with power on for 7 seconds followed by off for 3 seconds per cycle (n = 8). Eight ablations were performed in each of the two animals used in the study. All eight ablations per animal were

conducted using the same DMWA applicator (a different DMWA applicator was used in each animal). Continuous and pulsed mode ablations were alternated to control for any gradual degradation in applicator performance. Upon completion of each ablation the applicator was removed and a wooden dowel, marked with colored bands corresponding to the ablation number, was inserted along the applicator track to enable proper localization and identification of the thermal lesion post-procedure.

Pigs were euthanized at the conclusion of the ablation procedure while still under anesthesia. Euthanasia was performed by intravenous injection of sodium pentobarbital 390 mg/ml at a rate of 0.2 ml/kg of body weight. Following euthanasia, the livers were harvested, sectioned in ~5 mm thick axial slices, and stained for viability with triphenyltetrazolium chloride (TTC), enabling more accurate identification of ablation zone extents [12]. The sections were then fixed in 10 % buffered formalin and embedded in paraffin blocks. Approximately 5 μm thick hematoxylin and eosin (H&E) stained sections were obtained from the paraffin embedded samples for histologic examination.

5.3 Results

The simulated continuous power *ex vivo* model 55 °C contour at 300 s had a forward depth of 14.24 mm compared to 13 +/- 0.8 mm experimental (+9.5%) and a backward depth of 3.85 mm simulated vs 2.0 +/- 0.0 mm experimental (+92.5%). The simulated continuous power *in vivo* model 55 °C contour at 300 s had a forward depth of 10.54 mm compared to 11.3 +/- 2.9 mm experimental (-6.7%) and a backward depth of 0.96 mm simulated vs 0.7 +/- 0.6 mm experimental (+37.1%). The simulated forward and backward 55 °C contour depths for the

pulsed power models are listed in Table 5-2 below. The percentages in Table 5-2: Simulated Ablation Depths are refenced to the 100% duty cycle, 300 s base *in vivo* simulation (line 2).

Table 5-2: Simulated Ablation Depths

Power (W)	T (s)	DC (%)	Duration (s)	ω_{bl} (W/m3/K)	Fwd (mm)		Bkwd (mm)	
53.7		100	300	0	14.24		3.85	
53.7		100	300	40000	10.54		0.96	
53.7	5	50	600	40000	6.84	-35.1%	-1.88	295.9%
53.7	5	75	400	40000	9.02	-14.4%	-0.77	180.6%
53.7	10	50	600	40000	7.52	-28.7%	-1.51	257.2%
53.7	10	75	400	0	14.30	35.7%	2.813	-193.0%
53.7	10	75	400	20000	11.16	5.9%	0.66	31.5%
53.7	10	75	400	40000	9.49	-10.0%	-0.35	136.1%
53.7	10	75	400	60000	8.45	-19.8%	-0.78	181.5%
53.7	20	50	600	40000	7.74	-26.6%	-1.19	223.6%
53.7	20	75	400	10000	9.55	-9.4%	-0.21	122.2%

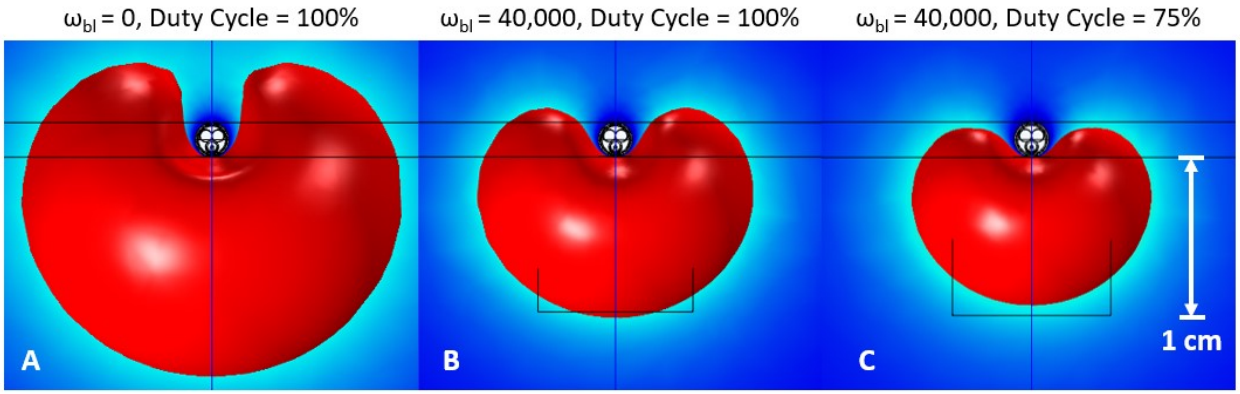

Figure 5-4: Simulated continuous power *ex vivo* (A) and *in vivo* (B) and pulsed power *in vivo* (C) ablation zone 55 °C contours.

Table 5-3 lists the experimentally observed *ex vivo* ablation zones. Of note, applicator S2.1 suffered a failure and only 2 continuous and 2 pulsed ablations are provided in its dataset compared to 4 for all other applicators. Aggregated data of all 4 applicators shows power pulsing

with a 70% duty cycle while applying equivalent total energy resulted in a 51.7% smaller backward ablation depth, a 2.3% larger forward ablation depth, and a 115.2% greater directivity ratio.

Table 5-3: *Ex Vivo* Continuous and Pulsed Power Experimental Results at 80 W.

App #	DC (%)	*n*	Fwd (mm)	Bkwd (mm)	DR	W (mm)	$T_{applicator}$ (°C)	T_{liver} (°C)	$P_{reflected}$ (W)
JVIR	100	4	**13.3 ± 1.0**	**2.3 ± 0.5**	**5.8**	23.3 ± 1.0			
F1.1	100	4	12.8 ± 0.5	2.0 ± 1.4	6.4 ± 5.0	21.0 ± 1.4	22.9 ± 1.0	37.2 ± 2.0	2.5 ± 2.0
F1.2	100	4	13.3 ± 1.0	2.8 ± 1.0	4.8 ± 1.8	23.0 ± 1.6	31.8 ± 14.2	37.1 ± 0.8	4.3 ± 1.4
S2.1	100	2	14.0 ± 1.4	3.5 ± 0.7	4.0 ± 0.4	22.5 ± 0.7	23.0 ± 2.1	37.2 ± 1.2	2.0 ± 0.7
S2.2	100	4	13.0 ± 0.0	3.3 ± 0.5	4.0 ± 0.5	22.0 ± 0.0	27.8 ± 2.5	36.6 ± 1.7	5.3 ± 0.9
AVG			**13.3**	**2.9**	**4.6**	22.1	26.4	37.0	3.5
F1.1	70	4	12.8 ± 1.0	1.8 ± 0.5	7.3 ± 3.4	21.5 ± 1.0	22.7 ± 1.5	35.2 ± 1.1	2.0 ± 1.7
F1.2	70	4	14.0 ± 0.8	2.3 ± 1.0	6.2 ± 4.4	22.5 ± 1.7	32.6 ± 3.5	37.3 ± 1.3	4.1 ± 0.9
S2.1	70	2	14.5 ± 2.1	0.5 ± 0.7	29.0	22.5 ± 0.7	22.9 ± 1.8	37.3 ± 1.0	2.0 ± 0.7
S2.2	70	4	13.0 ± 0.8	1.0 ± 0.6	13.0 ± 3.8	22.0 ± 0.5	26.4 ± 2.3	35.6 ± 1.8	5.5 ± 0.8
AVG			**13.6**	**1.4**	**9.9**	22.1	26.1	36.3	3.4

Table 5-4 lists the experimental results for the *in vivo* ablations. Of note, applicator F1.2 experienced a slow continual degradation in performance resulting in rising internal temperatures and reflected power. Two of the continuous power ablations with F1.2 experienced internal temperatures > 60 °C and were discarded from the data set. Two of the F1.1 ablations, one continuous and one pulsed, could not be accurately identified post-excision of the liver and are therefore also not included in the data set. One F1.1 continuous ablation had a backward ablation zone that extended to contact the outer surface of the liver while one F1.1 and one F1.2 pulsed ablation had a forward ablation zone that extended to contact the outer surface of the liver due to

inadvertent applicator placement near these surfaces. Though these ablations had slightly distorted shapes, their measurements are included in the *in vivo* dataset. Aggregated data of both applicators shows power pulsing with a 70% duty cycle while applying equivalent total energy resulted in a 40.1% smaller backward ablation depth, a 1.0% smaller forward ablation depth, and a 59.6% greater directivity ratio.

Table 5-4: *In Vivo* Continuous and Pulsed Power Experimental Results at 100 W.

App #	DC (%)	*n*	Fwd (mm)	Bkwd (mm)	DR	W (mm)	$T_{applicator}$ (°C)	$P_{reflected}$ (W)
JVIR	100	3	**11.3 ± 2.9**	**0.7 ± 0.6**	**16.1**			
Simulation	100		**10.5**	**1.0**	**11.0**	17.9		
F1.1	100	3	9.7 ± 0.6	2.3 ± 0.6	4.1 ± 0.9	14.0 ± 2.0	24.5 ± 3.9	3.8 ± 4.0
F1.2	100	2	10.5 ± 0.7	2.0 ± 0.0	5.3 ± 0.4	13.5 ± 0.7	48.3 ± 3.8	10.0 ± 0.7
AVG			**10.1**	**2.2**	**4.7**	13.8	36.1	7.4
Simulation	75		**9.5**	**-0.3**	**-31.6**	15.2		
F1.1	70	3	11.0 ± 1.7	1.7 ± 0.6	6.6 ± 2.6	17.3 ± 3.1	24.5 ± 1.8	4.0 ± 2.8
F1.2	70	4	9.0 ± 2.4	1.0 ± 0.0	9.0 ± 2.4	12.0 ± 2.2	47.1 ± 6.7	10.4 ± 0.6
AVG			**10.0**	**1.3**	**7.5**	14.7	35.3	7.6

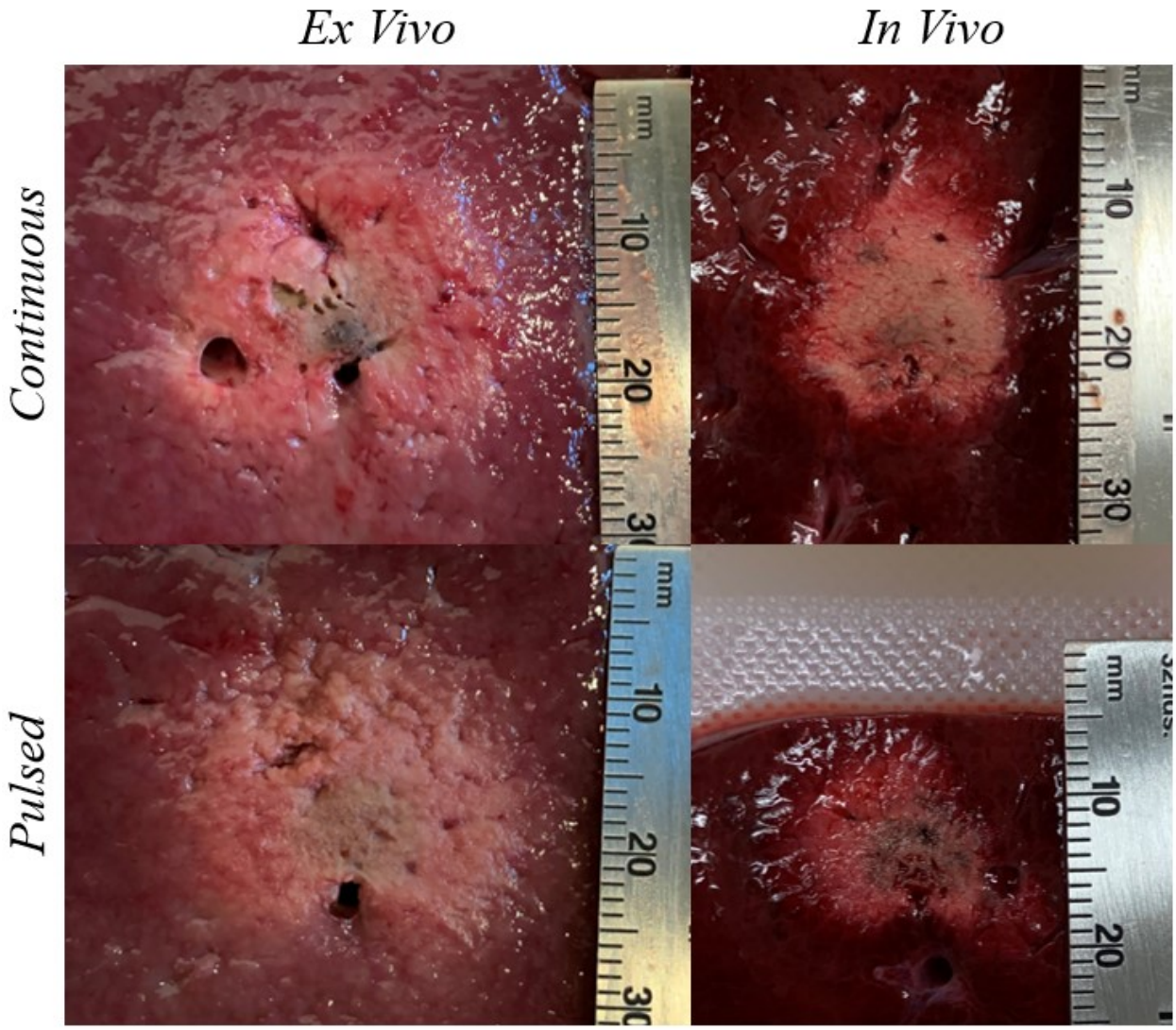

Figure 5-5: *Ex vivo* (80 W applied power) and *in vivo* (100 W applied power) ablation zones with continuous and pulsed power (70% duty cycle) using applicator F1.2.

5.4 Discussion

Power pulsing simulations at a 75% duty cycle showed a 136% reduction in backward ablation depth while *ex vivo* and *in vivo* experiments at a 70% duty cycle showed a 51.7% and 40.1% reduction in backward ablation depth, respectively. *Ex vivo* and *in vivo* data showed pulsing has minimal positive or negative impact on forward ablation depth, essentially in line with prior studies that showed power pulsing protocols had limited impact on the size or

sphericity of omni-directional ablation zones [22], [84], [85]. Though power pulsing does not seem to offer an improvement in forward ablation depth, reduced backward heating, confirmed by simulation and both *ex vivo* and *in vivo* experiments, resulted in an overall improvement in the directivity ratio for DMWA. With further development, power pulsing protocols may be warranted in a subset of niche DMWA cases were minimizing backward heating is especially important. Examples of such cases may include tumors near critical structures where thermoprotective techniques cannot be employed or treating metastatic tumors in the vertebral body near the spinal cord.

However, this study had several limitations. The variation in ablation zone size and shape when using a pulsed power scheme instead of continuous power is very small in absolute terms. The variation is also especially small in relative terms compared to the potential error in measuring experimental ablation zones where the potential failure to cut perpendicular to the applicator axis, potential failure to slice along the maximal plane, and difficulty accurately identifying faint and diffuse ablation zone boundaries all contributing to measurement inaccuracy. Several of the *in vivo* ablations were also located near the liver surface or large veins or arteries which skewed their shape – this is because there is very limited accessible liver available with sufficient thickness in a 45-50 kg pig to conduct this research. Furthermore, one of the developmental DMWA applicators (F1.2) used in both the *ex vivo* and *in vivo* datasets clearly suffered a continuous degradation in performance which could have skewed experimental results. As such, not enough experimental datapoints were collected to draw a definitive conclusion about power pulsing ability to affect a DMWA applicator's directivity ratio in a clinically relevant setting. Though this study focused on constant power, equivalent energy input

power pulsing schemes, further work should be conducted to determine if altering the input power, i.e. doubling the generator power, has a more significant effect on ablation directivity.

Finally, the significant discrepancy between the continuous power simulated and experimental backward ablation depth (+92.5% *ex* vivo and +37.1% *in* vivo) while there was better agreement with forward ablation depth (+9.5% *ex* vivo and -6.7% *in* vivo) may indicate the computational model's isothermal applicator boundary condition fails to fully account for the substantial cooling effect of the circulating cooling within the applicator and its ability to provide an additional degree of thermal protection to the tissues in the non-target direction – especially during the time it is providing active cooling to the tissues adjacent to the applicator while MW power is off. Given the significant affect applicator forced cooling has on the backward ablation depth, additional work is needed better develop the thermal and heat transfer physics in the DMWA applicator computational model.

5.5 Conclusion

Power pulsing simulations showed a 136% reduction in backward ablation depth while *ex vivo* and *in vivo* experiments showed a 52% and 40% reduction in backward ablation depth. Power pulsing simulations showed a 10% reduction in forward ablation depth while *ex vivo* and *in vivo* experiments showed a 2.3% increase and 1.0% reduction in forward ablation depth, respectively. The resulting improvement in directivity ratio for power pulsing experiments compared to continuous power experiments in *ex vivo* and *in* vivo tissue was 115% and 6.5% respectively (simulations predicted negative backward heating). Applying pulsed power during DMWA has demonstrated some potential to reduce backward heating with limited impact to forward ablation depth, therefore increasing the resulting directivity ratio of the ablation zone.

Power pulsing may have increased benefit for low-perfused vs. highly perfused tissues. Further data is necessary to better quantify the benefits of DMWA power pulsing in a clinically relevant setting.

Chapter 6 - Bone DMWA

6.1 Introduction

According to the National Cancer Institute, there will be an estimated 1,762,450 new cases of cancer diagnosed and 606,880 cancer deaths in 2019 [95]. Approximately 39.3 percent of men and women will be diagnosed with cancer of any site at some point during their lifetime [95]. Although cancer mortality rates have declined 1.5% per year on average from 2007-2016 [95], the United States national expenditure for cancer care reached $147.3 billion in 2017 and costs are likely to increase as the population ages, cancer prevalence increases, and new more expensive treatment options are adopted [96]. Furthermore, improved treatments are allowing patients to live longer with cancer, putting them at increased risk for developing metastatic disease [97].

Bone is the third most common site where metastatic cancer spreads [97]. Bladder, breast, kidney, lung, melanoma, prostate, thyroid, and uterine cancer all commonly metastasize to bone and often bone can be the first site attacked [97], [98]. Bone is attacked in 60-84% of all metastatic cases, and approximately 70% of those patients have resulting bone pain [97]. Bone metastases can also increase a patient's risk of fractures, spinal cord compression, hypercalcemia, and other associated complications which may increase mortality [97].

Common treatments for primary bone cancer include surgery, chemotherapy, and radiation therapy. Surgery may require special techniques to remove the tumor and then replace the lost bone with bone from another area of a patient's body, metal, or hard plastic [99]. Chemotherapy and radiation therapy may be less invasive, however, none of these typical treatment options may be possible, effective, tolerable, or fast-acting enough for a very ill patient who has progressed to an advanced stage of metastatic cancer. Minimally invasive options,

including thermal ablation systems, are being investigated and developed for use in bone. For example, a recently introduced clinical RF ablation system has been approved for indications including; palliative treatment in spinal procedures by ablation of metastatic malignant lesions in a vertebral body, coagulation and ablation of tissue in bone during surgical procedures including palliation of pain associated with metastatic lesions involving bone in patients who have failed or are not candidates for standard therapy, and ablation of benign bone tumors such as osteoid osteoma [100].

Of the possible thermal ablation energy modalities, each offers a different set of clinical advantages and disadvantages specific to use in bone. Cryoablation, which uses the Joule-Thomson effect to create rapid cooling though the expansion of gases in a cryoprobe chamber offers the advantage of creating a visible ice ball on CT [101], however, the multiple freeze-thaw cycles can be time consuming, especially if the resulting treatment zone requires backfill with structural cement or epoxy post thaw [48]. Cryoablation procedures are also more expensive (than radiofrequency or microwave ablation). Radiofrequency (RF) systems are typically the lowest cost, and can be configured to provide some spatial control, however, they rely on ionic agitation caused by the passage of high-frequency alternating current, which may have limited effect in high impedance (low conductivity) tissues such as bone [102], [103]. The extent of the RFA thermal treatment zone cannot be visualized in real-time by conventional imaging methods and therefore may risk thermal injury to nearby healthy critical anatomy. The use of high intensity ultrasound has also been proposed for treatment of tumors surrounded by bone, as the high acoustic absorption coefficient helps to confine the treatment zone primarily to the target, thereby protecting adjacent critical structures [49], [50].

During MWA, the cellular damage results from kinetic heating of polar molecules (such as water and proteins) that rapidly oscillate as they try to align with the applied electromagnetic waves propagating through tissue. MWA offers the advantages of rapid treatment times and the ability to radiate though high impedance tissue, however, similar to RFA, the extent of the thermal treatment zone cannot be determined in real-time with currently available imaging tools. However, advances in the development of a directional MWA applicator may afford the necessary spatial control of heating to enable precision MWA treatment in areas in close proximity to heat-sensitive critical anatomical structures [38]. An example use case for directional MWA may be treatment of metastatic disease in the vertebral body that is impinging on the spinal cord. However, very little basic science/engineering research investigating the use of MWA in bone has been reported in the literature.

Many MWA devices are designed and optimized for use in liver tissue. This is because liver is not only a common clinical MWA site, but also because it is a relatively homogenous tissue which enables consistent and repeatable experimental evaluation and liver's electrical and thermal properties are well known [104]. These MWA applicators are increasingly being used in other tissues such as lung, kidney, and even bone. However, bone tissue has substantially different electrical and thermal properties than liver and other tissue [105], and many of the prospective ablation sites are in close proximity to critical structures such as the spinal cord. Therefore, high-powered MWA applicators designed for large volume ablation in highly perfused organs may not be well suited for bone applications. The present report proposes a computational modeling-based approach to simulate a directional microwave ablation (DMWA) applicator performance in bone and analyze the suitability of using DMWA applicators for treating metastatic disease within the vertebral body.

6.2 Methods

6.2.1 Applicator

The MWA applicator considered for this study is an experimental 2.45 GHz, , water-cooled, 14-gauge design which has been previously characterized in *ex vivo* and *in vivo* liver tissues [38]. The only modification made to the applicator design specifically for use in bone was removal of the steel trocar tip which would not be needed since the applicator would be inserted through a pre-drilled hole rather than by direct penetration of the tissue.

6.2.2 Computational Model

A 3D finite element method (FEM) solver (COMSOL Multiphysics v5.5, COMSOL, INC. Burlington, MA) was used to model the electromagnetic radiation pattern and subsequent heat transfer from the MWA applicator in a manner similar to that reported by McWilliams et al. and Sebek et al [86], [87]. The model was used to solve the Helmholtz electromagnetic wave equation:

Equation 6-1:

$$\nabla^2 \mathbf{E} - k_0^2 \left(\varepsilon_r - \frac{j\sigma}{\omega \varepsilon_0} \right) \mathbf{E} = 0$$

where, **E** [V/m] is the electric field, k_0 [m^{-1}] is the free-space wavenumber, ε_r is relative permittivity, σ [S/m] is effective conductivity, ω [rad/s] is angular frequency, and ε_0 [F/m] is permittivity of free-space.

Ex vivo simulations were modeled for approximately 45 kg pigs with vertebral body dimensions of 2.5 cm wide, 2.0 cm deep, and 2.5 cm tall. The cortical bone surrounding the

cancellous bone was 2 mm thick. The spinal canal, with spinal cord tissue properties, was 1.0 cm in diameter. 7.5 mm thick cartilaginous tissue representing intervertebral discs were placed cranial and caudal to the vertebral body. The distal 6 cm of the DMWA applicator was modeled with an entry though the lateral wall of the vertebral body and the back of the applicator positioned approximately 2 mm from the spinal canal aiming ventrally. The encompassing 8 cm wide x 4 cm tall x 4 cm deep domain was modeled as air or muscle to simulate experimental setups with different amounts of soft tissue surrounding the vertebrae. Although not a preferred clinical approach, the applicator insertion path shown in Figure 6-1 was selected to facilitate more repeatable *ex vivo* experimentation in porcine tissue with relatively small vertebral bodies and without the aid of image guidance.

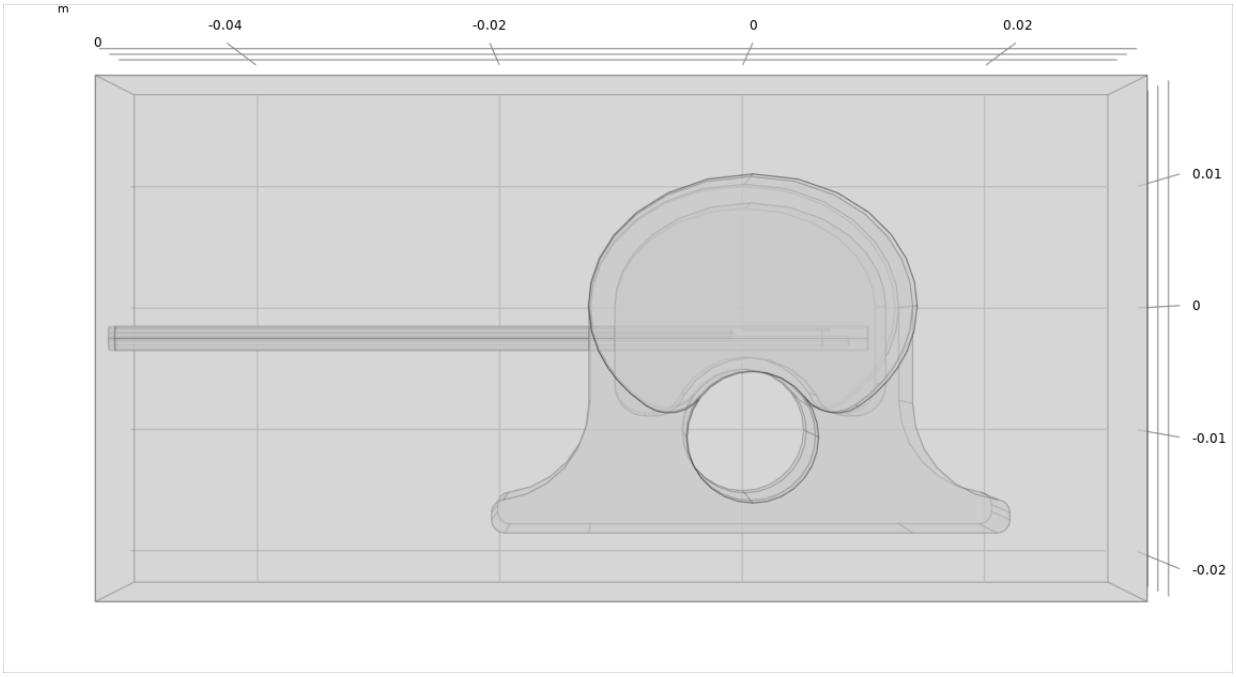

Figure 6-1: Model geometry used to simulate *ex vivo* ablation of a 45 kg pig vertebral body

To demonstrate bone DMWA in a clinically relevant site with a currently employed approach, *in vivo* ablations were modeled for humans. Vertebral body dimensions were 4.5 cm wide (laterolateral), 3 cm deep (cranial-caudal), and 2.5 cm tall (anterior-posterior). The cortical bone surrounding the cancellous bone was 3 mm thick. The spinal canal, with spinal cord tissue properties, was 2 cm wide by 1.5 cm deep. 7.5 mm thick cartilage tissues representing vertebral discs were placed above (cranial to) and below (caudal to) the vertebral body. A tumor centered in the middle of the vertebral body was modeled as a 2 cm diameter sphere with biophysical properties mimicking muscle tissue (soft tissue tumor within an osteolytic lesion) or cortical bone (osteoblastic lesion). The vertebrae and applicator models were surrounded by rectangular and cylindrical domains of muscle tissue, respectively. The distal 6 cm of two DMWA applicators were modeled with a 10° angled posterior entry through the pedicles of a vertebrae, as shown in Figure 6-3.

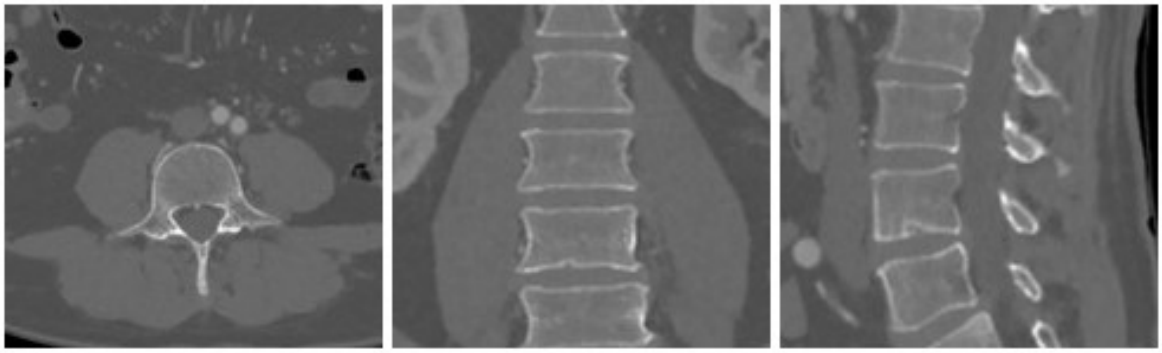

Figure 6-2: CT image of human vertebrae axial slice (left), coronal slice (middle), and sagittal slice (right). Images courtesy of Dr. Francois Cornelis.

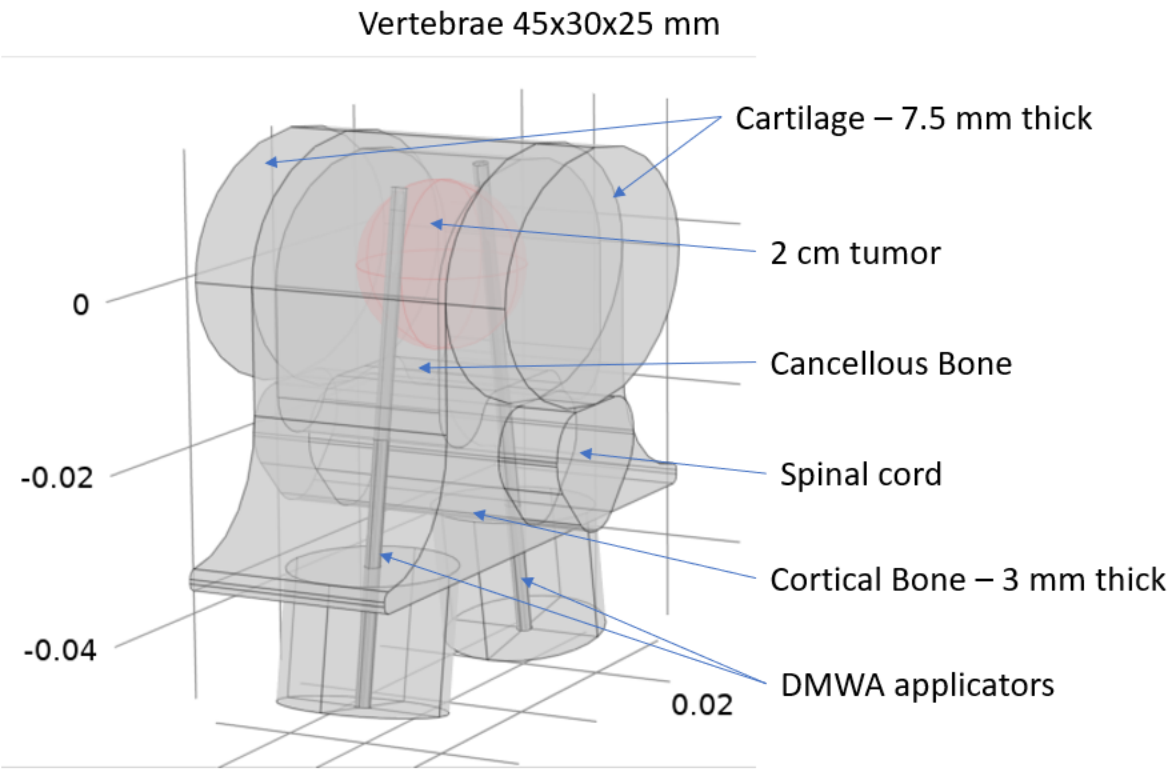

Figure 6-3: Geometry of model used for simulating *in vivo* ablation in human vertebral body

Scattering boundary conditions were applied at the extents of the models. The material electromagnetic properties used in simulation are given in Table 6-1: Tissue biophysical properties. All metallic elements were modeled as perfect electrical conductors with infinite conductivity. A port boundary condition was established at the proximal end of the coaxial cable dielectric and used to set the applicator's forward power accounting for approximately 50% attenuation losses in interconnecting cabling and the within the applicator. *Ex vivo* simulations investigated applied powers of 40 and 60 W (60, 80 and 120 W generator setpoint) for 3.5 or 5 minutes while *in vivo* simulations investigated an applied power of 40W (80 W generator setpoint) for 5 minutes.

Table 6-1: Tissue biophysical properties

Parameter	units	cortical bone	cancellous bone	cartilage	muscle	spinal cord	liver
Relative permittivity		11.4	18.5	38.8	52.7	30.1	43
Electric conductivity	S/m	0.39	0.81	1.76	1.74	1.09	1.69
Thermal conductivity	W/m/C	0.32	0.31	0.49	0.49	0.51	0.52
Density	kg/m^3	1908	1178	1100	1090	1075	1079
Specific heat capacity	J/kg/C	1313	2274	3568	3421	3630	3540
Heat transfer rate	ml/min/kg	10	30	35	37	160	860
Blood perfusion rate	W/m^3/K	683	2049	2390	2527	10928	58736

The electromagnetic loss in the tissue domain (Q_{mw}) was computed from the tissue's electrical conductivity (σ) and the simulated electric field ($\mathbf{E}$) based on:

Equation 6-2:

$$\mathrm{Q}_{mw} = \frac{1}{2}\sigma \cdot \|\mathbf{E}\|^2$$

Which was then coupled with Pennes' bioheat equation to compute the transient temperature profiles within the tissue:

Equation 6-3:

$$\rho c(\mathrm{T})\frac{\partial \mathrm{T}}{\partial t} = \nabla \cdot k(T)\nabla \mathrm{T} + \mathrm{Q}_{mw} - \omega_{bl}(\mathrm{T} - \mathrm{T}_{bl})$$

where ρc is volumetric heat capacity [$\mathrm{Jm^{-3}K^{-1}}$], T is temperature [K], k is thermal conductivity [$\mathrm{Wm^{-1}K^{-1}}$], ω_{bl} is blood perfusion [$\mathrm{Wm^{-3}K^{-1}}$], and T_{bl} is the temperature of blood. Table 6-1 lists the tissue thermal properties used in simulation.

The initial temperature of the tissue domain was set to 20 °C or 37 °C for *ex vivo* simulations to model specimens at room temperature or heated back to physiologic temperatures in a water bath, respectively. Follow-on simulations were also conducted at an initial temperature of 30 °C, as it was discovered that the 37 °C warmed *ex vivo* experimental specimens had cooled to an average temperature of 30.2 °C due to losses to ambient during the time it took to remove them from the water bath and commence the ablation experiments. A convective heat transfer boundary condition with a heat transfer coefficient of 10 W/(m^2*K) and external temperature of 20 °C was modeled at the extents of the vertebrae to account for heat loss to ambient. *In vivo* simulation initial tissue temperature was 37 °C to mimic living tissue and thermal insulation boundary conditions were used at the model extents. To simulate the forced cooling of the applicator, a 30 °C isothermal boundary condition was applied to the outer surface of the applicator. The use of isothermal boundary conditions to model forced cooling of the applicator has been previously proposed in literature [93] and is an approximation to account for microwave heating of the chilled cooling water near the antenna, heat transfer from attenuation losses in the applicator transmission cable, and heat transfer from the surrounding tissue to the applicator surface. Since the temperature dependence of the electrical and thermal variables of bone tissue have not been reported in the literature, *ex vivo* simulations were modeled with all tissue properties as static variables or modeled with the cancellous tissue to have the same temperature dependence as soft tissue to test the range of expected possibilities. For *in vivo* simulations tissue biophysical properties were all modeled as static properties other than the osteolytic tumor domain because (1) temperatures were not expected to be significantly elevated in these other tissue domains, and (2) as previously mentioned, the temperature-dependence of biophysical properties in bone is not known and may not vary in a similar fashion as known

tissues such as liver or muscle. For the osteolytic tumor domain, temperature dependence was implemented for tissue relative permittivity and conductivity to account for changes as tissue is heated and desiccated [90], [94], and for tissue specific heat capacity to account for the latent heat of vaporization of the water in the tissue. For *in vivo* simulations, separate heat source nodes were used for different tissue types to model their varying levels of perfusion. At a tissue temperature of 60 °C, blood perfusion, ω_{bl}, was simulated to go to 0, simulating microvascular stasis. An implicit transient solver was used with a maximum time step of 10 s, where at each step temperature dependent thermal and electrical properties were updated. For the *in vivo* simulations, an isothermal temperature contour at 55 °C (red) was used to mark the extent of the simulated thermal ablation zone [8] and an isothermal contour at 45 °C (green) was used to mark the extend of tissue which may be at risk of any thermal injury.

A non-uniform tetrahedral mesh was constructed with maximum edge size of 0.01 mm at the port boundary, 0.2 mm throughout the applicator, and 3 mm in the tissue domains. The maximum applicator mesh edge size was determined when further reducing the maximum element edge size did not change the resulting simulated S_{11} by more than 0.1 dB. With the above mesh settings, a coupled electromagnetic -heat transfer 300 second *in vivo* simulation took 147 minutes to compute with an Intel Xeon-W processor and 64 GB of memory.

6.2.3 Ex Vivo Experiments

Spinal columns were excised from approximately 45 kg pigs within 2 hours from the time they were euthanized. The thoracic and lumbar sections of the spinal column were separated into three-vertebrae segments. The ribs, transverse processes, and soft tissues surrounding the ventral and lateral sides of the vertebral bodies were removed. One set of vertebrae was allowed cooled

to room temperature during their preparation while a second was placed in plastic bags and warmed to 37 °C in a water bath. A cordless power drill with a 3/32” drill bit was used to provide a pathway for the DMWA applicator. The pathway was centered along the craniocaudal axis on the lateral wall of the vertebral body, perpendicular and approximately 2-3 mm ventral to the spinal canal. The pathway extended laterally through almost the entire width of the vertebral body, with the goal of abutting, but not penetrating the cortex on the opposite side. A 0.7 mm diameter K-wire (IMEX Veterinary, IN., Longview, TX) was placed in a pin vice and used to provide a pathway for a 0.6 mm diameter fiber optic temperature sensor (Neoptix, Quebec City, Canada), placed parallel to the axis of the spinal column, approximately 10 mm ventral from the DMWA applicator, and about in-line with the cross-section of maximum heating. A second fiber optic temperature sensor was placed in the spinal canal outside of the spinal cord dura mater, parallel to the first temperature sensor and in the same cross-sectional place as the DMWA applicator and was held in direct contact with the ventral wall of the canal by a cotton swab.

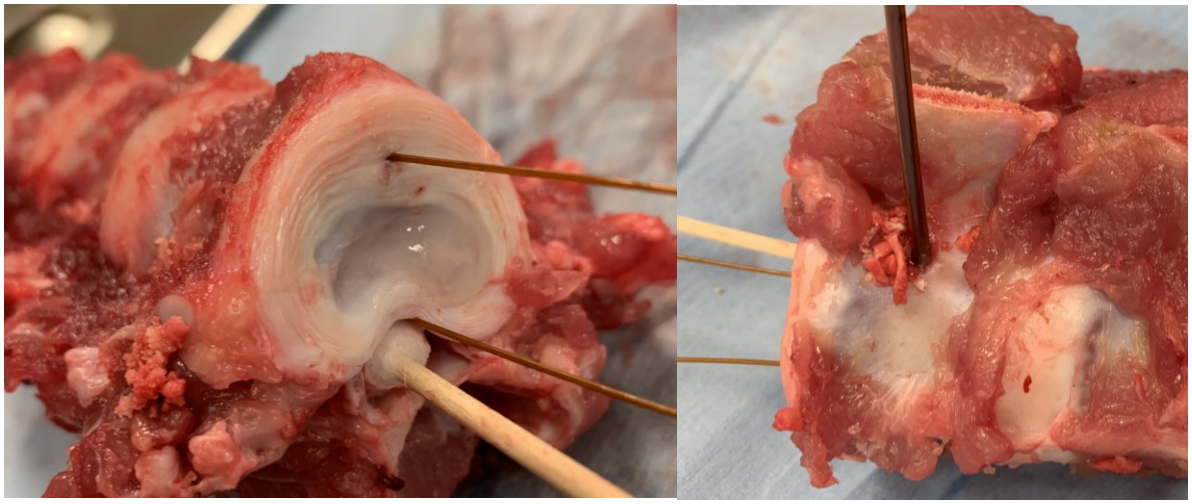

Figure 6-4: Images of temperature sensor (left) and DMWA (right) placement within *ex vivo* porcine vertebral body

An experimental microwave generator (Energize Medical, Lenexa, KS) was used to power the DMWA applicator. A peristaltic pump (Energize Medical, Lenexa, KS) circulated cooling water from an ice bath through the DMWA applicator at a flowrate of approximately 50 mL/min. Ablations were performed at 120 W (generator setting) for 5 min (n = 6) and 80W (generator setting) for 3.5 min (n = 8) for the room temperature samples and at 80 W (generator setting) for 3.5 min for the 37 °C samples (n = 6). Ablations were conducted within 3-5 hours after euthanasia without refrigeration or freezing of the samples.

Post-ablation, the vertebrae were cross-sectioned with a bandsaw across the axial plane (parallel to the probe pathway) at or immediately adjacent to DMWA applicator pathway. Any visible ablation zone, as indicated by a whitened or grayed discoloration of the marrow-filled cancellous bone tissue was measured with the distance extending axially defined as ablation depth and the distance extending along the applicator shaft defined as ablation height. Two specimens were further cut longitudinally (sagittal plane) to give an estimate of ablation width. Eleven of the specimens, including the two longitudinal sections, were fixed in 10% neutral buffered formalin, decalcified in 5% formic acid solution, embedded in paraffin, sectioned 5 μm thick, and hematoxylin and eosin (H&E) stained for histologic analysis by light microscopy. H&E stained slides were digitally scanned at 40X objective magnification and entered into Aperio eSlide Manager (Leica Biosystems, Buffalo Grove, IL).

The specific location of the T1 and T2 temperature sensors could not be identified on the histology slides. The eSlide Manager caliper tool was used to measure the perpendicular distance from the margin of applicator tract to the endosteal surface of the cortex in the forward direction (optimal T1 placement) and the perpendicular distance from the applicator tract to the periosteal surface within the spinal canal (optimal T2 placement), as shown in Figure 6-5. These

measurements were taken to set the absolute maximum distance T1 could have been positioned and the absolute minimum distance T2 could have been positioned for comparison to the distances recorded during the *ex vivo* experiments and ultimately the distances used to select final T1 and T2 temperatures from the computational models.

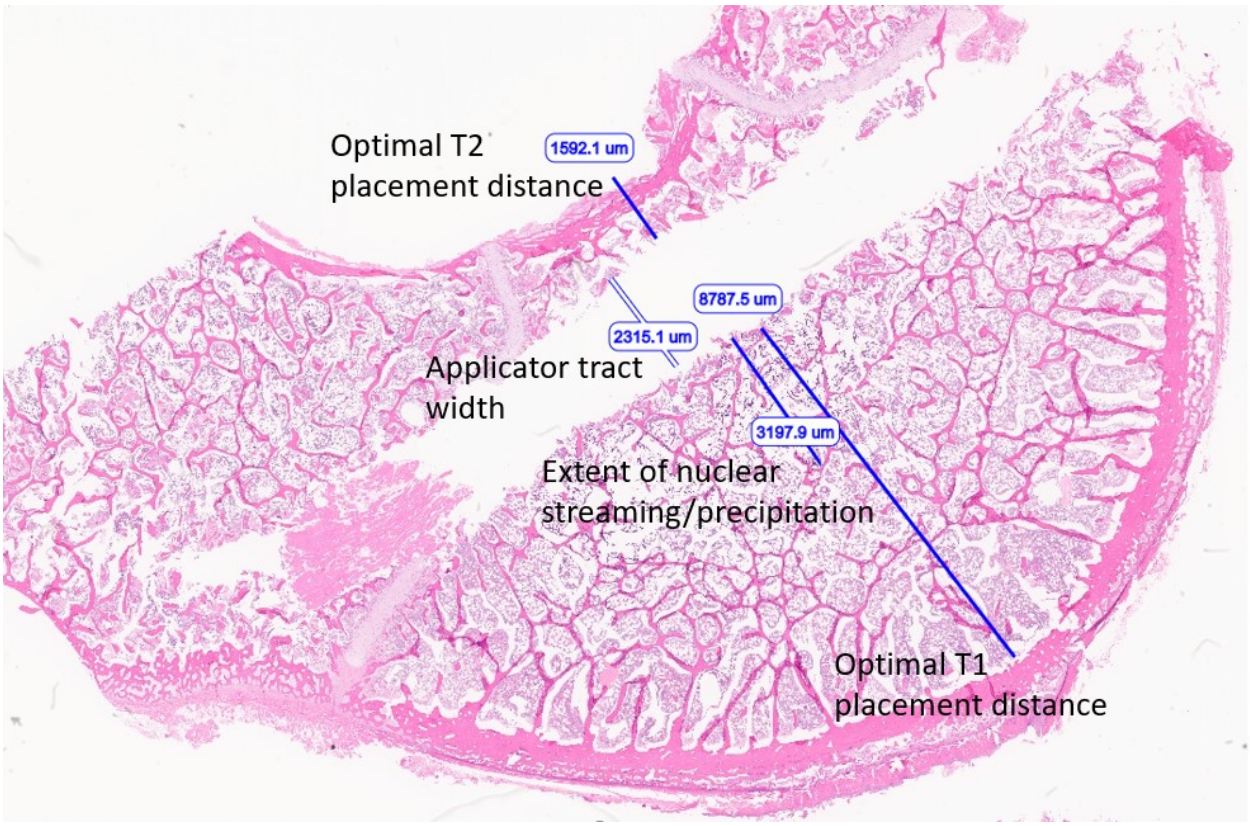

Figure 6-5: Measurement techniques to verify maximum positioning of T1 and minimum positioning of T2.

6.3 Results

The simulated temperature at a location of 9.5 mm perpendicular from the DMWA applicator in the forward direction (T1), and the 2.5 mm from the DMWA applicator in the backward direction (T2) for the various *ex vivo* models are listed in Table 6-2, Table 6-3, and Table 6-4. The extents of the 55 or 60 °C isothermal contour did not correlate well to the region of visible discoloration in the experimental results and therefore the dimensions of the 80 °C

isothermal contours were used to report simulated ablation zone extents. Simulated final temperature distributions of various 80 W, 3.5 minute, 20 °C initial temperature models are shown in Figure 6-6, Figure 6-7, and Figure 6-8.

Table 6-2: **Simulated ex vivo bone ablation results, vertebrae surrounded by 20 °C air, no tissue property temperature dependence modeled.**

P (W)	Time (min)	T_{bone}	D (mm)	L (mm)	$T1_i$	$T1_f$	$\Delta T1$	$T2_i$	$T2_f$	$\Delta T2$
80	3.5	20	3.7	9.0	20.0	51.3	31.3	20.0	33.4	13.4
80	3.5	30	5.4	10.2	30.0	62.5	32.5	30.0	39.6	9.6
80	3.5	37	6.5	11.5	37.0	68.9	31.9	37.0	43.8	6.8
120	5	20	9.7	18.8	20.0	81.4	61.4	20.0	41.8	21.8

Table 6-3: **Simulated *ex vivo* bone ablation results, vertebrae surrounded by 20 °C air, tissue property temperature dependence modeled the same as soft tissue.**

P (W)	Time (min)	T_{bone}	D (mm)	L (mm)	$T1_i$	$T1_f$	$\Delta T1$	$T2_i$	$T2_f$	$\Delta T2$
80	3.5	20	1.9	2.6	20.0	50.5	30.5	20.0	33.8	13.8
80	3.5	30	1.6	2.4	30.0	43.8	13.8	30.0	42.2	12.2
80	3.5	37	1.8	2.5	37.0	49.2	12.2	37.0	46.7	9.7
120	5	20	6.1	11.0	20.0	70.8	50.8	20.0	44.3	24.3

Table 6-4: **Simulated *ex vivo* bone ablation results, vertebrae surrounded by muscle tissue, no tissue property temperature dependence modeled.**

P (W)	Time (min)	T_{bone}	D (mm)	L (mm)	$T1_i$	$T1_f$	$\Delta T1$	$T2_i$	$T2_f$	$\Delta T2$
80	3.5	20	2.6	8.6	20.0	36.4	16.4	20.0	33.9	13.9
80	3.5	37	4.3	10.3	37.0	52.6	15.6	37.0	44.5	7.5
120	5	20	6.1	13.4	20.0	50.8	30.8	20.0	42.0	22.0
120*	5	20	3.4	10.0	20.0	46.6	26.6	20.0	42.2	22.2

*denotes a simulation which included bone tissue biophysical property temperature dependence

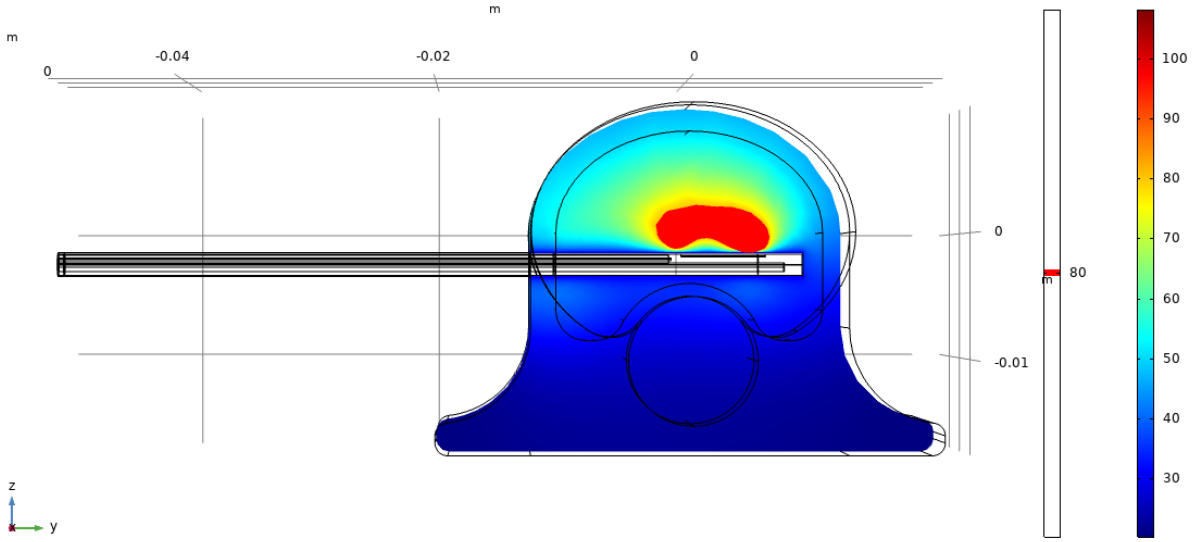

Figure 6-6: **80 W, 3.5 minute *ex vivo* ablation simulation with initial tissue temperature of 20 °C surrounded by 20 °C air convective boundary and static tissue biophysical properties**

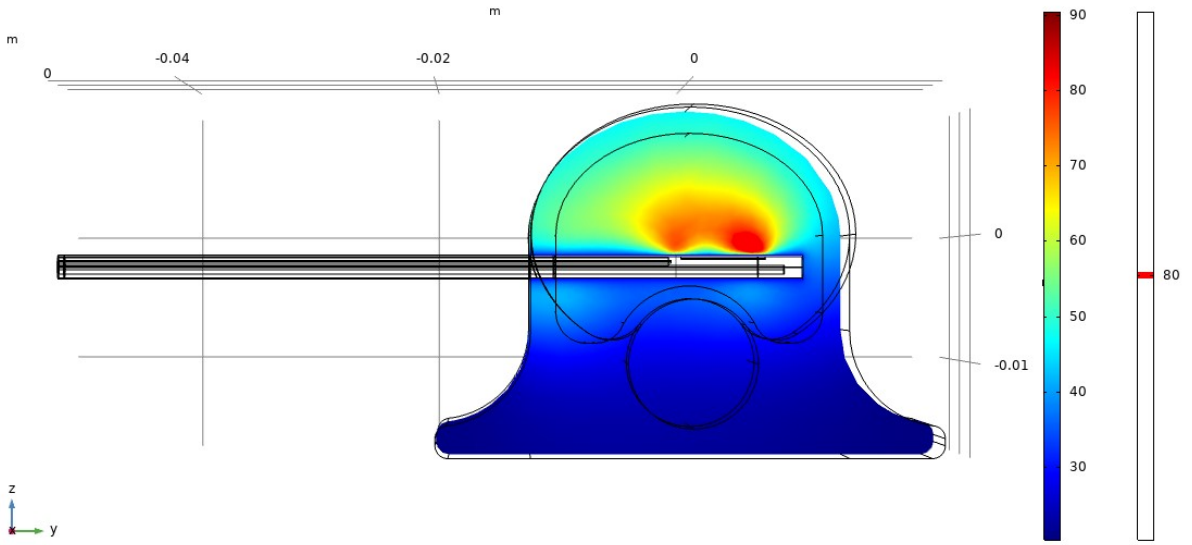

Figure 6-7: **80 W, 3.5 minute *ex vivo* ablation simulation with initial tissue temperature of 20 °C surrounded by 20 °C air convective boundary and biophysical properties with the same temperature dependence as soft tissue.**

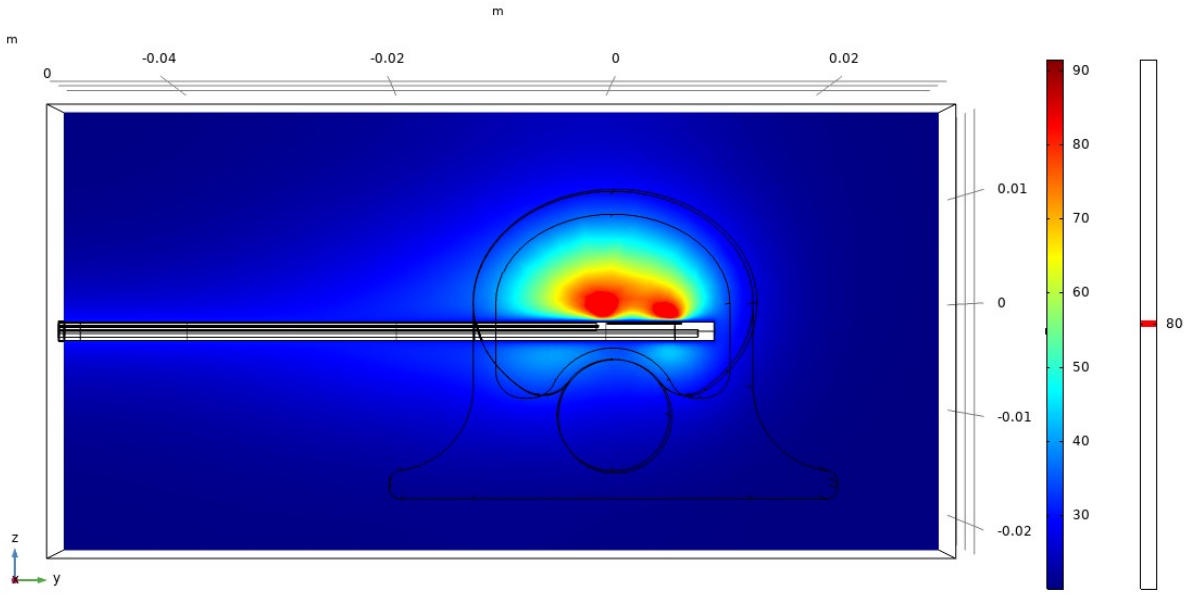

Figure 6-8: **80 W, 3.5 minute *ex vivo* ablation simulation with initial tissue temperature of 20 °C surrounded by 20 °C muscle and static tissue biophysical properties**

For the *ex vivo* experiments, measurements of the visible ablation zone, as defined by the whitened or greyed region, as well as T1 and T2 measurements are provided in Table 6-5. Of note, one set of T1 and T2 measurements was excluded from the 120 W experimental set due to a data logging error.

Table 6-5: Bone ablation experimental results

P (W)	t (min)	*n*	D_{T1} (mm)	D_{T2} (mm)	D (mm)	L (mm)	$T1_i$	$T1_f$	$\Delta T1$	$T2_i$	$T2_f$	$\Delta T2$
80	210	7	9.3	4.3	3.0	9.0	19.9	53.4	33.6	20.9	35.9	15.0
			±0.9	±0.0	±0.5	±1.5	±0.8	±2.9	±2.9	±0.5	±1.5	±1.5
80	210	6	9.3	5.3	5.5	10.5	30.2	63.7	33.5	35.1	45.9	10.8
			±1.0	±0.5	±0.5	±0.8	±3.7	±9.8	±9.1	±4.0	±4.3	±5.8
120	5	6*	9.8	5.0	7.8	14.0	17.2	80.3	63.2	17.5	49.8	32.3
			±1.0	±0.0	±1.0	±2.0	±1.7	±9.8	±9.5	±1.2	±4.8	±4.1

*one sample was excluded from the T1 and T2 measurements

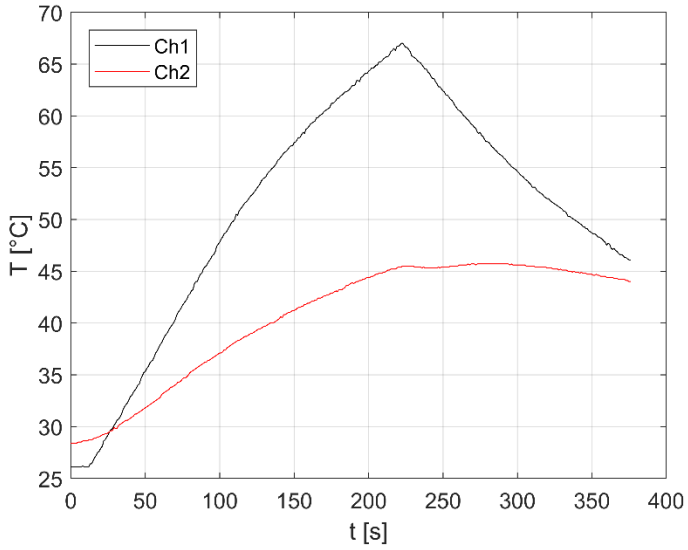

Figure 6-9: Graph of T1 and T2 during 80 W, 3.5 minute ablation

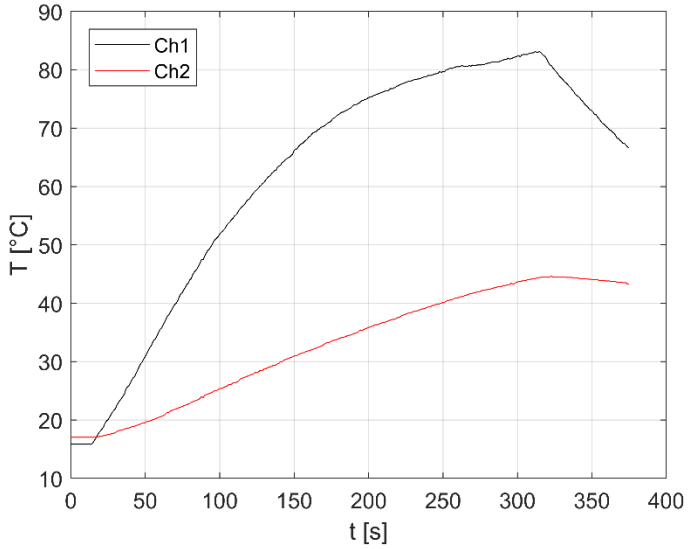

Figure 6-10: Graph of T1 and T2 during 120 W, 5 minute ablation

The T1 distance averaged among all experimental measurements was 9.5 mm. The maximum possible T1 distance measured and averaged among all histology slides was 10.1 mm with a range of 8.3 to 12.7 mm. The T2 distance averaged among all experimental measurements

was 4.8 mm. The minimum possible T2 distance measured and averaged among all histology slides was 2.4 mm with a range of 1.4 to 3.6 mm.

The differences in simulated to experimentally measured T1 and T2 temperatures are displayed in Table 6-6 and Table 6-7, respectively.

Table 6-6: Bone ablation experimental vs. simulated ΔT1 in *ex vivo* vertebrae

Power	T_{bone} ideal	Time	Experiment	Simulation static tissue properties		Simulation T-dependent tissue properties	
(W)	(°C)	(min)	ΔT1	ΔT1	Δexp-sim	ΔT1	Δexp-sim
80	20	3.5	33.6	31.3	-7%	30.5	-9%
80	37	3.5	33.5	31.9	-5%	12.2	-64%
120	20	3.5	63.2	61.4	-3%	50.8	-20%

Table 6-7: Bone ablation experimental vs. simulated ΔT2 in *ex vivo* vertebrae

Power	T_{bone} ideal	Time	Experiment	Simulation static tissue properties		Simulation T-dependent tissue properties	
(W)	(°C)	(min)	ΔT2	ΔT2	Δexp-sim	ΔT2	Δexp-sim
80	20	3.5	15.0	13.4	-11%	13.8	-8%
80	37	3.5	10.8	6.8	-37%	9.7	-10%
120	20	3.5	32.3	21.8	-33%	24.3	-25%

A gross image of a longituduinal section of an experimental ablation zone and the corresponding histologic image are show in Figure 6-11. Figure 6-12 is a longitudinal (sagittal plane) section, cut across half of a cross sectional (transverse plane) slice of an ablation zone that includes an adjacent unablated vertabra and associated intervertebral disc and the corresponding histologic image. Figure 6-13 shows 10x magnification of H&E stained sections of intensely heated, moderately heated, and healthy bone tissue.

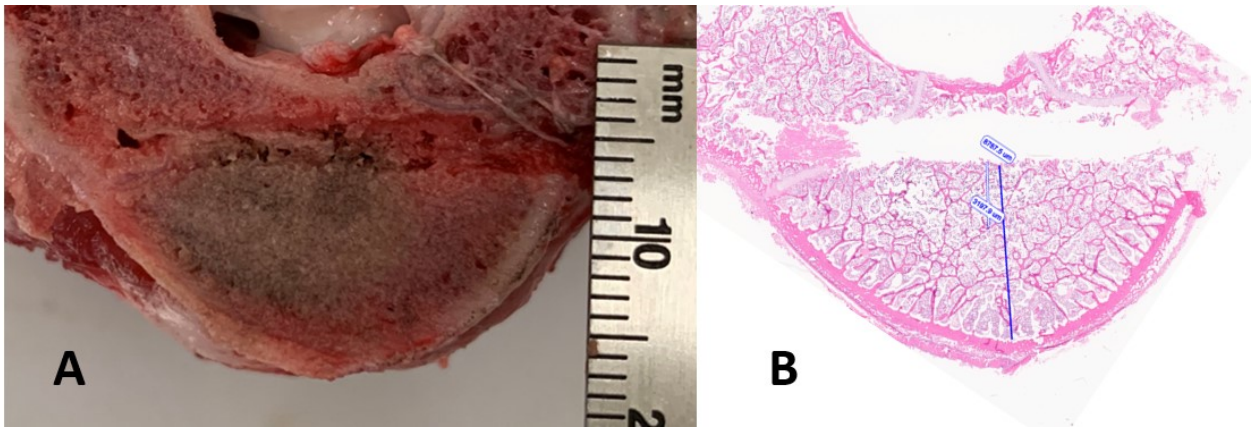

Figure 6-11: Gross image of an axial slice, along the DMWA applicator pathway, of 120 W, 5 minute, room temperature initial temperature *ex vivo* ablation zone (A) and corresponding H&E stained slide at 1x magnification (B)

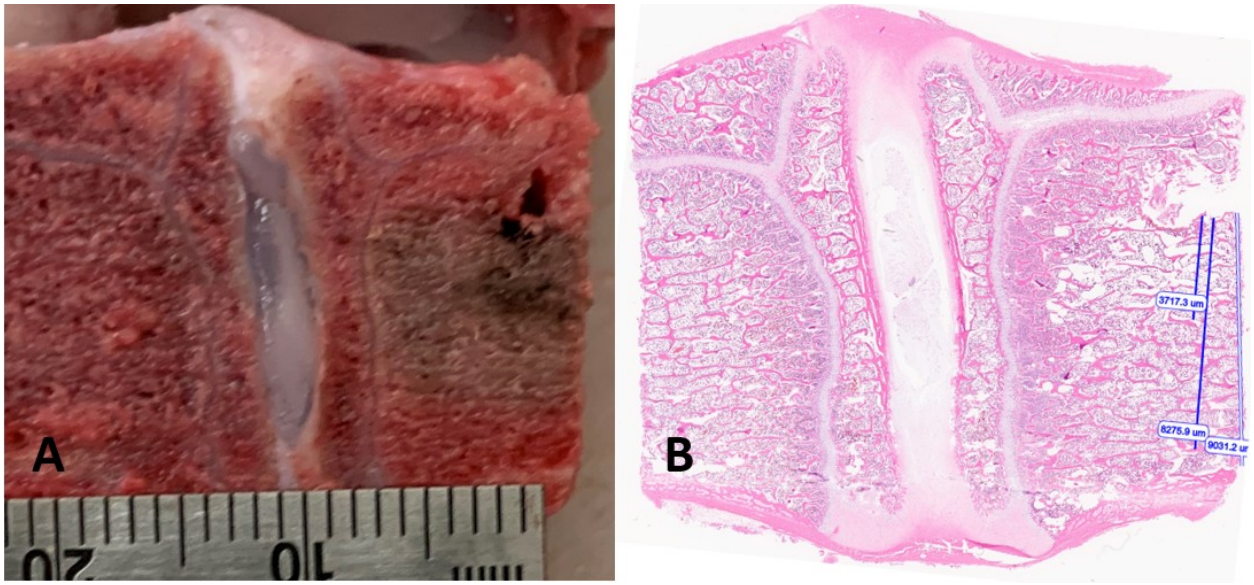

Figure 6-12: Gross image of a sagittal plane section of approximately half of a cross-sectional (axial plane) slice of 120 W, 5 minute, room temperature initial temperature *ex vivo* ablation zone (right side of A), the adjacent unablated vertebrae (left side of A) and associated intervertebral disc; Corresponding H&E stained slide section at 1x magnification (B)

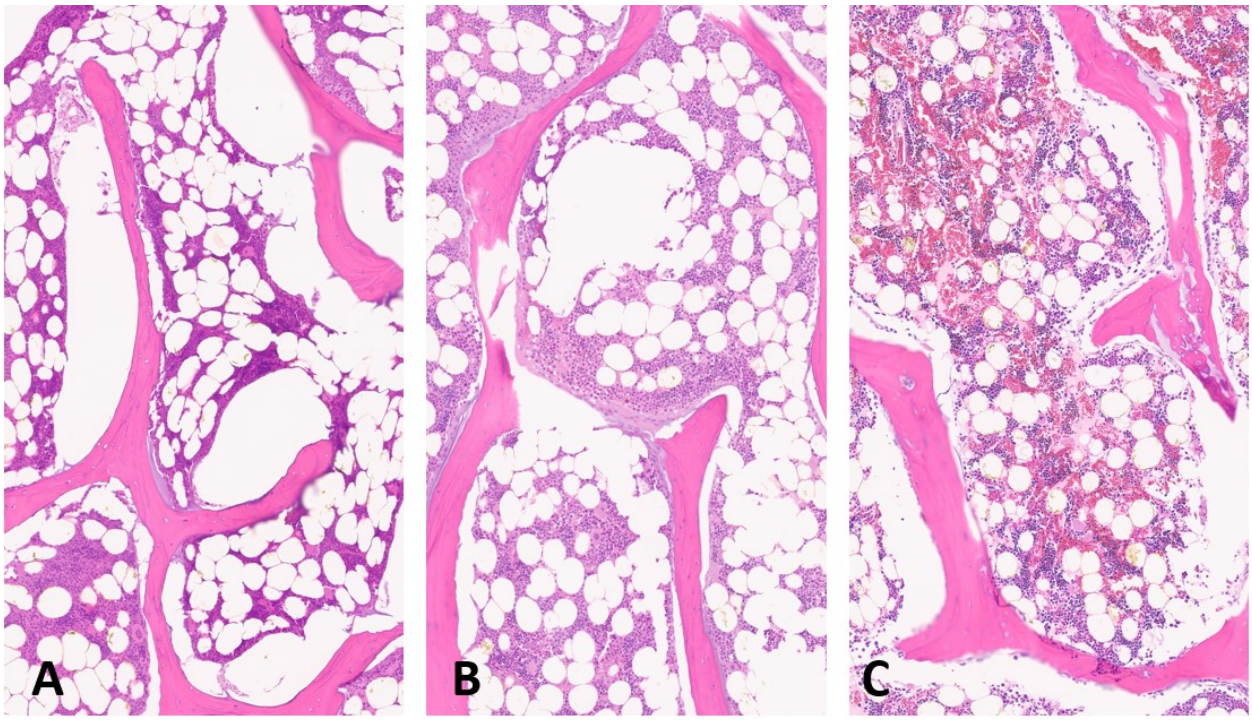

Figure 6-13: H&E stained, 5 µm thick, sections at 10x magnification showing a region very near the DMWA applicator antenna where intense heating caused loss of cellular detail within the marrow with precipitation and clumping of debris (A), a region more distant from the DMWA applicator where heating caused red blood cell lysis and structural preservation of blood cell precursors (myeloid/lymphoid) is present (B), and normal vertebrae from an unablated specimen (C).

Figure 6-14 and Figure 6-15 show the extents of the 45 and 55 °C isothermal contours representing the zone of possible thermal damage and zone of complete thermal ablation, respectively, during an 80 W each, 5-minute two DMWA applicator procedure in a normal human vertebrae. Figure 6-16and Figure 6-17 shows the extents of the same isothermal contours if the vertebrae contained a 2 cm spherical tumor having biophysical properties mimicking normal muscle tissue. Figure 6-18 and Figure 6-19 shows the extents of the same isothermal contours if the vertebrae contained a 2 cm spherical tumor having biophysical properties mimicking cortical bone tissue.

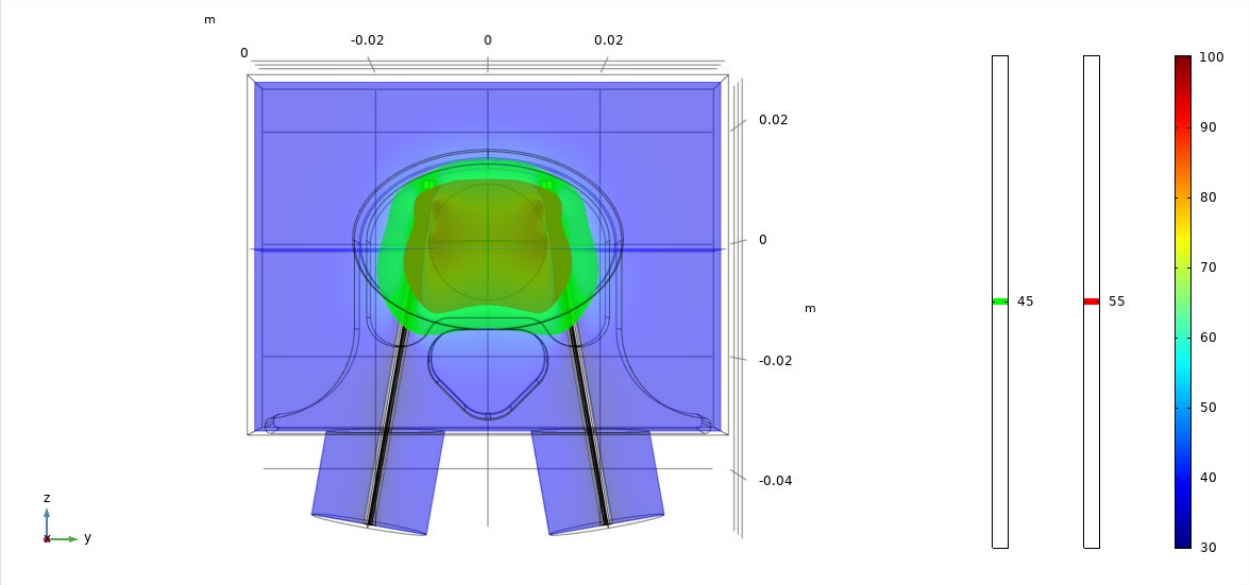

Figure 6-14: 80 W each, 5 minute, two-DMWA applicator human vertebrae *in vivo* ablation simulation with no tumor – YZ plane. The 55 °C isothermal contour is transparent red while the 45 °C isothermal contour is transparent green.

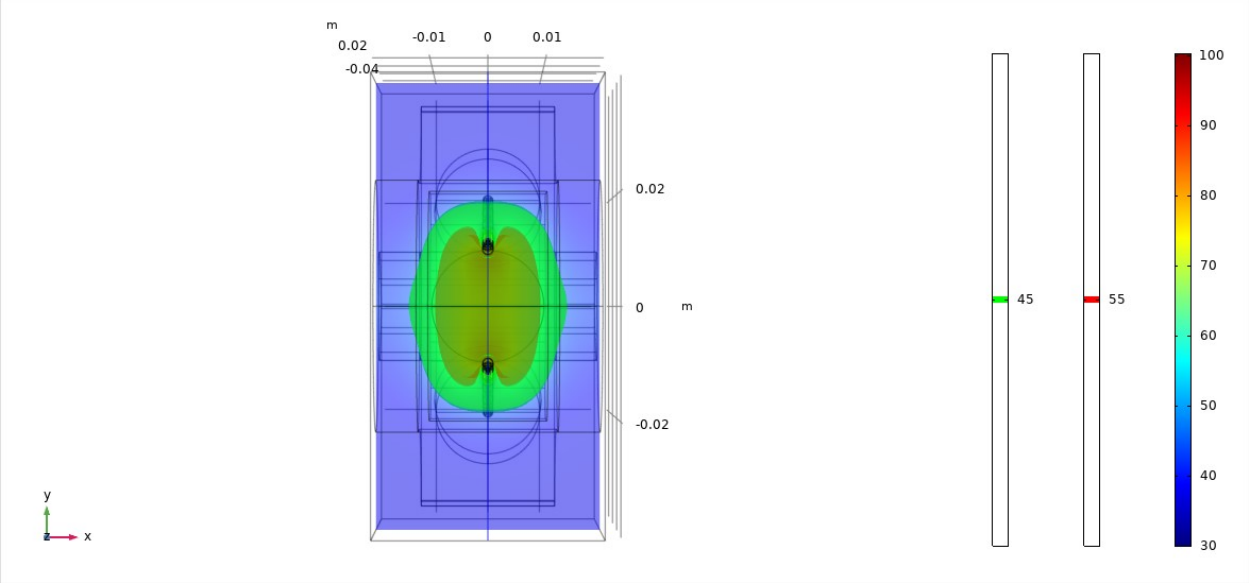

Figure 6-15: 80 W each, 5 minute, two-DMWA applicator human vertebrae *in vivo* ablation simulation with no tumor – XY plane. The 55 °C isothermal contour is transparent red while the 45 °C isothermal contour is transparent green.

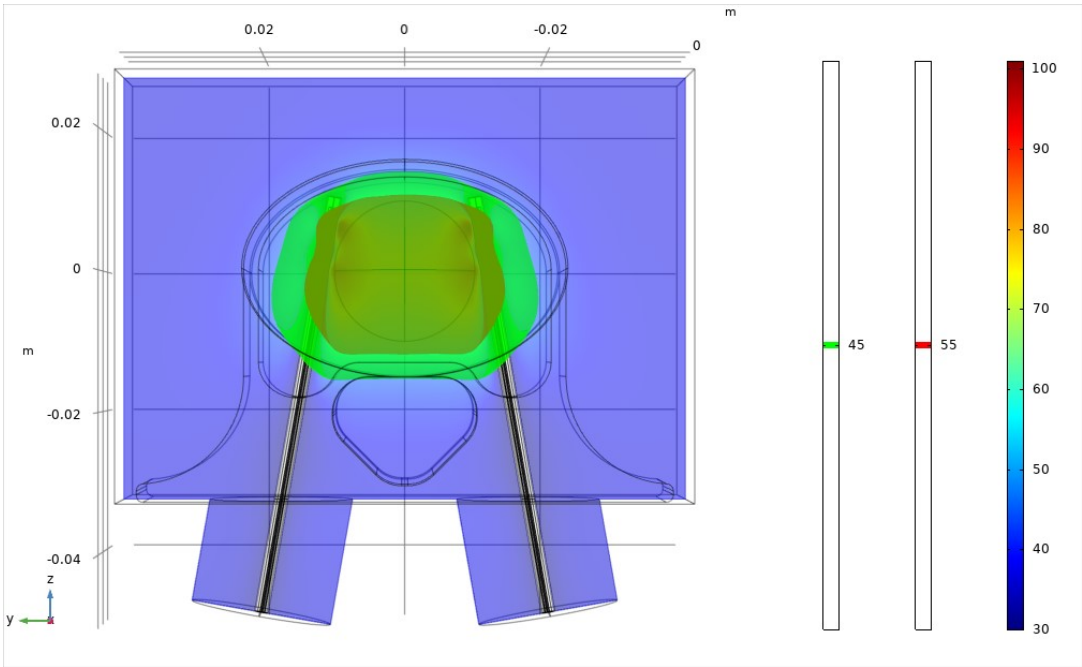

Figure 6-16: 80 W each, 5 minute, two-DMWA applicator human vertebrae *in vivo* ablation simulation with a 2 cm tumor with biophysical properties mimicking muscle – YZ plane. The 55 °C isothermal contour is transparent red while the 45 °C isothermal contour is transparent green.

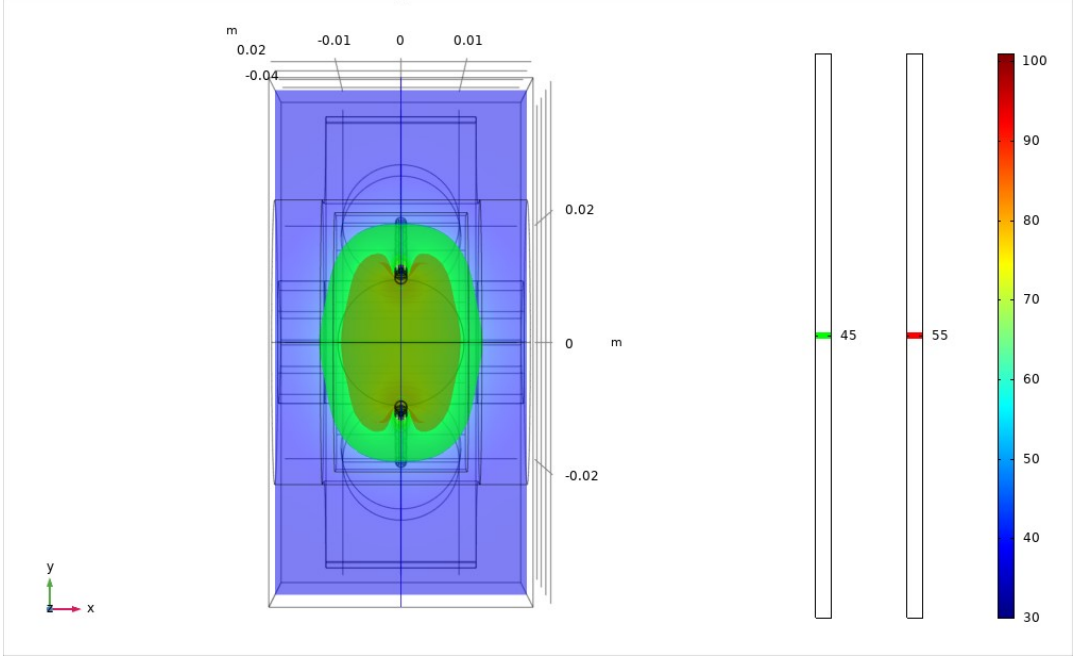

Figure 6-17: 80 W each, 5 minute, two-DMWA applicator human vertebrae in vivo ablation simulation with a 2 cm tumor with biophysical properties mimicking muscle – XY plane. The 55 °C isothermal contour is transparent red while the 45 °C isothermal contour is transparent green.

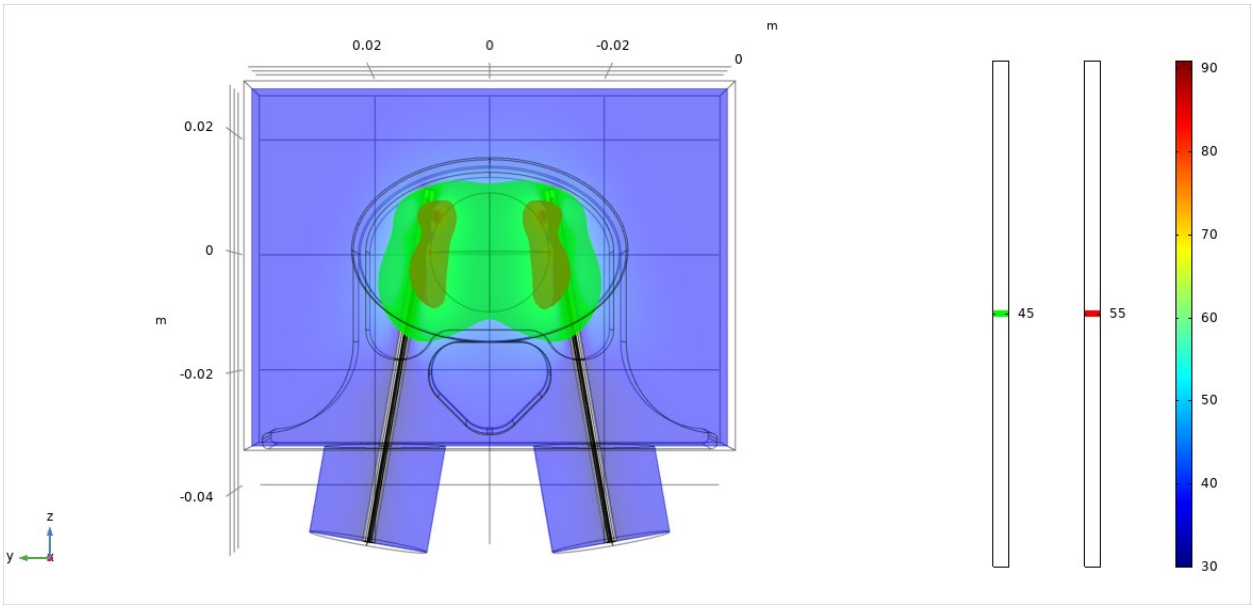

Figure 6-18: 80 W each, 5 minute, two-DMWA applicator human vertebrae in vivo ablation simulation with a 2 cm tumor with biophysical properties mimicking cortical bone – YZ plane. The 55 °C isothermal contour is transparent red while the 45 °C isothermal contour is transparent green.

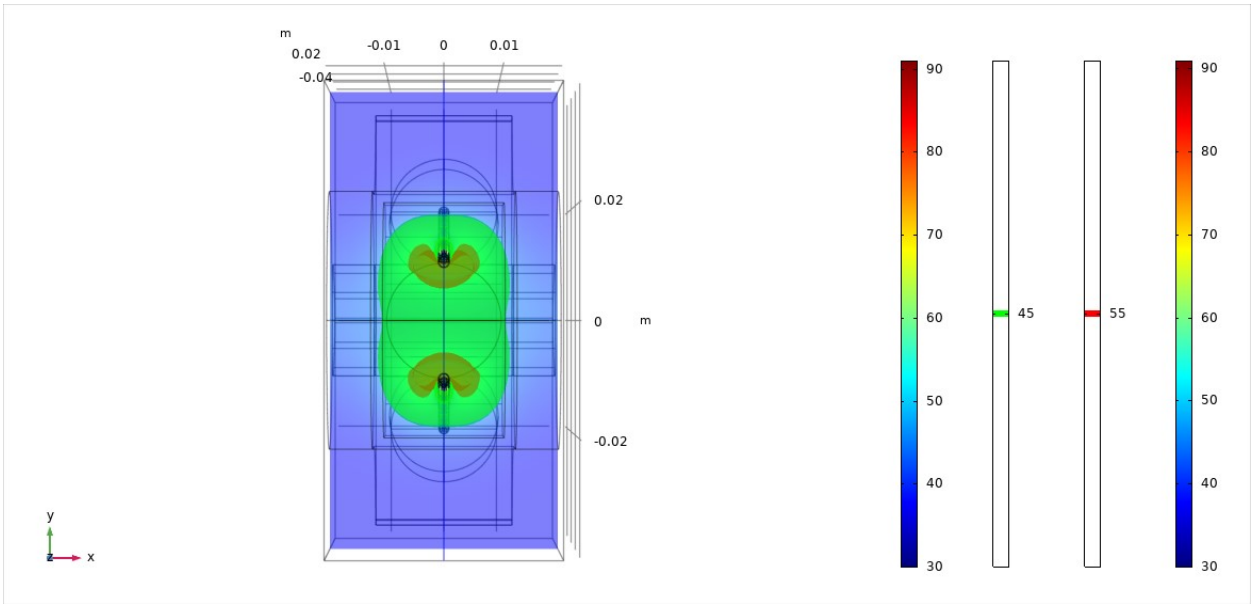

Figure 6-19: 80 W each, 5 minute, two-DMWA applicator human vertebrae in vivo ablation simulation with a 2 cm tumor with biophysical properties mimicking cortical bone – XY plane. The 55 °C isothermal contour is transparent red while the 45 °C isothermal contour is transparent green.

6.4 Discussion

The primary uses of bone MWA would likely be treating metastatic tumors that have biophysical properties similar to soft tissues, and osteoid osteoma that has biophysical properties similar to bone tissue [102]. The interactions of microwaves in soft tissues (liver, lung, kidney, etc.) throughout the course of a MWA procedure, including how the biophysical properties of those tissues change at elevated temperatures, is relatively well understood. However, how microwaves interact in bone and how bone tissue biophysical properties change during thermal ablation has not been rigorously presented in the literature.

First, there was a large difference in the extents of the simulated 55 or 60 °C isothermal contours compared to the extents of the visibly discolored regions in the experimental tissue specimens post-ablation, with the visible ablation zone being much smaller than the simulated 55 or 60 °C contours. However, the T1 measurement data showing temperatures rising to averages of 53.4 – 80.3 °C approximately 9.5 mm from the applicator suggests the visible region of discoloration in *ex vivo* bone is not a good indicator of the extents of the 55-60 °C heating like it is in other soft tissues. This may be due to reduced or different mechanisms of changes in the physical properties of the bone tissue that otherwise lead to coloration changes in soft tissues at ablative temperatures. Based on histology, it seems the whitening of the ablation zone may be caused by the lysis of red blood cells, which seems to occur throughout a region that extends slightly beyond the macroscopically visible discolored region. The extents of the macroscopically visible ablation zones for each power/time/starting temperature *ex* vivo experiment model correlated to slightly different specific temperatures. The 80 °C contour was selected for uniformly reporting the simulated "ablation zone" for correlation to experimental results. However, this may not have a clinically relevant meaning, as it likely underestimates the

zone region of tissue that receives an ablative thermal dose. Further confounding these results, the boundary of visible discoloration in the bone ablation samples is quite faint, making it difficult to accurately measure. Furthermore, the process of using a bandsaw to section the *ex vivo* vertebrae may alter the cut surface of the specimen, impacting accurate gross, and perhaps even histologic assessment of ablation zone extents.

Given that bone tissues already have a relative permittivity and electrical conductivity about one half (cancellous bone) to one quarter (cortical bone) of most soft tissue [106], this study made an initial assumption that those values would not change appreciably during thermal ablation (bone has less water content to dehydrate, fewer proteins to desiccate, 70% inorganic hydroxyapatite constitution). However, to test the full range of possible bone tissue temperature dependence, *ex vivo* simulations were also run that modeled bone tissue with the same temperature dependence exhibited by soft tissues. As previously discussed, because the extent of the grossly visible ablation zone cannot be reliably used as an indicator of ablation zone temperature without further study, the temperature data recorded from experiments was used to validate the computational models.

However, since each vertebra has a non-uniform size and shape, and placement of the DMWA applicator and the temperature sensors had to be referenced external to the vertebrae at the time of the experiments, there was significant uncertainty as to the exact placement of the temperature sensors. This would have a high impact on correlating simulated and experimental results. The exact placement of T1 and T2 during the ablation experiments could also not be identified on the histology slides, however, the maximum T1 and minimum T2 placement distances could be calculated. The average T1 distance, based on histologic measurement, showed 10.1 mm as the maximum T1 distance. This means the average distance of 9.5 mm for

T1 placement recorded during the ablation procedure could have been accurate. A much larger discrepancy was observed between the average T2 distance recorded during the ablation procedure (4.8 mm) and the optimal minimum T2 distance averaged from the histology slide measurements (2.4 mm). This may be because the spinal canal has a non-uniform diameter though a vertebra (it widens towards the center), which is not accounted for with externally referenced distance measurements. The optimal minimum T2 distance measured and averaged from the histology slides was likely more representative of actual T2 placement than what was measured during the experiments and therefore used to determine the simulated T2 temperatures. For both T1 and T2, there could have been error in placing the temperature sensors exactly within the same vertebral cross-sectional plane as the DMWA applicator. An analysis of this range of possible error could not be reconstructed post-experiment, but in general, less than optimal placement would have resulted in lower experimental T1 temperatures, but potentially higher experimental T2 measurements due to the sidelobes of the DMWA applicator radiation pattern.

Though bone tissue properties likely do exhibit some temperature dependent changes during microwave ablation, based on the differences in simulated vs experimental temperatures at T1 and T2 shown in Table 6-6and Table 6-7, it seems the static tissue property model predicts T1 temperature significantly better while the temperature-dependent tissue property model predicts T2 measurement only moderately better. Considering there is less certainty in the experimental placement of T2, a computational model assuming static bone tissue biophysical properties could be an acceptable starting point for developing an *in vivo* model of using DMWA to treat metastatic disease in human vertebrae.

It is important to note that the pigs used in the experimental study were young and their vertebral bodies would likely have a higher composition of bone marrow than that of a more mature model [107]. Further study should be conducted to determine if a different tissue composition within the vertebral body would have a meaningful impact on the microwave ablation zone when treating metastatic disease in elderly patients.

Although the very high T1 temperatures observed in *ex vivo* simulations and experimentation may be concerning, considering the need for spatial control of thermal damage in clinical use, the high T1 temperatures may be caused by the experimental setup where a relatively small tissue sample was surrounded by air. Air is a thermally insulative material compared to soft tissues, which means much of the heat input within the tissue specimen would be contained in it, creating a sort of "oven effect", causing elevated temperatures. Simulations in which the surrounding medium of air was replaced with muscle showed much lower final temperatures at T1 (Table 6-4and Figure 6-8). Further *ex vivo* experimentation could be conducted with more soft tissues surrounding the vertebral specimens, however, the surrounding soft tissue will make exact placement and measurement of the DMWA applicator and temperature sensors more challenging.

Expanding the computational model to include tissue-specific blood perfusion distributed cooling effects showed a two-applicator DMWA procedure has the potential to fully ablate (raise the temperature to 55 °C) a 2 cm spherical osteolytic lesion in the center of a human vertebrae while limiting the spinal cord temperature to below 45 °C. These modeling results show DMWA applicators, previously optimized for use in liver tissues, still offer the necessary spatial control of the thermal ablation zone to provide minimally invasive curative or palliative treatment of bone tumors.

6.5 Conclusion

The physics of microwave ablation in bone have not been extensively studied previously. However, based on the experimental evidence presented, the extent of microwave transmission and heating in bone tissues can be effectively modeled and simulated. Advanced computational models show DMWA has potential for clinical application treating metastatic tumors in the vertebral body and potentially other bone sites.

Chapter 7 - Conclusion and Future Work

Over the past several decades, there has been substantial development of thermal ablation technologies as a minimally invasive treatment option for patients who are otherwise not good candidates for surgery, chemotherapy, or radiation therapy. Microwave ablation (MWA) in particular has seen a growing increase in popularity due to its ability to rapidly heat relatively large volumes of tissue in both highly perfused and low-impedance tissues. Recent technical and clinically-motivated development in the field of MWA has focused on incremental improvements in the size and sphericity achievable by current omni-directional applicators, techniques for post-procedural imaging assessment of treatment outcome, and the development and integration of treatment planning tools to aid in the placement of the applicators and proper selection of the thermal dose. However, all current commercial MWA systems are configured to deliver maximum power to achieve the largest possible ablation zones in highly perfused organs, the tradeoff being a lack of precise spatial control of the thermal treatment zone when used in diverse clinical environments.

A directional microwave ablation (DMWA) applicator offers many of the same benefits of traditional MWA such as fast treatment times and the ability to radiate through low-impedance tissues, but also has the potential to provide the improved spatial control necessary for precision treatment. In Chapter 2, we described some of the new treatment approaches that could be enabled by DMWA and discussed some of the clinical sites where DMWA could provide improved treatment of niche cases or even offer new ability to provide a minimally invasive treatment option, both within and beyond interventional oncology. These include precise ablation of tumors in the kidney and lung, metastases in bone, and benign targets in the

adrenal or thyroid glands, among other potential targets. Though these proposed various treatment techniques and clinical uses range from moderately beneficial to disruptive, DMWA use beyond soft tissue cancer tumor ablation will require significantly more experimental and clinical evidence to support FDA approval and insurance reimbursement – the joint keys to treating patients en masse.

However, though prior DMWA applicator designs have been proposed in the literature, and some have even achieved FDA clearance, none are currently in clinical use. The challenges of minimizing the size of a MW frequency directional antenna, delivering sufficient energy to ablate a clinically meaningful tissue volume, and constructing a device small but robust enough for clinical use sum to be a technically challenging task. In Chapter 3 we described our methodology to balance electromagnetic and thermal performance with clinical usability requirements in the development of a practical DMWA design. Chapters 4 describe experimental evaluation of our best hand-built DMWA prototypes in a clinically relevant testing environment. The consequences of our design methodology was a DMWA applicator that can be highly directional (high forward to backward ablation depth ratio, > 10.0), but creates substantially smaller ablation zones (10-15 mm forward depth) than existing omni-directional ablations (30-40 mm short axis width).

Looking to enhance the directional performance of the DMWA applicator, in Chapter 5 we showed a 10 second period, 70% duty cycle, 100 W generator setting power pulsing protocol showed a 40.1% reduction in the backward ablation depth, a 1.0% reduction in the forward ablation depth, and a 59.6% increase in the directivity ratio in *in vivo* liver.

Looking to begin building a description of biophysics of microwave heating in bone needed to support DMWA's clinical use treating metastatic and primary disease in bone tissue,

Chapter 6 shows a computational model with static bone tissue biophysical properties was able to predict the temperature change during DMWA in the forward direction within 3 – 7% and in the backward direction within 11 – 37% of what was recorded during *ex vivo* DMWA in freshly excised bone. This computational model was further modified to include tissue-specific perfusion values and demonstrated two DMWA applicators operated at a 80 W generator setting each for 5 minutes could heat the entirety of a 2 cm metastatic tumor in the center of vertebral body to ablative temperature (55 °C) without exceeding 45 °C in the spinal canal.

Based on the presented research and experimental evidence, we strongly believe the current DMWA applicator design can meet several compelling clinical needs at its current performance level. Therefore, we have begun extensive efforts to advance the technologies presented in this dissertation towards a stage where they can be evaluated in the clinical setting. In order to translate the technology from an academic engineering research lab setting, we have collaborated with experienced medical device manufacturers to design devices suitable for manufacturing at scale within a quality-controlled environment. Furthermore, we have engaged in close collaboration with clinical end-users to guide the further development of the system. As described in Chapter 3, these efforts have since yielded significant progress and technical success and we are eager to proceed to working on the next major milestones towards delivering a new medical device suitable for evaluation in the clinical setting. Briefly, our planned next steps towards this translation include:

1. Conduct focus groups with clinical experts to determine where improvements should be made in the applicator physical properties and ergonomics as well as improvements to the generator user interface.
    a. Transmission bundle weight, flexibility, and overall length

b. Applicator shaft rigidity/mechanical performance
c. Applicator hub/handle size
d. Applicator shaft marker band placement
e. Need for external and/or imaging indicators of directionality
f. Types of clinical uses, including outside oncology, which could be a good fit for DMWA including anticipated frequency of cases
g. Number of generator MW output channels and other features desired
h. Water cooling pump interface options for multiple applicators

2. Enter design controls and begin developing a quality system and design history file
3. Select a predicate system and conduct performance and safety testing (based on the possible predicates, clinical data is not expected to be necessary), biocompatibility testing, self-life testing, etc.
4. File for FDA 510(k) clearance for a class II device.
5. Obtain institutional approval to conduct first-in-human testing.

References

[1] M. Ahmed, C. L. Brace, F. T. Lee, and S. N. Goldberg, "Principles of and advances in percutaneous ablation," *Radiology*, vol. 258, no. 2, pp. 351–369, Feb. 2011, doi: 10.1148/radiol.10081634.

[2] "Key Statistics for Lung Cancer." https://www.cancer.org/cancer/non-small-cell-lung-cancer/about/key-statistics.html (accessed May 24, 2017).

[3] "Key Statistics About Kidney Cancer." https://www.cancer.org/cancer/kidney-cancer/about/key-statistics.html (accessed Feb. 14, 2020).

[4] "Key Statistics for Lung Cancer." https://www.cancer.org/cancer/non-small-cell-lung-cancer/about/key-statistics.html (accessed Feb. 19, 2018).

[5] "Cancer today." http://gco.iarc.fr/today/home (accessed Feb. 14, 2020).

[6] P. Wust *et al.*, "Hyperthermia in combined treatment of cancer," *The Lancet Oncology*, vol. 3, no. 8, pp. 487–497, Aug. 2002, doi: 10.1016/S1470-2045(02)00818-5.

[7] J. A. Pearce, "Comparative analysis of mathematical models of cell death and thermal damage processes," *International Journal of Hyperthermia*, vol. 29, no. 4, pp. 262–280, Jun. 2013, doi: 10.3109/02656736.2013.786140.

[8] W. C. Dewey, "Arrhenius relationships from the molecule and cell to the clinic," *International Journal of Hyperthermia*, vol. 25, no. 1, pp. 3–20, Feb. 2009, doi: 10.1080/02656730902747919.

[9] Salgaonkar Vasant A. *et al.*, "Model-based feasibility assessment and evaluation of prostate hyperthermia with a commercial MR-guided endorectal HIFU ablation array," *Medical Physics*, vol. 41, no. 3, p. 033301, Feb. 2014, doi: 10.1118/1.4866226.

[10] C. J. Diederich, W. H. Nau, and P. R. Stauffer, “Ultrasound applicators for interstitial thermal coagulation,” *IEEE Transactions on Ultrasonics, Ferroelectrics, and Frequency Control*, vol. 46, no. 5, pp. 1218–1228, Sep. 1999, doi: 10.1109/58.796127.

[11] C. M. Pacella, G. Francica, D. Costanzo, and G. Giuseppe, “Laser Ablation for Small Hepatocellular Carcinoma,” *Radiology Research and Practice*, 2011. https://www.hindawi.com/journals/rrp/2011/595627/ (accessed Apr. 01, 2018).

[12] G. Shafirstein *et al.*, “Conductive interstitial thermal therapy (CITT) inhibits recurrence and metastasis in rabbit VX2 carcinoma model,” *International Journal of Hyperthermia*, vol. 25, no. 6, pp. 446–454, Sep. 2009, doi: 10.1080/02656730903013618.

[13] S. N. Goldberg, “Radiofrequency tumor ablation: principles and techniques,” *Eur. J. Ultrasound Off. J. Eur. Fed. Soc. Ultrasound Med. Biol.*, vol. 13, no. 2, pp. 129–147, Jun. 2001.

[14] M. Atoui, S. Gunda, D. Lakkireddy, and S. Mahapatra, “Radiofrequency Ablation to Prevent Sudden Cardiac Death,” *Methodist Debakey Cardiovasc J*, vol. 11, no. 2, pp. 121–128, 2015, doi: 10.14797/mdcj-11-2-121.

[15] L. A. Mynderse, C. G. Roehrborn, A. W. Partin, G. M. Preminger, and E. P. Coté, “Results of a 5-Year Multicenter Trial of a New Generation Cooled High Energy Transurethral Microwave Thermal Therapy Catheter for Benign Prostatic Hyperplasia,” *The Journal of Urology*, vol. 185, no. 5, pp. 1804–1810, May 2011, doi: 10.1016/j.juro.2010.12.054.

[16] J. Wong, N. Bremer, P. D. Weyker, and C. A. J. Webb, “Ultrasound-Guided Genicular Nerve Thermal Radiofrequency Ablation for Chronic Knee Pain,” *Case Rep Anesthesiol*, vol. 2016, 2016, doi: 10.1155/2016/8292450.

[17] T. P. Ryan and C. L. Brace, “Interstitial microwave treatment for cancer: historical basis and current techniques in antenna design and performance,” *Int J Hyperthermia*, vol. 33, no. 1, pp. 3–14, Feb. 2017, doi: 10.1080/02656736.2016.1214884.

[18] B. T. McWilliams, E. E. Schnell, S. Curto, T. M. Fahrbach, and P. Prakash, “A Directional Interstitial Antenna for Microwave Tissue Ablation: Theoretical and Experimental Investigation,” *IEEE Trans Biomed Eng*, vol. 62, no. 9, pp. 2144–2150, Sep. 2015, doi: 10.1109/TBME.2015.2413672.

[19] J. Sebek, S. Curto, R. Bortel, and P. Prakash, “Analysis of minimally invasive directional antennas for microwave tissue ablation,” *Int J Hyperthermia*, vol. 33, no. 1, pp. 51–60, Feb. 2017, doi: 10.1080/02656736.2016.1195519.

[20] Y. Mohtashami, S. C. Hagness, and N. Behdad, “A Hybrid Slot/Monopole Antenna With Directional Heating Patterns for Microwave Ablation,” *IEEE Transactions on Antennas and Propagation*, vol. 65, no. 8, pp. 3889–3896, Aug. 2017, doi: 10.1109/TAP.2017.2714020.

[21] D. Berube, “Electrode arrangement for use in a medical instrument,” US 6,673,068 B1, Oct. 29, 2002.

[22] M. Bedoya, A. M. del Rio, J. Chiang, and C. L. Brace, “Microwave ablation energy delivery: Influence of power pulsing on ablation results in an ex vivo and in vivo liver model,” *Medical Physics*, vol. 41, no. 12, p. 123301, 2014, doi: 10.1118/1.4901312.

[23] R. L. Cazzato *et al.*, “Spinal Tumor Ablation: Indications, Techniques, and Clinical Management,” *Tech Vasc Interv Radiol*, vol. 23, no. 2, p. 100677, Jun. 2020, doi: 10.1016/j.tvir.2020.100677.

[24] D. K. Singh, A. Katyan, N. Kumar, K. Nigam, B. Jaiswal, and R. N. Misra, “CT-guided radiofrequency ablation of osteoid osteoma: established concepts and new ideas,” *Br J Radiol*, vol. 93, no. 1114, p. 20200266, Oct. 2020, doi: 10.1259/bjr.20200266.

[25] R. C. Ward, T. T. Healey, and D. E. Dupuy, “Microwave ablation devices for interventional oncology,” *Expert Rev Med Devices*, vol. 10, no. 2, pp. 225–238, Mar. 2013, doi: 10.1586/erd.12.77.

[26] K. F. C. and D. E. Dupuy, “Thermal ablation of tumours: biological mechanisms and advances in therapy,” *Nat. Rev. Cancer*, vol. 14, no. 3, pp. 199–208, 2014.

[27] J. M. Lawrenz, H. Ilaslan, S. A. Lietman, M. J. Joyce, C. S. Winalski, and N. W. Mesko, “Minimally invasive techniques for pain palliation in extraspinal bone metastases: a review of conventional methods and cryoablation,” *Current Orthopaedic Practice*, vol. 27, no. 5, pp. 547–552, Oct. 2016, doi: 10.1097/BCO.0000000000000417.

[28] R. S. of N. A. (RSNA) and A. C. of Radiology (ACR), “Radiofrequency Ablation (RFA) | Microwave Ablation (MWA) - Lung Tumors.” https://www.radiologyinfo.org/en/info.cfm?pg=rfalung (accessed Oct. 27, 2020).

[29] C. L. Brace, “Radiofrequency and Microwave Ablation of the Liver, Lung, Kidney, and Bone: What Are the Differences?,” *Current Problems in Diagnostic Radiology*, vol. 38, no. 3, pp. 135–143, May 2009, doi: 10.1067/j.cpradiol.2007.10.001.

[30] S. J. S. Ruiter, W. J. Heerink, and K. P. de Jong, “Liver microwave ablation: a systematic review of various FDA-approved systems,” *Eur Radiol*, vol. 29, no. 8, pp. 4026–4035, Aug. 2019, doi: 10.1007/s00330-018-5842-z.

[31] 42] M. Kuang, “Liver Cancer: Increased Microwave Delivery to Ablation Zone with Cooled-Shaft Antenna—Experimental and Clinical Studies 1,” *Radiology*, vol. 242, no. 3, pp. 914–924, 2007.

[32] M. G. Lubner, J. L. Hinshaw, A. Andreano, L. Sampson, F. T. Lee, and C. L. Brace, “High-powered microwave ablation with a small-gauge, gas-cooled antenna: initial ex vivo and in vivo results,” *J Vasc Interv Radiol*, vol. 23, no. 3, pp. 405–411, Mar. 2012, doi: 10.1016/j.jvir.2011.11.003.

[33] R. Hoffmann *et al.*, “Comparison of four microwave ablation devices: an experimental study in ex vivo bovine liver,” *Radiology*, vol. 268, no. 1, pp. 89–97, Jul. 2013, doi: 10.1148/radiol.13121127.

[34] M. Alonzo, A. Bos, S. Bennett, and H. Ferral, “The Emprint™ Ablation System with Thermosphere™ Technology: One of the Newer Next-Generation Microwave Ablation Technologies,” *Semin Intervent Radiol*, vol. 32, no. 4, pp. 335–338, Dec. 2015, doi: 10.1055/s-0035-1564811.

[35] D. J. Gillies *et al.*, “Deep learning segmentation of general interventional tools in two-dimensional ultrasound images,” *Med Phys*, Aug. 2020, doi: 10.1002/mp.14427.

[36] J. Garnon *et al.*, “Adjunctive Thermoprotection During Percutaneous Thermal Ablation Procedures: Review of Current Techniques,” *Cardiovasc Intervent Radiol*, vol. 42, no. 3, pp. 344–357, Mar. 2019, doi: 10.1007/s00270-018-2089-7.

[37] J. Smirniotopoulos, W. Cheng, S. Krohmer, S. Kee, and B. Pua, “Interventional Oncology: Keeping Out of Trouble in Ablation Techniques,” *Techniques in Vascular and Interventional Radiology*, vol. 21, no. 4, pp. 223–227, Dec. 2018, doi: 10.1053/j.tvir.2018.07.003.

[38] A. Pfannenstiel *et al.*, "Directional Microwave Ablation: Experimental Evaluation of a 2.45-GHz Applicator in Ex Vivo and In Vivo Liver," *Journal of Vascular and Interventional Radiology*, vol. 31, no. 7, pp. 1170-1177.e2, Jul. 2020, doi: 10.1016/j.jvir.2020.01.016.

[39] P. A. Patel, L. Ingram, I. D. C. Wilson, and D. J. Breen, "No-touch wedge ablation technique of microwave ablation for the treatment of subcapsular tumors in the liver," *J Vasc Interv Radiol*, vol. 24, no. 8, pp. 1257–1262, Aug. 2013, doi: 10.1016/j.jvir.2013.04.014.

[40] D. Haemmerich and F. T. Lee, "Multiple applicator approaches for radiofrequency and microwave ablation," *Int J Hyperthermia*, vol. 21, no. 2, pp. 93–106, Mar. 2005, doi: 10.1080/02656730412331286894.

[41] M. F. Meloni *et al.*, "Microwave ablation in primary and secondary liver tumours: technical and clinical approaches," *Int J Hyperthermia*, vol. 33, no. 1, pp. 15–24, Feb. 2017, doi: 10.1080/02656736.2016.1209694.

[42] A. Kambadakone *et al.*, "Imaging guided percutaneous interventions in hepatic dome lesions: Tips and tricks," *World J Hepatol*, vol. 9, no. 19, pp. 840–849, Jul. 2017, doi: 10.4254/wjh.v9.i19.840.

[43] K. R. Kim and S. Thomas, "Complications of Image-Guided Thermal Ablation of Liver and Kidney Neoplasms," *Semin Intervent Radiol*, vol. 31, no. 2, pp. 138–148, Jun. 2014, doi: 10.1055/s-0034-1373789.

[44] Z. Liu, M. Ahmed, Y. Weinstein, M. Yi, R. L. Mahajan, and S. N. Goldberg, "Characterization of the RF ablation-induced 'oven effect': the importance of background

tissue thermal conductivity on tissue heating," *Int J Hyperthermia*, vol. 22, no. 4, pp. 327–342, Jun. 2006, doi: 10.1080/02656730600609122.

[45] L. Sidoff and D. Dupuy, "Clinical experiences with microwave thermal ablation of lung malignancies," *International Journal of Hyperthermia*, 2016.

[46] J. Sebek, R. Bortel, and P. Prakash, "Broadband lung dielectric properties over the ablative temperature range: Experimental measurements and parametric models," *Med Phys*, vol. 46, no. 10, pp. 4291–4303, Oct. 2019, doi: 10.1002/mp.13704.

[47] A. Pfannenstiel, T. Keast, S. Kramer, H. Wibowo, and P. Prakash, "Flexible microwave ablation applicator for the treatment of pulmonary malignancies," in *SPIE 10066 Energy-based Treatment of Tissue and Assessment*, 2017, pp. 100660M-1-100660M–13, Accessed: Apr. 10, 2017. [Online]. Available: http://dx.doi.org/10.1117/12.2255504.

[48] A. Kastler, H. Alnassan, S. Aubry, and B. Kastler, "Microwave Thermal Ablation of Spinal Metastatic Bone Tumors," *Journal of Vascular and Interventional Radiology*, vol. 25, no. 9, pp. 1470–1475, Sep. 2014, doi: 10.1016/j.jvir.2014.06.007.

[49] S. J. Scott *et al.*, "Approaches for modelling interstitial ultrasound ablation of tumours within or adjacent to bone: theoretical and experimental evaluations," *Int J Hyperthermia*, vol. 29, no. 7, pp. 629–642, Nov. 2013, doi: 10.3109/02656736.2013.841327.

[50] S. J. Scott, V. Salgaonkar, P. Prakash, E. C. Burdette, and C. J. Diederich, "Interstitial ultrasound ablation of vertebral and paraspinal tumours: parametric and patient-specific simulations," *Int J Hyperthermia*, vol. 30, no. 4, pp. 228–244, Jun. 2014, doi: 10.3109/02656736.2014.915992.

[51] B. Tunc and M. Gulsoy, “Stereotaxic laser brain surgery with 1940-nm Tm:fiber laser: An in vivo study,” *Lasers in Surgery and Medicine*, vol. 51, no. 7, pp. 643–652, 2019, doi: 10.1002/lsm.23070.

[52] L. Winter *et al.*, “Magnetic resonance thermometry: Methodology, pitfalls and practical solutions,” *Int J Hyperthermia*, vol. 32, no. 1, pp. 63–75, 2016, doi: 10.3109/02656736.2015.1108462.

[53] P. Faridi, S. H. Bossmann, and P. Prakash, “Simulation-based design and characterization of a microwave applicator for MR-guided hyperthermia experimental studies in small animals,” *Biomed. Phys. Eng. Express*, vol. 6, no. 1, p. 015001, Nov. 2019, doi: 10.1088/2057-1976/ab36dd.

[54] P. T. Donlon *et al.*, “Using microwave thermal ablation to develop a subtotal, cortical-sparing approach to the management of primary aldosteronism,” *International Journal of Hyperthermia*, vol. 36, no. 1, pp. 905–914, Jan. 2019, doi: 10.1080/02656736.2019.1650205.

[55] F. J. Fintelmann *et al.*, “Catecholamine Surge during Image-Guided Ablation of Adrenal Gland Metastases: Predictors, Consequences, and Recommendations for Management,” *J Vasc Interv Radiol*, vol. 27, no. 3, pp. 395–402, Mar. 2016, doi: 10.1016/j.jvir.2015.11.034.

[56] J. Arias Garau, “Radiofrequency Denervation of the Cervical and Lumbar Spine,” *Phys Med Rehabil Clin N Am*, vol. 29, no. 1, pp. 139–154, 2018, doi: 10.1016/j.pmr.2017.08.011.

[57] “Uterine fibroids - Symptoms and causes,” *Mayo Clinic*. https://www.mayoclinic.org/diseases-conditions/uterine-fibroids/symptoms-causes/syc-20354288 (accessed Oct. 24, 2020).

[58] “Uterine fibroids,” *womenshealth.gov*, Dec. 15, 2016. https://www.womenshealth.gov/a-z-topics/uterine-fibroids (accessed Oct. 24, 2020).

[59] J. G. Garza-Leal *et al.*, “Transcervical, intrauterine ultrasound-guided radiofrequency ablation of uterine fibroids with the VizAblate System: safety, tolerability, and ablation results in a closed abdomen setting,” *Gynecol Surg*, vol. 8, no. 3, pp. 327–334, Sep. 2011, doi: 10.1007/s10397-010-0655-3.

[60] K. Walmsley and S. A. Kaplan, “TRANSURETHRAL MICROWAVE THERMOTHERAPY FOR BENIGN PROSTATE HYPERPLASIA: SEPARATING TRUTH FROM MARKETING HYPE,” *The Journal of Urology*, vol. 172, no. 4, Part 1, pp. 1249–1255, Oct. 2004, doi: 10.1097/01.ju.0000129967.30558.ca.

[61] “Esophageal varices - Symptoms and causes,” *Mayo Clinic*. https://www.mayoclinic.org/diseases-conditions/esophageal-varices/symptoms-causes/syc-20351538 (accessed Nov. 06, 2020).

[62] J. Sebek *et al.*, “Feasibility Assessment of Microwave Ablation for Treating Esophageal Varices,” *J. Med. Devices*, vol. 11, no. 3, pp. 031013-031013–8, Jul. 2017, doi: 10.1115/1.4037187.

[63] H. Fallahi, J. Sebek, and P. Prakash, “Broadband Dielectric Properties of Ex Vivo Bovine Liver Tissue Characterized at Ablative Temperatures,” *IEEE Transactions on Biomedical Engineering*, pp. 1–1, 2020, doi: 10.1109/TBME.2020.2996825.

[64] C. Rossmanna and D. Haemmerich, “Review of temperature dependence of thermal properties, dielectric properties, and perfusion of biological tissues at hyperthermic and ablation temperatures,” *Crit Rev Biomed Eng*, vol. 42, no. 6, pp. 467–492, 2014.

[65] G. D. Dodd, M. S. Frank, M. Aribandi, S. Chopra, and K. N. Chintapalli, "Radiofrequency thermal ablation: computer analysis of the size of the thermal injury created by overlapping ablations," *AJR Am J Roentgenol*, vol. 177, no. 4, pp. 777–782, Oct. 2001, doi: 10.2214/ajr.177.4.1770777.

[66] "Analysis of microwave ablation antenna optimization techniques - Etoz - 2018 - International Journal of RF and Microwave Computer-Aided Engineering - Wiley Online Library." https://onlinelibrary-wiley-com.er.lib.k-state.edu/doi/full/10.1002/mmce.21224 (accessed Apr. 01, 2018).

[67] H. Luyen, S. C. Hagness, and N. Behdad, "A Minimally Invasive Coax-Fed Microwave Ablation Antenna With a Tapered Balun," *IEEE Transactions on Antennas and Propagation*, vol. 65, no. 12, pp. 7280–7287, Dec. 2017, doi: 10.1109/TAP.2017.2755258.

[68] P. Prakash*, M. C. Converse, J. G. Webster, and D. M. Mahvi, "An Optimal Sliding Choke Antenna for Hepatic Microwave Ablation," *IEEE Transactions on Biomedical Engineering*, vol. 56, no. 10, pp. 2470–2476, Oct. 2009, doi: 10.1109/TBME.2009.2025264.

[69] Z. Ji and C. L. Brace, "Expanded modeling of temperature-dependent dielectric properties for microwave thermal ablation," *Phys Med Biol*, vol. 56, no. 16, pp. 5249–5264, Aug. 2011, doi: 10.1088/0031-9155/56/16/011.

[70] M. Lazebnik, M. C. Converse, J. H. Booske, and S. C. Hagness, "Ultrawideband temperature-dependent dielectric properties of animal liver tissue in the microwave frequency range," *Phys Med Biol*, vol. 51, no. 7, pp. 1941–1955, Apr. 2006, doi: 10.1088/0031-9155/51/7/022.

[71] V. Lopresto, R. Pinto, G. A. Lovisolo, and M. Cavagnaro, “Changes in the dielectric properties of ex vivo bovine liver during microwave thermal ablation at 2.45 GHz,” *Phys Med Biol*, vol. 57, no. 8, pp. 2309–2327, Apr. 2012, doi: 10.1088/0031-9155/57/8/2309.

[72] H. Fallahi and P. Prakash, “Measurement of Broadband Temperature-Dependent Dielectric Properties of Liver Tissue,” in *2018 IEEE International Microwave Biomedical Conference (IMBioC)*, Jun. 2018, pp. 91–93, doi: 10.1109/IMBIOC.2018.8428845.

[73] J. Sebek, R. Bortel, and P. Prakash, “Broadband lung dielectric properties over the ablative temperature range: Experimental measurements and parametric models,” *Med Phys*, Jul. 2019, doi: 10.1002/mp.13704.

[74] “US6471696B1 - Google Patents.” https://patents.google.com/patent/US6471696B1/en (accessed Sep. 27, 2017).

[75] H. Fallahi and P. Prakash, “Antenna Designs for Microwave Tissue Ablation,” *CRB*, vol. 46, no. 6, 2018, doi: 10.1615/CritRevBiomedEng.2018028554.

[76] V. Lopresto, R. Pinto, L. Farina, and M. Cavagnaro, “Treatment planning in microwave thermal ablation: clinical gaps and recent research advances,” *Int J Hyperthermia*, vol. 33, no. 1, pp. 83–100, 2017, doi: 10.1080/02656736.2016.1214883.

[77] J. Garnon *et al.*, “Adjunctive Thermoprotection During Percutaneous Thermal Ablation Procedures: Review of Current Techniques,” *CardioVascular and Interventional Radiology*, vol. 42, no. 3, pp. 344–357, 2019, doi: 10.1007/s00270-018-2089-7.

[78] J. E. Coad and J. C. Bischof, “Histologic differences between cryothermic and hyperthermic therapies,” Jun. 2003, vol. 4954, pp. 27–36, doi: 10.1117/12.476334.

[79] M. Ahmed, C. L. Brace, F. T. Lee, and S. N. Goldberg, “Principles of and advances in percutaneous ablation,” *Radiology*, vol. 258, no. 2, pp. 351–369, Feb. 2011, doi: 10.1148/radiol.10081634.

[80] N. A. Durick *et al.*, “Microwave ablation with triaxial antennas tuned for lung: results in an in vivo porcine model,” *Radiology*, vol. 247, no. 1, pp. 80–87, Apr. 2008, doi: 10.1148/radiol.2471062123.

[81] L. Ratanaprasatporn, K. P. Charpentier, M. Resnick, S. Lu, and D. Dupuy, “Intra-operative microwave ablation of liver malignancies with tumour permittivity feedback control: a prospective ablate and resect study,” *HPB*, vol. 15, no. 12, pp. 997–1001, 2013, doi: 10.1111/hpb.12084.

[82] C. L. Brace *et al.*, “Microwave Ablation with a Single Small-Gauge Triaxial Antenna: In Vivo Porcine Liver Model 1,” *Radiology*, vol. 242, no. 2, 2007.

[83] D. J. Schutt and D. Haemmerich, “Effects of variation in perfusion rates and of perfusion models in computational models of radio frequency tumor ablation,” *Med Phys*, vol. 35, no. 8, pp. 3462–3470, Aug. 2008, doi: 10.1118/1.2948388.

[84] T. C. H. Hui *et al.*, “Microwave ablation of the liver in a live porcine model: the impact of power, time and total energy on ablation zone size and shape,” *International Journal of Hyperthermia*, vol. 37, no. 1, pp. 668–676, Jan. 2020, doi: 10.1080/02656736.2020.1774083.

[85] C. Prud’homme *et al.*, “Lung microwave ablation – an in vivo swine tumor model experiment to evaluate ablation zones,” *International Journal of Hyperthermia*, vol. 37, no. 1, pp. 879–886, Jan. 2020, doi: 10.1080/02656736.2020.1787530.

[86] B. T. McWilliams, E. E. Schnell, S. Curto, T. M. Fahrbach, and P. Prakash, "A Directional Interstitial Antenna for Microwave Tissue Ablation: Theoretical and Experimental Investigation," *IEEE Transactions on Biomedical Engineering*, vol. 62, no. 9, pp. 2144–2150, Sep. 2015, doi: 10.1109/TBME.2015.2413672.

[87] J. Sebek, S. Curto, R. Bortel, and P. Prakash, "Analysis of minimally invasive directional antennas for microwave tissue ablation," *Int J Hyperthermia*, vol. 33, no. 1, pp. 51–60, Feb. 2017, doi: 10.1080/02656736.2016.1195519.

[88] C. A. Balanis, *Advanced Engineering Electromagnetics*. Hoboken, NJ, USA: Wiley, 1982.

[89] S. Gabriel, R. W. Lau, and C. Gabriel, "The dielectric properties of biological tissues: III. Parametric models for the dielectric spectrum of tissues," *Phys. Med. Biol.*, vol. 41, no. 11, p. 2271, 1996, doi: 10.1088/0031-9155/41/11/003.

[90] V. Lopresto, R. Pinto, and M. Cavagnaro, "Experimental characterisation of the thermal lesion induced by microwave ablation," *International Journal of Hyperthermia*, vol. 30, no. 2, pp. 110–118, Mar. 2014, doi: 10.3109/02656736.2013.879744.

[91] Z. Ji and C. L. Brace, "Expanded modeling of temperature-dependent dielectric properties for microwave thermal ablation," *Phys. Med. Biol.*, vol. 56, no. 16, p. 5249, 2011, doi: 10.1088/0031-9155/56/16/011.

[92] S. K. Hall, E. H. Ooi, and S. J. Payne, "Cell death, perfusion and electrical parameters are critical in models of hepatic radiofrequency ablation," *International Journal of Hyperthermia*, vol. 31, no. 5, pp. 538–550, Aug. 2015, doi: 10.3109/02656736.2015.1032370.

[93] Deshazer Garron, Hagmann Mark, Merck Derek, Sebek Jan, Moore Kent B., and Prakash Punit, "Computational modeling of 915 MHz microwave ablation: Comparative assessment

of temperature-dependent tissue dielectric models," *Medical Physics*, vol. 44, no. 9, pp. 4859–4868, May 2017, doi: 10.1002/mp.12359.

[94] C. L. Brace, "Temperature-dependent dielectric properties of liver tissue measured during thermal ablation: Toward an improved numerical model," in *2008 30th Annual International Conference of the IEEE Engineering in Medicine and Biology Society*, Aug. 2008, pp. 230–233, doi: 10.1109/IEMBS.2008.4649132.

[95] "Cancer of Any Site - Cancer Stat Facts," *SEER*. https://seer.cancer.gov/statfacts/html/all.html (accessed Nov. 19, 2019).

[96] "Financial Burden of Cancer Care | Cancer Trends Progress Report." https://progressreport.cancer.gov/after/economic_burden (accessed Nov. 19, 2019).

[97] K. L. Schulman and J. Kohles, "Economic burden of metastatic bone disease in the U.S.," *Cancer*, vol. 109, no. 11, pp. 2334–2342, 2007, doi: 10.1002/cncr.22678.

[98] "Metastatic Cancer," *National Cancer Institute*, May 12, 2015. https://www.cancer.gov/types/metastatic-cancer (accessed Nov. 19, 2019).

[99] "Bone cancer - Diagnosis and treatment - Mayo Clinic." https://www.mayoclinic.org/diseases-conditions/bone-cancer/diagnosis-treatment/drc-20350221 (accessed Nov. 19, 2019).

[100] Medtronic, "OsteoCool Radiofrequency Ablation System." https://www.medtronic.com/us-en/healthcare-professionals/products/spinal-orthopaedic/tumor-management/osteocool-ablation-system-rf.html (accessed Nov. 19, 2019).

[101] J. Morris *et al.*, "Dual-Energy CT Monitoring of Cryoablation Zone Growth in the Spinal Column and Bony Pelvis: A Laboratory Study," *Journal of Vascular and Interventional Radiology*, vol. 30, no. 9, pp. 1496–1503, Sep. 2019, doi: 10.1016/j.jvir.2019.01.030.

[102] R. M. Irastorza, M. Trujillo, J. Martel Villagrán, and E. Berjano, "Computer modelling of RF ablation in cortical osteoid osteoma: Assessment of the insulating effect of the reactive zone," *Int J Hyperthermia*, vol. 32, no. 3, pp. 221–230, 2016, doi: 10.3109/02656736.2015.1135998.

[103] J. Matschek, E. Bullinger, F. von Haeseler, M. Skalej, and R. Findeisen, "Mathematical 3D modelling and sensitivity analysis of multipolar radiofrequency ablation in the spine," *Mathematical Biosciences*, vol. 284, pp. 51–60, Feb. 2017, doi: 10.1016/j.mbs.2016.06.008.

[104] C. Amabile *et al.*, "Microwave ablation of primary and secondary liver tumours: ex vivo, in vivo, and clinical characterisation," *Int J Hyperthermia*, vol. 33, no. 1, pp. 34–42, 2017, doi: 10.1080/02656736.2016.1196830.

[105] P. Meaney, T. Rydholm, and H. Brisby, "A Transmission-Based Dielectric Property Probe for Clinical Applications," *Sensors (Basel)*, vol. 18, no. 10, Oct. 2018, doi: 10.3390/s18103484.

[106] "Dielectric Properties » IT'IS Foundation." https://itis.swiss/virtual-population/tissue-properties/database/dielectric-properties/ (accessed Nov. 13, 2020).

[107] T. Baum *et al.*, "Anatomical Variation of Age-Related Changes in Vertebral Bone Marrow Composition Using Chemical Shift Encoding-Based Water–Fat Magnetic Resonance Imaging," *Front Endocrinol (Lausanne)*, vol. 9, Apr. 2018, doi: 10.3389/fendo.2018.00141.